Accelerated Discovery of Electrocatalysts for Electrochemical Ammonia Synthesis

Kolen, M.

DOI
10.4233/uuid:0ba71b5c-56c3-4830-bc5d-506538d045a3

Publication date
2023

Document Version
Final published version

Citation (APA)
Kolen, M. (2023). *Accelerated Discovery of Electrocatalysts for Electrochemical Ammonia Synthesis*. [Dissertation (TU Delft), Delft University of Technology]. https://doi.org/10.4233/uuid:0ba71b5c-56c3-4830-bc5d-506538d045a3

Important note
To cite this publication, please use the final published version (if applicable).
Please check the document version above.

Accelerated Discovery of Electrocatalysts for Electrochemical Ammonia Synthesis

Accelerated Discovery of Electrocatalysts for Electrochemical Ammonia Synthesis

Dissertation

for the purpose of obtaining the degree of doctor
at Delft University of Technology
by the authority of the Rector Magnificus, Prof.dr.ir. T.H.J.J. van der Hagen,
chair of the Board of Doctorates
to be publicly defended on
Monday 27 February 2023 at 17:30 o'clock

by

Martin KOLEN

Master of Science in Chemical Engineering,
RWTH Aachen University, Germany
Born in Essen, Germany.

This dissertation has been approved by the promotors.

Composition of the doctoral committee:

Rector Magnificus,	chairperson
Prof. dr. F.M. Mulder	Delft University of Technology, promotor
Prof. dr. W.A. Smith	Delft University of Technology, copromotor
Independent members:	
Prof. dr. M.T. Tromp	University of Groningen
Dr. A. Anastasopol	TNO
Prof. dr. B. Dam	Delft University of Technology
Prof. dr. J.J.C. Geerlings	Delft University of Technology
Dr. R. Kortlever	Delft University of Technology

This research received funding from the Netherlands Organization for Scientific Research (NWO) under project number 15234 in the framework of the Direct Electrolytic Ammonia Project.

Printed by: Ridderprint

Cover artwork: Generated with the AI-art tool Midjourney using the prompt: "accelerated discovery of materials"

ISBN: 978-94-6458-951-1

An electronic version of this dissertation is available at
http://repository.tudelft.nl/.

Contents

1 Introduction

1.1. The Necessity for Climate Change Mitigation

Human activities have caused rapid changes across the global climate system which are unprecedented over many centuries to thousands of years. The global mean temperature has increased approximately 1°C above preindustrial levels which has led to severe negative consequences for humans such as more frequent and more extreme weather events, water and food scarcity, ill health and premature deaths, sea level rise, heavy precipitation and drought. If climate change continues unabatedly these consequences will become much more severe with the possibility of pushing ecosystems to tipping points beyond which abrupt possibly irreversible changes are occurring. The degree of severity of climate change impacts depends on how rapidly global warming can be halted.[1] To prevent the worst consequences of climate change the global temperature rise must be limited to well below 2°C above preindustrial levels.[1, 2]

The global temperature rise is directly dependent on the concentration of greenhouse gases (GHG) like carbon dioxide (CO_2) and methane (CH_4) in the atmosphere. Therefore, efforts to mitigate climate change are directed at reducing GHG emissions from human activities. According to the International Panel on Climate Change (IPCC), the concentration of CO_2 equivalent in the atmosphere cannot exceed 500 ppm for a 50% chance of staying below 2°C global temperature rise. The current increase of the CO_2 concentration in the atmosphere amounts about 2.4 ppm per year which means that in order to reach this goal, the global GHG emissions have to reach zero within only a few decades.[3]

Most GHG emissions are produced during the conversion of fossil fuels into products or energy. Approximately 63% of global GHG emissions are produced by the sectors electricity and heat generation, industry, and transportation.[4] To decarbonise these sectors, clean alternative technologies to the current fossil fuel based ones must be developed and scaled rapidly. The sharp increase of the share of renewable electricity in recent years has shown that this is possible but a key requirement is that sufficiently cheap clean alternative technologies are available.[5, 6] However, for many industries (e.g. chemical industry, heavy transportation industry, steel industry) there are no cost-competitive, CO_2-neutral alternative technologies, yet. To decarbonise these industries, innovations are needed to overcome the technological challenges that prevent cost-competitiveness.[7, 8]

1

1.2. Synthetic Fuels for Decarbonisation

Cheap renewable electricity from solar and wind has the potential to deliver the necessary energy for the decarbonization of industries which are currently difficult to decarbonise. For example, industrial ammonia (NH_3) synthesis could be decarbonised by substituting the hydrogen (H_2) feedstock which is currently produced from fossil fuels with H_2 produced from water and renewable electricity in a process called water electrolysis.[9] However, chemical processes have to run continuously but renewable electricity production has large temporal and geographical variability due to its dependence on sun and wind intensity. Any surplus energy produced from a spike in renewable energy generation potential then has to be either stored or curtailed. Unfortunately, large scale energy storage is too expensive at the moment which means that a lot of the produced electricity would have to be curtailed. This lowers the efficiency of the process and prevents cost-competitiveness. It is estimated that by 2050 an additional 0.2 EJ/day short-term storage and 30 EJ long-term storage will be needed worldwide.[10] Therefore, the development of cheap, large-scale energy storage will be an important step towards halting global warming.

Energy storage on the EJ-scale requires synthetic fuels because other options like batteries or pumped-storage hydroelectricity have either insufficient energy density or are only available in certain regions of the world.[10] Hydrogen is a promising synthetic fuel for long-term energy storage, because it has high gravimetric energy density and it can be produced without GHG emissions by electrolysis. The so-called green H_2 can be stored in tanks during times of excess renewable energy generation potential and converted back into electricity using fuel cells or gas turbines during times when the power demand is higher than the renewable electricity production. However, due to its low volumetric energy density, H_2 must be stored in cryogenically liquefied form or it must be compressed to 200-900 bar, which requires a lot of energy. In addition, technologies to transport H_2 at the required scale are not mature yet and are also anticipated to significantly increase the cost of green H_2.[11, 12] Possibly, other energy carriers have better economics than H_2 for certain applications.

1.3. Electrochemical Ammonia Synthesis

Ammonia is a basic chemical with an annual production volume of 150 million tons. The high gravimetric energy density of NH_3 (5.18 kWh/kg at 25°C, 10 bar) makes it promising as an energy carrier. In addition, NH_3 can be stored and transported using existing infrastructure with smaller energy efficiency losses than H_2 because NH_3 liquefies already at around 10 bar.[9, 13] Currently, NH_3 is produced from CH_4 and nitrogen (N_2) in the Haber-Bosch Process. The Haber-Bosch Process is responsible for 1-1.8% of the global CO_2 emissions which makes it one of the chemical processes with the highest CO_2 emissions in the world.[9, 14, 15] The NH_3 from the Haber-Bosch Process is mostly used for synthetic nitrogen-fertilizers. Without these fertilizers earth could not produce enough food for its current human population.

Most of the CO_2 emissions of the Haber-Bosch-Process are produced during the steam reforming of CH_4 to produce H_2 which is later converted into NH_3. Therefore, a straight forward way to avoid these GHG emissions would be to produce the H_2 from electrolysis (using renewable electricity) instead. The green NH_3 produced this way could be used as a fertilizer, fuel or energy storage system. However, a chemical process like the Haber-Bosch-Process has to operate continuously which means that the production rate cannot be adjusted depending on renewable electricity production. To ensure continuous production, large energy storage systems have to installed together with the Haber-Bosch unit which increases the cost of the system.[9, 14, 15]

A promising concept to increase the flexibility of green NH_3 synthesis is electrochemical NH_3 synthesis. The idea of this concept is to replace the hydrogen evolution reaction (HER; Equation 1.1), which occurs at the cathode in a water electrolyser, with the nitrogen reduction reaction (NRR; Equation 1.2) which converts (N_2) directly into NH_3.[16] Because NH_3 is synthesized directly in an electrolyzer, the NH_3 production rate can be adjusted more rapidly than in a continuously operated chemical process. If successfully developed, this technology could, in theory, have an energy efficiency that is similar to the efficiency of water electrolysis today (around 80%) and further reduce the capital cost of the total process by removing the need for a separate NH_3 synthesis unit. In addition, an electrochemical process to produce NH_3 might be more tolerant to impurities in the N_2 supply than the Haber-Bosch Process which would lower the cost even further. The production of NH_3 in modular electrolyzers instead of giant chemical plants might also enable cost-efficient local production of NH_3 in remote regions.[9]

$$\begin{gathered} 2H_2O + 2e^- <=> 2H_2 + 2OH^- \\ E^0 = -0.828V\ vs.\ SHE\ at\ pH = 14 \end{gathered} \tag{1.1}$$

$$\begin{gathered} N_2 + 6H_2O + 6e^- <=> 2NH_3 + 6OH^- \\ E^0 = -0.763V\ vs.\ SHE\ at\ pH = 14 \end{gathered} \tag{1.2}$$

Due to its large potential impact on climate change mitigation, electrochemical NH_3 synthesis has attracted considerable research interest in recent years. Several different mechanisms have been proposed for the reaction. In the direct NRR mechanism, N_2 is adsorbed onto the catalyst surface and then hydrogenated to NH_3 via proton and electron transfers.[9] The direct NRR mechanism can be further categorized into either an associative Heyrovsky type mechanism where only one bond of the N_2 triple bond is broken before hydrogenation, and a dissociative Heyrovsky type mechanism (shown in Figure 1.1A) were the triple bond is fully broken before hydrogenation.[17] The lithium-mediated mechanism starts with the electrodeposition of metallic lithium from the electrolyte (Figure 1.1B). Then, Li_3N is spontaneously formed and hydrogenated to NH_3 in subsequent proton-electron

1

transfers.[9] The H-permeation mechanism (Figure 1.2) starts with the electrochemical generation of atomic hydrogen on a Nickel foil which is exposed to a N_2 atmosphere on the side that is not facing the electrolyte (exit side). A portion of the electrochemically generated atomic hydrogen permeates through the foil and hydrogenates the nitrogen in a thin nickel nitride film that covers the exit side. The nitrogen desorbs from the surface after hydrogenation to NH_3 and leaves a vacancy in which N_2 can adsorb. The adsorbed N_2 is subsequently hydrogenated to NH_3 by the permeating atomic hydrogen, too.[18]

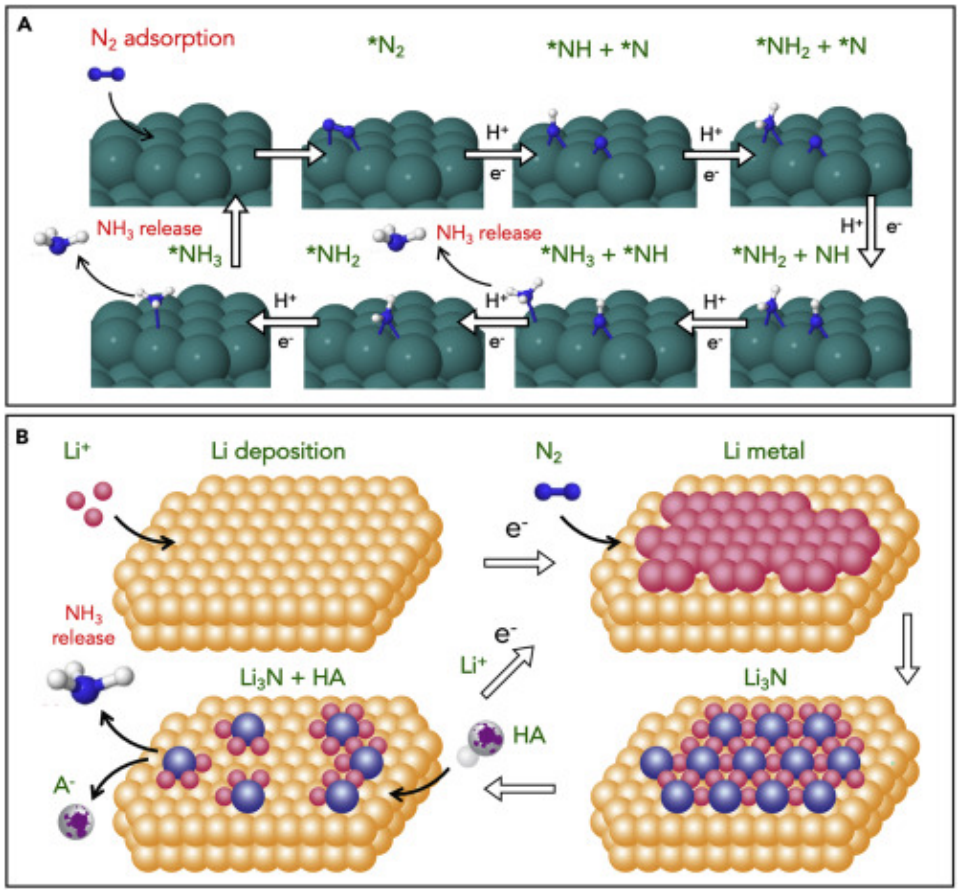

Figure 1.1: Mechanisms of electrochemical NH_3 synthesis. A) direct NRR mechanism. Molecular nitrogen is dissociatively chemisorbed on the catalyst surface and subsequently hydrogenated to NH_3 in Heyrovsky steps. B) Lithium-mediated NRR mechanism. Metallic lithium is produced on the surface of the electrode where it reacts with N_2 to form Li_3N which is electrochemically hydrogenated to NH_3. Reprinted from Ref [9] with permission from Elsevier.

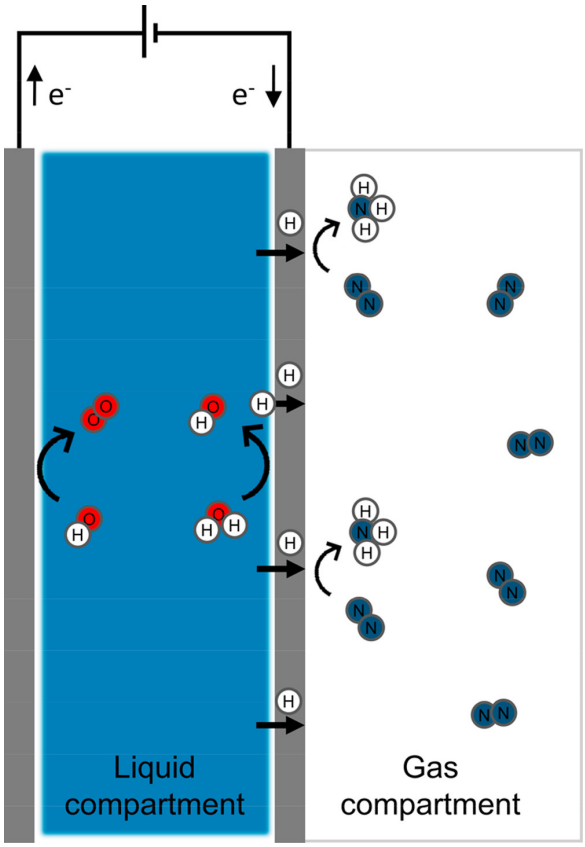

Figure 1.2: H-perm mechanism for electrochemical NH_3 synthesis. A nickel foil separates an electrolyte-filled compartment from a N_2-filled gas compartment. Atomic hydrogen is electrochemically generated on the electrolyte side of the Ni foil and permeates through the Ni foil to the N_2 side where it hydrogenates adsorbed N_2. Reprinted with permission from Ref [18]. Copyright 2021 American Chemical Society.

Depending on the mechanism different challenges limit the technological maturity of electrochemical NH_3 synthesis. In the case of the Li-mediated mechanism, high production rates and faradaic efficiencies can be achieved but the high energy requirement to reduce Li limits the maximum thermodynamically possible energy efficiency to 26% (assuming a faradaic efficiency of 80%). In addition, metallic lithium is incompatible with an aqueous electrolyte which means that protons have to be supplied from a different source, such as H_2, which has to be generated in a separate process.[19, 20] Both, the direct NRR mechanism and the H-permeation mechanism produce NH_3 at very low production rates (typically below 0.1 nmol s^{-1} cm^{-2}) which is three orders of magnitude below commercially interesting rates.[9, 18] The focus of this dissertation is on increasing the NH_3 production rates for the direct NRR mechanism.

The difficulty of obtaining higher NH_3 production rates with the direct NRR mech-

anism is caused by the more favourable HER in aqueous electrolyte. A selective electrocatalyst for NRR is needed to promote the reaction over the competing HER. The difficulty of finding a selective electrocatalyst for NRR is commonly attributed to the very stable N_2 triple bond which needs to be activated and subsequently hydrogenated in a 6-electron transfer process to produce NH_3. In comparison, to produce H_2 from HER only 2 electron transfers are needed.[21] In addition, DFT calculations on single metal surfaces suggest that a minimum overpotential of 0.5 V is necessary for NRR to overcome the correlation between the binding energies of key intermediates (so-called scaling relations).[22] These considerations suggest that a large number of negative results can be expected when attempting to develop selective electrocatalysts for NRR.

Nevertheless, materials consisting of elements from all over the periodic table have been reported to be active catalysts for NRR.[23] Several investigations to assess the reliability of these reports came to the conclusion that none of the reports used a sufficiently rigorous experimental protocol to prove unambiguously that the produced NH_3 originated from NRR activity and not from NH_3 contamination in the electrolyte.[24–26] The uncertainty around the reliability of reports of NRR activity is caused by the low NH_3 production from NRR which has to be accumulated in the electrolyte until the detection limit of the liquid NH_3 detection is reached. The problem is, that with the current low NH_3 production rates of NRR, NH_3 concentrations in the electrolyte are on par with common NH_3 contamination sources. Therefore, common NH_3 contaminations can be easily mistaken for NRR activity. [27]

Ammonia contamination in the electrolyte can originate from a wide variety of sources including catalyst precursors[19, 28–30], feed gases (N_2, Ar, $^{15}N_2$)[31, 32], breath[25], atmosphere[33, 34] nitrile gloves[25], nafion[33, 35], sample vials and cell surfaces[19]). False positives from NH_3 contaminations have led to retractions and refutations of results which were believed to be groundbreaking.[36, 37] The difficulty of distinguishing false positives from NRR activity has led to several cases where a lot of resources were invested into a potential catalyst only to find out in the end that NRR activity originated from contamination.[26, 32] Clearly, an experimental protocol which produces reliable results is crucial for NRR catalyst development.

As pointed out previously, the chances of finding a selective catalyst for NRR on the first attempt are very slim according to theoretical considerations because of the more favourable HER. Therefore, an experimental workflow for NRR catalyst development must be capable of quickly filtering out a large number of negative results. However, the current experimental workflow for NRR catalyst development is extremely slow due to long electrolysis steps, frequent control experiments and time-consuming NH_3 quantification.[27] These bottlenecks in the NRR experimental workflow have to be removed to address the complexity of finding a selective catalyst for NRR. In summary, we have identified two barriers which inhibit the development of a selective NRR catalyst: the slow experimental throughput of NRR experiments and the unreliable quantification of NRR activity with current experi-

mental protocols.

1.4. Thesis Outline

In order to improve the experimental workflow for NRR, we systematically analyze in Chapters 2 and 3 what currently prevents fast and reliable NRR research and how these limitations can be overcome. In Chapter 2, the focus is on the development of a suitable NH_3 detection method to replace the time-consuming, error-prone spectrophotometric NH_3 detection methods that are currently used for NRR research. In Chapter 3, we analyze how the deficiencies of current NRR experimental protocols are linked to the cell design that is typically used to measure the NRR activity of catalysts. Based on our findings, we propose an alternative cell design that circumvents these deficiencies. After discussing how to remove the barriers for fast and reliable one-at-a-time catalyst testing in Chapters 2 and 3, we describe in Chapter 4 how to accelerate NRR catalyst development further by including automation and parallelization techniques in the experimental workflow. We use the resulting high-throughput electrocatalyst screening workflow to screen 528 bimetallic catalysts for NRR activity. Finally in Chapter 5, we describe a pressure balancing system for high-pressure electrolysis in flow cells which can be used to improve the selectivity of NRR by shifting the thermodynamic equilibrium towards NRR.

1

References

[1] IPCC, *Summary for Policymakers. In: Climate Change 2022 Impacts, Adaptation and Vulnerability*, Tech. Rep. 6 (2022).

[2] United Nations, *Paris Agreement,* (2015).

[3] Intergovernmental Panel on Climate Change and O. Edenhofer, eds., *Climate Change 2014: Mitigation of Climate Change: Working Group III Contribution to the Fifth Assessment Report of the Intergovernmental Panel on Climate Change* (Cambridge University Press, New York, NY, 2014).

[4] V. Masson-Delmotte, H.-O. Pörtner, J. Skea, P. Zhai, D. Roberts, P. R. Shukla, A. Pirani, R. Pidcock, Y. Chen, E. Lonnoy, W. Moufouma-Okia, C. Péan, S. Connors, J. B. R. Matthews, X. Zhou, M. I. Gomis, T. Maycock, M. Tignor, and T. Waterfield, *An IPCC Special Report on the impacts of global warming of 1.5°C above pre-industrial levels and related global greenhouse gas emission pathways, in the context of strengthening the global response to the threat of climate change, sustainable development, and efforts to eradicate poverty,* , 630 (2019).

[5] International Renewable Energy Agency, *Renewable Energy Prospects for the European Union*, Tech. Rep. (2018).

[6] International Renewable Energy Agency, *Renewable Power: Climate-safe Energy Competes on Cost Alone*, Tech. Rep. (2018).

[7] J. Rockström, O. Gaffney, J. Rogelj, M. Meinshausen, N. Nakicenovic, and H. J. Schellnhuber, *A roadmap for rapid decarbonization,* Science **355**, 1269 (2017).

[8] P. De Luna, C. Hahn, D. Higgins, S. A. Jaffer, T. F. Jaramillo, and E. H. Sargent, *What would it take for renewably powered electrosynthesis to displace petrochemical processes?* Science **364**, eaav3506 (2019).

[9] D. R. MacFarlane, P. V. Cherepanov, J. Choi, B. H. Suryanto, R. Y. Hodgetts, J. M. Bakker, F. M. Ferrero Vallana, and A. N. Simonov, *A Roadmap to the Ammonia Economy,* Joule **4**, 1186 (2020).

[10] F. M. Mulder, *Implications of diurnal and seasonal variations in renewable energy generation for large scale energy storage,* Journal of Renewable and Sustainable Energy **6**, 033105 (2014).

[11] G. Parks, R. Boyd, J. Cornish, and R. Remick, *Hydrogen Station Compression, Storage, and Dispensing Technical Status and Costs: Systems Integration*, Tech. Rep. NREL/BK-6A10-58564, 1130621 (2014).

[12] Hydrogen Council, McKinsey & Company, *Hydrogen Insights Report*, Tech. Rep. (2021).

[13] R. Lan and S. Tao, *Ammonia as a Suitable Fuel for Fuel Cells,* Frontiers in Energy Research **2** (2014), 10.3389/fenrg.2014.00035.

[14] A. Valera-Medina, H. Xiao, M. Owen-Jones, W. David, and P. Bowen, *Ammonia for power,* Progress in Energy and Combustion Science **69**, 63 (2018).

[15] The Royal Society, *Ammonia: Zero-Carbon Fertiliser, Fuel and Energy Store.* (2020).

[16] N. Cao and G. Zheng, *Aqueous electrocatalytic N2 reduction under ambient conditions,* Nano Research **11**, 2992 (2018).

[17] E. Skúlason, T. Bligaard, S. Gudmundsdóttir, F. Studt, J. Rossmeisl, F. Abild-Pedersen, T. Vegge, H. Jónsson, and J. K. Nørskov, *A theoretical evaluation of possible transition metal electro-catalysts for N $_2$ reduction,* Phys. Chem. Chem. Phys. **14**, 1235 (2012).

[18] D. Ripepi, R. Zaffaroni, H. Schreuders, B. Boshuizen, and F. M. Mulder, *Ammonia Synthesis at Ambient Conditions via Electrochemical Atomic Hydrogen Permeation,* ACS Energy Letters **6**, 3817 (2021).

[19] W. Yu, P. Buabthong, C. G. Read, N. F. Dalleska, N. S. Lewis, H.-J. Lewerenz, H. B. Gray, and K. Brinkert, *Cathodic NH $_4$ $^+$ leaching of nitrogen impurities in CoMo thin-film electrodes in aqueous acidic solutions,* Sustainable Energy & Fuels **4**, 5080 (2020).

[20] B. H. R. Suryanto, K. Matuszek, J. Choi, R. Y. Hodgetts, H.-L. Du, J. M. Bakker, C. S. M. Kang, P. V. Cherepanov, A. N. Simonov, and D. R. MacFarlane, *Nitrogen reduction to ammonia at high efficiency and rates based on a phosphonium proton shuttle,* Science **372**, 1187 (2021).

[21] A. R. Singh, B. A. Rohr, M. J. Statt, J. A. Schwalbe, M. Cargnello, and J. K. Nørskov, *Strategies toward Selective Electrochemical Ammonia Synthesis,* ACS Catalysis **9**, 8316 (2019).

[22] J. H. Montoya, C. Tsai, A. Vojvodic, and J. K. Nørskov, *The Challenge of Electrochemical Ammonia Synthesis: A New Perspective on the Role of Nitrogen Scaling Relations,* ChemSusChem **8**, 2180 (2015).

[23] Y. Ren, C. Yu, X. Tan, H. Huang, Q. Wei, and J. Qiu, *Strategies to suppress hydrogen evolution for highly selective electrocatalytic nitrogen reduction: Challenges and perspectives,* Energy & Environmental Science **14**, 1176 (2021).

[24] L. F. Greenlee, J. N. Renner, and S. L. Foster, *The Use of Controls for Consistent and Accurate Measurements of Electrocatalytic Ammonia Synthesis from Dinitrogen,* ACS Catalysis **8**, 7820 (2018).

[25] S. Z. Andersen, V. Čolić, S. Yang, J. A. Schwalbe, A. C. Nielander, J. M. McEnaney, K. Enemark-Rasmussen, J. G. Baker, A. R. Singh, B. A. Rohr, M. J. Statt,

S. J. Blair, S. Mezzavilla, J. Kibsgaard, P. C. K. Vesborg, M. Cargnello, S. F. Bent, T. F. Jaramillo, I. E. L. Stephens, J. K. Nørskov, and I. Chorkendorff, *A rigorous electrochemical ammonia synthesis protocol with quantitative isotope measurements,* Nature **570**, 504 (2019).

[26] J. Choi, B. H. R. Suryanto, D. Wang, H.-L. Du, R. Y. Hodgetts, F. M. Ferrero Vallana, D. R. MacFarlane, and A. N. Simonov, *Identification and elimination of false positives in electrochemical nitrogen reduction studies,* Nature Communications **11**, 5546 (2020).

[27] M. Kolen, W. A. Smith, and F. M. Mulder, *Accelerating ^{1} H NMR Detection of Aqueous Ammonia,* ACS Omega **6**, 5698 (2021).

[28] Y. Chen, H. Liu, N. Ha, S. Licht, S. Gu, and W. Li, *Revealing nitrogen-containing species in commercial catalysts used for ammonia electrosynthesis,* Nature Catalysis (2020), 10.1038/s41929-020-00527-4.

[29] H.-L. Du, T. R. Gengenbach, R. Hodgetts, D. R. MacFarlane, and A. N. Simonov, *Critical Assessment of the Electrocatalytic Activity of Vanadium and Niobium Nitrides toward Dinitrogen Reduction to Ammonia,* ACS Sustainable Chemistry & Engineering **7**, 6839 (2019).

[30] D. L. Boucher, J. A. Davies, J. G. Edwards, and A. Mennad, *An investigation of the putative photosynthesis of ammonia on iron-doped titania and other metal oxides,* Journal of Photochemistry and Photobiology A: Chemistry **88**, 53 (1995).

[31] R. Dabundo, M. F. Lehmann, L. Treibergs, C. R. Tobias, M. A. Altabet, P. H. Moisander, and J. Granger, *The Contamination of Commercial 15N2 Gas Stocks with 15N–Labeled Nitrate and Ammonium and Consequences for Nitrogen Fixation Measurements,* PLoS ONE **9**, e110335 (2014).

[32] R. Y. Hodgetts, H.-L. Du, D. R. MacFarlane, and A. N. Simonov, *Electrochemically Induced Generation of Extraneous Nitrite and Ammonia in Organic Electrolyte Solutions During Nitrogen Reduction Experiments,* ChemElectroChem **8**, 1596 (2021).

[33] G. Y. Duan, Y. Ren, Y. Tang, Y. Z. Sun, Y. M. Chen, P. Y. Wan, and X. J. Yang, *Improving the Reliability and Accuracy of Ammonia Quantification in Electro- and Photochemical Synthesis,* ChemSusChem **13**, 88 (2020).

[34] C. Saigne, S. Kirchner, and M. Legrand, *ION-CHROMATOGRAPHIC MEASUREMENTS OF AMMONIUM, FLUORIDE, ACETATE, FORMATE AND METHANESULPHONATE IONS AT VERY LOW LEVELS IN ANTARCTIC ICE,* Analytica Chimica Acta, **203**, 11 (1987).

[35] H. Liu, Y. Zhang, and J. Luo, *The removal of inevitable NO species in catalysts and the selection of appropriate membrane for measuring electrocatalytic ammonia synthesis accurately,* Journal of Energy Chemistry **49**, 51 (2020).

[36] S. Licht, B. Cui, B. Wang, F.-F. Li, J. Lau, and S. Liu, *Retraction,* **369**, 780 (2020).

[37] J. Choi, H.-L. Du, C. K. Nguyen, B. H. R. Suryanto, A. N. Simonov, and D. R. MacFarlane, *Electroreduction of Nitrates, Nitrites, and Gaseous Nitrogen Oxides: A Potential Source of Ammonia in Dinitrogen Reduction Studies,* ACS Energy Letters **5**, 2095 (2020).

2
Accelerating ^{1}H NMR Detection of Aqueous Ammonia

Direct electrolytic N_2 reduction to ammonia (NH_3) is a renewable alternative to the Haber-Bosch-Process. The activity and selectivity of electrocatalysts is evaluated by measuring the amount of NH_3 in the electrolyte. Quantitative ^{1}H Nuclear Magnetic Resonance (qNMR) detection reduces the bench time to analyze samples of NH_3 (present in the assay as NH_4^+) compared to conventional spectrophotometric methods. However, many groups do not have access to an NMR spectrometer with sufficiently high sensitivity. We report that by adding 1 mM *paramagnetic Gd^{3+}-ions to the NMR sample the required analysis time can be reduced by an order of magnitude such that fast NH_4^+ detection becomes accessible with a standard NMR spectrometer. Accurate, internally calibrated quantification is possible over a wide pH-range.*

Parts of this chapter have been published in ACS Omega **6,8**, 5698–5704 (2021) [1].

2.1. Introduction

Ammonia (NH_3) is one of the largest chemical commodities responsible for about 1.5% of global energy use and associated CO_2 emissions from the Haber-Bosch Process. It's primary use is as a feedstock for nitrogen-based fertilizers. Electrochemical, fossil fuel free, methods to produce ammonia are gaining significant interest for the reduction of CO_2 emissions, and in addition to enable ammonia as carbon free energy carrier and storage.[2–4] Direct electrolytic N_2 reduction is a renewable alternative to synthesize NH_3. To suppress the undesirable hydrogen evolution reaction a selective electrocatalyst is needed.[5]

The activity and selectivity of electrocatalysts is quantified by measuring the accumulated NH_3 in the electrolyte with appropriate detection methods. Recently, a number of papers were published about the difficulty of obtaining reproducible results in nitrogen reduction research.[6, 7] Such difficulty is related to experimental procedures and e.g. significant amounts of NH_3 from dust, ambient air, $^{15}N_2$ and desorption from cell surfaces. Additionally, NOx contamination or nitrogen containing catalyst precursors can be reduced to NH_3 during electrolysis which can be falsely attributed to N_2 reduction.[8, 9] Reliable testing and analysis procedures including control experiments with isotope labelled $^{15}N_2$ are necessary to avoid false positives.[6] Conventional spectrophotometric NH_3 detection methods such as the indophenol blue method cannot distinguish between isotopologues of NH_3 and require considerable bench time.[10, 11] ^{1}H NMR spectroscopy is a fast, accessible and isotopically selective alternative to spectrophotometric methods for NH_3 detection but as we will show below the sensitivity on a standard 400 MHz spectrometers is insufficient.[12] Here we present a powerful liquid state NMR method with sufficient sensitivity on relatively easily accessible NMR spectrometers i.e. requiring limited field strength and normal sensitivity probes.

Several alternatives to spectrophotometric NH_3 detection methods have been proposed recently. Ion chromatography can be used for ammonia detection but isotopologues cannot be distinguished and an overlap of NH_4^+ with other cations poses a threat to the accuracy of the method.[13] Yu et al. proposed ultrahigh performance liquid chromatography - mass spectroscopy (UPLC-MS) to measure derivatized solutions of NH_3.[14] The method is very sensitive and capable of distinguishing isotopologues of NH_3 but requires careful control over the pH. Quantitative ^{1}H NMR has been widely adopted to quantify $^{15}NH_4^+$ from control experiments with $^{15}N_2$. The acidified form of ammonia, ammonium ($^{14}NH_4^+$) and it's isotopologue $^{15}NH_4^+$ have an unmistakable fingerprint in the ^{1}H NMR spectrum.[12]

Quantitative ^{1}H NMR is based on the proportional relationship between the signal integral I_x and the number of protons N_x responsible for that particular signal:

$$I_x = K_S N_x \tag{2.1}$$

where K_S is a proportionality factor that depends on the physio-chemical properties

of the sample. In order to achieve accurate quantification, changes in K_S have to be accounted for by a suitable quantification method.[15] Pulse Length based Concentration Determination (PULCON) uses the principle of reciprocity to correlate the absolute intensity of two spectra measured in different solutions.[16] Nielander et al. successfully applied the PULCON method to NH_4^+ quantification.[12]
Since fluctuations of K_S affect all resonances in the spectrum equally, the ratio of two peaks is independent of K_S and can therefore be used for quantification. Typically, an internal standard of known concentration is added as a reference. The concentration of NH_4^+ can be quantified either by relative or absolute quantification. For relative quantification, a calibration curve is generated by measuring standard solutions of NH_4^+ and an internal standard.[15] The prerequisites for accurate ammonia quantification with relative quantification were recently described.[17] Absolute quantification allows the calculation of the NH_4^+ concentration directly from the integral of the peaks of NH_4^+ and the internal standard without requiring a calibration curve according to:

$$C_{NH_4^+} = \frac{I_{NH_4^+}}{I_{std}} \frac{N_{std}}{N_{NH_4^+}} C_{std} \tag{2.2}$$

where I, N and C are the integral area, number of nuclei and concentration of NH_4^+ and standard, respectively. Absolute quantification requires that the total time spent to acquire one scan, the interscan delay t_{scan}, is at least 5 times the longest longitudinal relaxation time T_1 in the sample.[15] Despite the advantages of absolute quantification (calibration-free and robust) so far, no absolute quantification method has been proposed for ammonia detection. Hodgetts *et al.* reported that a d1, T_1 and proton exchange induced loss of coherence affects the NH_4^+ peak, rendering absolute quantification not suitable for NH_4^+ detection.[17] By adding a suitable paramagnetic salt accurate absolute quantification becomes possible because the T_1 of both, the internal standard and NH_4^+ are reduced so that there is insufficient time for the proton exchange to induce a loss of coherence as we will see below.
The lower limit of quantification (LOQ) of a detection method is the lowest concentration of NH_3 that can be measured within an acceptable time and with an acceptable accuracy. The LOQ depends on the sensitivity which is calculated from the signal-to-noise ratio (SNR) at a certain interscan delay t_{scan}:

$$Sensitivity = \frac{SNR}{\sqrt{t_{scan}}} \tag{2.3}$$

To reduce the minimum LOQ by a factor of 2, the analysis time has to be quadrupled.[18] Nielander et al. could detect 1 µM NH_4^+ in ethanol within 1 h ($t_{scan} = 2\ s$) with a 900 MHz NMR and cryo-probe.[12] The sensitivity difference between a 900 MHz NMR and a standard laboratory NMR (400 MHz) is substantial. The type of probe and the field strength difference leads to one order of magnitude lower sensitivity which leads to two orders of magnitude longer analysis time to achieve the same LOQ on a 400 MHz NMR without cryoprobe.[19] To compensate for the lower sensitivity longer experiments (typically several hours) are necessary to accumulate

enough NH_4^+ in the electrolyte to reach the detection limit which is unfavourable and which in addition increases the risk of false negatives due to deactivation and of false positives due to contamination. Higher ^{1}H NMR sensitivity is needed to enable laboratories with more standard NMR spectrometers to quantify NH_3 efficiently.

The type of the pulse sequence influences the NH_4^+ sensitivity strongly.[12, 17] The signal from the hydrogen atoms of the solvent has to be suppressed to avoid baseline distortions and low receiver gain. Nielander et al. showed that pulse sequences that utilize pulsed field gradients in combination with selective excitation pulses are very effective at suppressing water without removing the NH_4^+ signal.[12] These pulse sequences use pulsed field gradients to dephase the water resonance and selective pulses to ensure that during acquisition water is completely out of phase while NH_4^+ is in phase.[20].

The T_1 of a molecule influences the sensitivity because for a given interscan delay t_{scan}, T_1 determines the percentage of spins that can relax back to equilibrium in between scans. A smaller percentage relaxation leads to less acquired signal per scan according to:

$$M_z = M_0(1 - e^{-t_{scan}/T_1}) \tag{2.4}$$

where, M_Z and M_0 are the magnetization in z-axis following t_{scan} and at full relaxation, respectively. The interscan delay t_{scan} is comprised of the recycle delay d1 and the acquisition time. It is noteworthy that for some pulse sequences the percentage relaxation only depends on the recycle delay, not on the acquisition time, as will be discussed in more detail below. Reducing the interscan delay for example by fast sampling is a well-known strategy to improve the ^{1}H NMR sensitivity.[21] Another strategy to lower the interscan delay is to shorten the T_1 of the analyte which has the advantage that the same percentage relaxation can be achieved at a lower interscan delay.[15] T_1 is determined by the fluctuating magnetic interactions due to nearby magnetic moment fluctuations and due to positional changes of surrounding nuclei and moments. Interactions with unpaired electrons of paramagnetic substances are 1000 times larger than typical interactions between nuclear magnetic moments. Therefore, a small amount of a paramagnetic substance is sufficient to lower T_1 drastically.[22] This concept is applied in contrast agents for medical Magnetic Resonance Imaging (MRI). The so-called paramagnetic relaxation enhancement (PRE) is also a common strategy to overcome sensitivity barriers for small organic molecules and proteins, because as the T_1 decreases more scans can be acquired in the same amount of time.[19, 23, 24]

2.2. Results and discussion

The Gd^{3+}-ion is widely used for PRE in medical MRI due to it's large magnetic moment from seven unpaired electrons.[25] We investigated the influence of paramagnetic Gd^{3+}-ions on the sensitivity for aqueous ammonia detection to enable ^{1}H NMR as a routine analysis tool for NH_4^+ quantification, with the use of an internal

standard (absolute quantification). In agreement with Nielander et al. we found that pulse sequences that are suppressing the water resonance by dephasing it during acquisition are well suited for NH_4^+ detection.[12] With Excitation Sculpting (ES) the water resonance is suppressed effectively and a flat baseline is obtained around the NH_4^+ triplet. However, at 40 µM NH_4^+ the SNR is only 13.6 for a 12.8 min measurement on a 400 MHz NMR with room temperature probe (see Figure 2.1a). With this sensitivity, it takes 4 hours until the accumulated ammonia in the electrolyte produced by a catalyst with intermediate activity becomes quantifiable by NMR (calculation in Section 2.5). Therefore, we sought to improve the sensitivity by adding 1 mM of paramagnetic Gd^{3+} to the NMR tube. Maleic acid (MA) was added as an internal standard to quantify the amount of NH_4^+ with absolute quantification. The singlet of maleic acid at ca. 6.21 ppm is sufficiently separated from the NH_4^+ triplet at ca. 6.9 ppm. The T_1 of both, NH_4^+ and MA decreases drastically after the addition of Gd^{3+}. The T_1 decreases from 2.16 s to 0.14 s and from 2.05 s to 0.13 s for NH_4^+ and MA, respectively (Figure 2.1d). This 15.4-fold reduction of the T_1 of NH_4^+ enables a reduction of the interscan delay by the same factor which according to Equation 2.3, leads to a potential 3.9-fold sensitivity increase ($\sqrt{15.4} = 3.9$). The linewidth of NH_4^+ increases only slightly with the addition of Gd^{3+} from 3.6 Hz to 4.2 Hz.

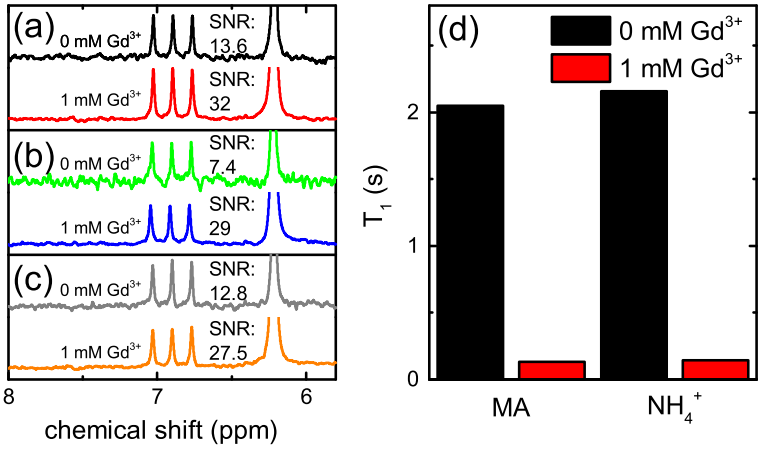

Figure 2.1: ^1H NMR sensitivity gain from 0 mM Gd^{3+} (**black**, **green** and **gray**) to 1 mM Gd^{3+} (**red**, **blue**, **orange**) in the NMR tube measured with different acquisition parameters and pulse sequences. **(a)** 40 µM NH_4^+ measured with identical total acquisition time (12.8 min) and a recycle delay d1 of 10 s and 0.75 s for 0 mM Gd^{3+} and 1 mM Gd^{3+}, respectively. Pulse sequence: Excitation Sculpting. **(b)** 40 µM NH_4^+ measured with identical total acquisition time (10.7 min) and recycle delay (0.5 s). Pulse sequence: Excitation Sculpting. **(c)** 40 µM NH_4^+ measured with the same acquisition parameters as (b) but with the DPFGSE pulse sequence. All SNR values are averages from a triplet measurement. **(d)** Effect of 1 mM Gd^{3+} on T_1 of NH_4^+ and maleic acid. Field strength: 400 MHz.

To show that the measured sensitivity gain matches the sensitivity gain predicted from T_1 measurements, we measured a sample of 40 µM NH_4^+ with and without 1 mM Gd^{3+} using different acquisition parameters (Figure 2.1a–c). In Figure 2.1a the total analysis time is identical in both measurements and the d1 is set to $5T_1$ so that NH_4^+ has the same percentage relaxation in both cases. With 1 mM Gd^{3+}, the sensitivity is significantly (factor 2.4) higher but not as much as expected from the T_1 decrease (factor 3.9). We will later show that a sensitivity gain close to the predicted value can be measured directly by removing an additional 90° pulse that is by default included in the ES pulse sequence. With the default version of ES the sensitivity gain is lower than expected from the T_1 decrease because the additional 90° pulse removes the contribution of the acquisition time to the percentage relaxation. Consequently, the acquisition time only adds time to the total analysis time without improving signal strength and the percentage relaxation depends only on d1. Since the acquisition time makes up a larger fraction of the interscan delay at low interscan delays the decrease of sensitivity is more pronounced with 1 mM Gd^{3+} where the acquisition time makes up 0.75 s of the total 1.5 s interscan delay. Without Gd^{3+} only 2 s out of 12 s interscan delay are acquisition time leading to a smaller sensitivity loss. In other words, the interscan delay could be a factor 1.2 and 2 smaller for 0 mM Gd^{3+} and 1 mM Gd^{3+}, respectively. Therefore, the sensitivity gain with 1 mM Gd^{3+} would increase by a factor 1.3 ($\sqrt{\frac{2}{1.2}} = 1.3$) from 2.4 to 3.1 if the sensitivity loss would have been equal in both cases. Taking into account 15% sensitivity loss due to line broadening the sensitivity gain is 3.6 which is close to the predicted value.

The experiment shown in Figure 2.1a is not sufficient to prove a sensitivity gain because it only shows that with a higher recycle delay less scans can be acquired in the same amount of time. Less scans will always lead to lower SNR. To prove a sensitivity increase, it is necessary to show that a larger recycle delay is necessary with 0 mM Gd^{3+} but not with 1 mM Gd^{3+}. This is shown in Figure 2.1b where both, 0 mM Gd^{3+} and 1 mM Gd^{3+} were measured with low recycle delay (0.5 s) and identical total acquisition time. The sensitivity without Gd^{3+} is 3.9 times lower indicating that a large fraction of the signal is lost due to low percentage relaxation. The percentage relaxation at a recycle delay of 0.5 s is 20.7% and 97.2% for a T_1 of 2.16 s and 0.14 s, respectively. Therefore, 4.7 times more signal can be expected with 1 mM Gd^{3+} in the same amount of time. We assume that 15% of that signal increase is lost due to line broadening with Gd^{3+} which results in a sensitivity improvement by a factor of 4.08. This value agrees well with the experimentally observed value of 3.9.

To study if adding Gd^{3+} also improves the sensitivity with other pulse sequences, we measured the sensitivity gain with the Double Pulsed Field Gradient Spin Echo (DPFGSE) pulse sequence (Figure 2.1c) using the same acquisition parameters as in Figure 2.1b. The sensitivity gain with DPFGSE (2.1) is lower than with ES (3.9). The reason for this is that with DPFGSE the percentage relaxation has to be calculated

using the full interscan delay including acquisition time, not just the d1 as for ES. Using the same methodology as in b) we calculate the percentage relaxation with and without Gd^{3+} and arrive at an expected sensitivity gain of 1.8 which agrees well with the experimentally measured value. The sensitivity gain is lower than in (b) because with 1 mM Gd^{3+} the chosen t_{scan} of 1.25 s is almost 9 times longer than the T_1 of NH_4^+ which means that t_{scan} is much longer than the necessary $5T_1$ and as a result sensitivity is lost. The previous examples demonstrate that after addition of 1 mM Gd^{3+} a significant sensitivity gain is observed with different acquisition parameters and pulse sequences and this sensitivity gain agrees well with the expected values predicted from T_1 measurements.

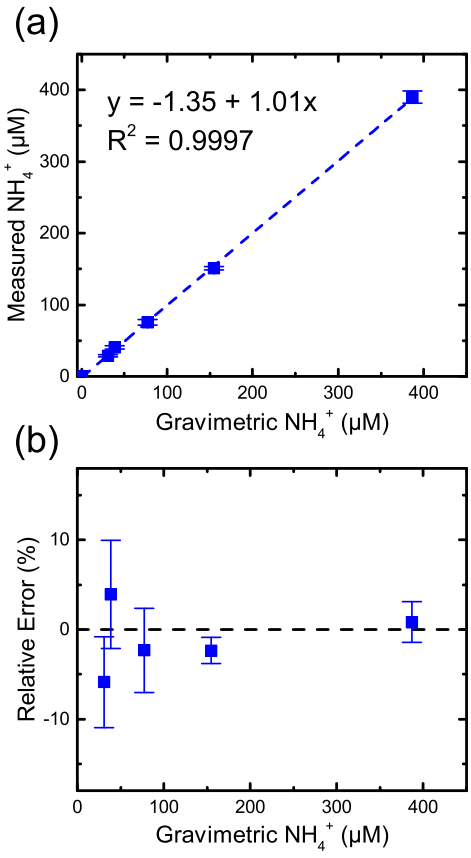

Figure 2.2: **(a)** Linearity and **(b)** accuracy of NH_4^+ quantification with 1 mM Gd^{3+}. Error bars around each point represent the standard deviation for each triplicate measurement. Pulse sequence: Excitation Sculpting, recycle delay: 0.5 s, acquisition time: 0.75 s total analysis time: 10.7 min, field strength: 400 MHz.

We measured the accuracy of the NH_4^+ quantification with 1 mM Gd^{3+} by calculating the NH_4^+ concentration from the intensities of MA and NH_4^+ using Equation 2.2 and comparing it to the gravimetrically measured concentration (Figure 2.2a,b). The method has very good linearity (R^2 = 0.999) and an acceptable relative error (≤10%) in the NH_4^+ concentration range from 30 µM to 388 µM with the ES pulse sequence. The relative error is randomly distributed around the abscissa which suggests that it is caused by integration errors. Higher accuracy (relative error ≤5.3%) was obtained with isotope labelled $^{15}NH_4^+$ (see Figure 2.6). $^{15}NH_4^+$ can be quantified with higher accuracy because it appears in the NMR spectrum as a doublet which has inherently higher SNR than the $^{14}NH_4^+$ triplet.

The pH of the catholyte, which is used for detection, can vary over time due to acidic or alkaline species produced in the electrochemical reaction, or because of migration of ions induced by the electric field.[26, 27] N_2 reduction experiments are especially prone to pH changes because the electrolyte volume is minimised to maximise the signal for ammonia detection. Both, UPLC-MS and the indophenol method are sensitive to pH changes, because the pH influences the reaction that is carried out prior to analysis.[10, 14] Therefore, additional dilution steps can be necessary to measure accurately with these methods.

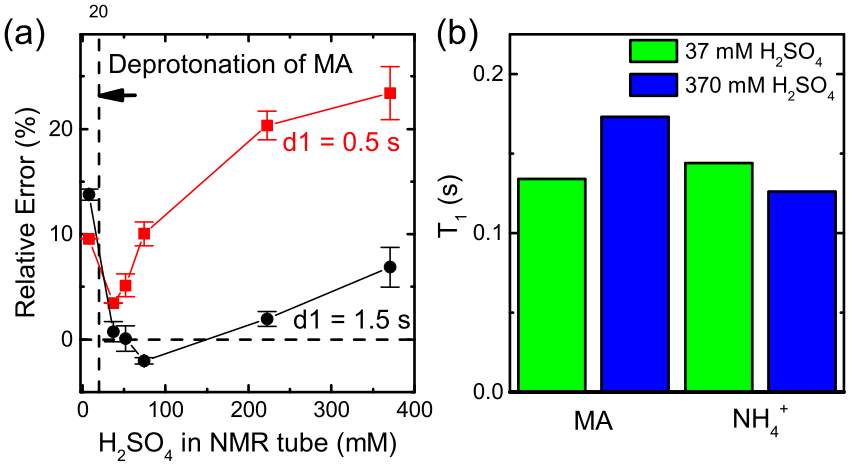

Figure 2.3: Influence of H_2SO_4 concentration in the NMR tube on accuracy of NH_4^+ quantification with a d1 of 0.5 s (**red**) and a d1 of 1.5 s (**black**). Error bars around each point represent the standard deviation for each triplicate measurement. **(a)** T_1 of NH_4^+ and maleic acid at two different H_2SO_4 concentrations. **(b)** Acquisition parameters: at=0.75 s, nt=512, Pulse sequence: Excitation Sculpting, field strength: 400 MHz.

To investigate if the accuracy of our ^{1}H NMR method depends on the pH, we acidified a sample of 388 µM NH_3 with different concentrations of H_2SO_4 (Figure 2.3a). Based on the previous finding that the T_1 of NH_4^+ and MA are very close to each other we chose a recycle delay of 0.5 s ($3T_1$) for this experiment. For acid concen-

trations above 37 mM H_2SO_4 the relative error continuously increases the more acid is added. To investigate if the growing relative error might be caused by changing T_1 values we measured the T_1 of NH_4^+ and MA at 370 mM H_2SO_4 (Figure 2.3b). The gap between the T_1 of NH_4^+ and MA is slightly larger at 370 mM H_2SO_4 than at 37 mM H_2SO_4 which might explain the larger error. After increasing the recycle delay from 0.5 s to 1.5 s to compensate for the increased T_1 gap the relative error decreases to <2% between 37 and 222 mM H_2SO_4. This suggests that the detection method is accurate over a wide pH-range if a higher d1 is chosen to compensate for T_1 changes.

In Figure 2.3, even with a high recycle delay of 1.5 s an unusually high error remains at the highest and lowest acid concentration. The error at the lowest acid concentrations is in agreement with the results by Hodgetts *et al.* and is caused by deprotonation of MA below 20 mM H_2SO_4.[17] Spectra acquired at the highest acid concentration had phasing issues which had to be corrected by post-processing the spectrum using the autophasing algorithm in the software package MestReNova. We suspect that the phasing issues are caused by tuning and matching which becomes more difficult at high salt concentrations.[15] To achieve maximum accuracy, the acid concentration should not exceed 222 mM.

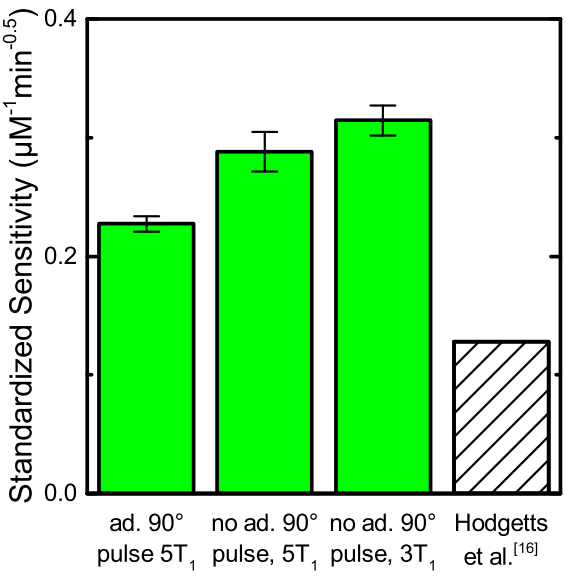

Figure 2.4: Effect on sensitivity of removing the additional 90° pulse from Excitation Sculpting pulse sequence and reducing the interscan delay from 0.72 s ($5T_1$) to 0.43 s ($3T_1$) (**green**). Comparison with literature sensitivity in water. A "standardized sensitivity" was calculated to compare sensitivities measured on different spectrometers (see main text). Error bars around each point represent the standard deviation for each triplicate measurement. NH_4^+: 40 µM, Gd^{3+}: 1 mM, field strength: 400 MHz.

As discussed previously, with the default settings of the ES pulse sequence, the acquisition time does not contribute to the percentage relaxation so that sensitivity is lost. To determine the maximum sensitivity for NH_4^+ detection with 1 mM Gd^{3+} we deactivated the additional 90° pulse at the beginning of the pulse sequence so that both, acquisition time and recycle delay contribute to the percentage relaxation. This leads to a significant increase of the sensitivity (see Figure 2.4). The sensitivity can be further increased by reducing the interscan delay from $5T_1$ to $3T_1$ which is feasible in this case because the T_1 of NH_4^+ and MA are very close to each other. The SNR of a 40 µM NH_4^+ sample measured for 14.6 min (interscan delay $3T_1$) is 47.4. This corresponds to a 1.4-fold sensitivity increase compared with the the activated 90° pulse. The relative error is similar with an interscan delay of $5T_1$ and $3T_1$ (<6%) indicating that the interscan delay can be reduced without sacrificing accuracy. As discussed above, at high acid concentrations a higher recycle than $3T_1$ might be necessary to compensate for T_1 changes.

We remeasured the sensitivity gain after addition of 1 mM Gd^{3+} to obtain a direct measurement of the sensitivity gain without the interference of the additional 90° pulse. A 3.9-fold and 3.6-fold sensitivity increase is measured with 1 mM Gd^{3+} for an interscan delay of $5T_1$ and $3T_1$, respectively. These values are consistent with the predicted sensitivity gain from the T_1 decrease (3.9). Taking into account the corrected sensitivity gain that we calculated from Figure 2.1a (3.1) we estimate that the sensitivity can be increased by a factor of 3.5 ± 0.4 with 1 mM Gd^{3+} which corresponds to an order of magnitude less analysis time or several hours less ammonia accumulation to reach the detection limit. This sensitivity improvement makes fast ^{1}H NMR NH_4^+ quantification accessible with a standard NMR spectrometer and reduces the cost of essential control experiments with expensive (≈ 500 euros/L) $^{15}N_2$.

It is difficult to compare the sensitivity of two different NMR detection methods if these methods were applied using different spectrometers. The sensitivity can vary an order of magnitude because of different field strength, probe hardware, NMR tubes, postprocessing methods etc.[19] We attempt to compare our sensitivity with the sensitivity measured by Hodgetts *et al.* by calculating a standardized sensitivity that takes into account the influence of field strength and type of probe (cryo- or room temperature probe) on sensitivity (Figure 2.4). The calculation of the standardized sensitivity can be found in Section 2.5. As expected, with 1 mM Gd^{3+} the standardized sensitivity is significantly higher than the value reported by Hodgetts *et al.* without Gd^{3+}.

2.3. Conclusion

In summary, the ^{1}H NMR analysis time required to quantify NH_4^+ in aqueous samples can be reduced by an order of magnitude by adding 1mM paramagnetic Gd^{3+}. This improvement makes ^{1}H NMR NH_4^+ quantification more accessible and reduces the cost of control experiments with $^{15}N_2$ which enables faster and more reliable N_2

reduction research. A large reduction of the T_1 of NH_4^+ and MA without significant line broadening causes the sensitivity increase. The method has very good linearity ($R^2 = 0.999$) and is accurate over a wide pH-range if the interscan delay is increased to compensate for small T_1 changes.

2.4. Materials and Methods

Materials

$^{14}NH_4Cl$ (99.995%), $^{15}NH_4Cl$ (≥ 98 atom %, ^{15}N ≥ 99 % CP), maleic acid (≥ 99%) and H_2SO_4 (≥ 97.5%) were obtained from Sigma Aldrich. Gadolinium(III) nitrate hexahydrate (99.9%) was obtained from Fisher Scientific. DMSO-d_6 (99.9% D, 0.03 % V/V Tetramethylsilan) was obtained from Cambridge Isotope Laboratories. Ultrapure water was produced with a Milli-Q Advantage A10 water purification system (resistivity: 18.2 MΩ at 25°C).

Sample preparation

Ammonia standard solutions (40–500 µM) were prepared fresh daily by adding a suitable amount of NH_4Cl to ultrapure water and performing serial dilutions to the required standard concentrations. In a typical experiment, 525 µL NH_4^+ standard solution was mixed with 50 µL 0.5 M H_2SO_4, 50 µL DMSO-d_6, 25 µL 12.5 mM maleic acid and 25 µL 27 mM Gd^{3+} solution inside an eppi. 600uL of this solution was transfered into a 5 mm thin wall NMR tube (Wilmad). All NH_4^+ concentrations are reported as concentration in the NMR tube unless otherwise noted. NMR tubes were closed with Norell Sample Vault NMR tube caps (Sigma Aldrich). NMR tubes were cleaned with ultrapure water and ethanol using an NMR tube cleaner. After cleaning, the NMR tubes were dried at 60°C for 1 h and stored in a dust-free environment.

^{1}H NMR data acquisition and processing

^{1}H NMR spectra were acquired on a 400 MHz pulsed Fourier transform NMR spectrometer equipped with an autosampler. An autotunable, temperature regulated Agilent OneNMR room temperature probe was used for all measurements. The temperature was set to 25°C and the receiver gain was optimised automatically. In order to avoid baseline distortions and low receiver gain, the water resonance has to be suppressed by a suitable pulse sequence. Good water suppression was obtained with pulse sequences that use pulsed field gradients to dephase the water magnetization and selective pulses to flip the NH_4^+ magnetization back into phase during acquisition. Two pulse sequences that were preinstalled in the software of our NMR system (vNMRj) were used in this work: Excitation Sculpting (vNMRj: ”waterES”) and double pulsed field gradient spin echo (vNMRj: ”selexcit”). The waterES pulse sequences has the following structure:

waterES: G1-P90-G1-d1-P90-G2-S180-P180-G2-G3-S180-P180-G3-aq

where, G1-G3 are z-gradients of different strengths, P90, P180 are hard pulses and S180 is a selective 180° pulse. During the acquisition time only the water res-

onance is out of phase whereas the rest of the spectrum is in phase leading to the desired suppression of the water resonance. The block "G1-P90-G1" dephases residual magnetization prior to the next scan and can be deactivated to increase sensitivity as described in the main text. The z-gradient G1 had a duration of 1.6 ms and a strength of 1.07 G cm^{-1}. The z-gradients G2 and G3 had a duration of 1 ms and a strength of 1.7 G cm^{-1}. The 180° selective pulses had the shape "Wsupp" with a width of 2.5 ms and a power of 13 dB. The selexcit pulse sequence has the following structure:

selexcit: P90-G1-S180-G1-G2-S180-G2-aq

where, G1 and G2 are z-gradients of different strengths, P90, P180 are hard pulses and S180 is a selective 180° pulse. During the acquisition time only the region defined by the selective 180° pulse is in phase whereas the rest of the spectrum is out of phase. The z-gradients G1 and G2 had a strength of 0.85 G cm^{-1} and 1.28 G cm^{-1}, respectively and a duration of 1 ms. The selective 180° pulse was defined as a "q3" pulse shape with a width of 5 ms and a power of 0 dB. The position and width of the selective pulse in frequency domain was set to 6.63 ppm and 540 Hz, respectively so that the pulse is positioned between the resonances of NH_4^+ and maleic acid. The pulse shapes "q3" and "Wsupp" that were used to create the shaped pulses in waterES and selexcit are standard pulse shapes available in the software package vNMRj. Equivalent pulse shapes should be available in other software packages.

The data was processed in the software package MestReNova (version: 12.0.1-20560) using the automated tools provided in this software. Unless otherwise noted an apodization of 4 Hz was applied followed by phasing and baseline correction. The peaks of NH_4^+ (t, ≈ 6.9 ppm, 4H) and MA (s, ≈ 6.21 ppm, 2H) were integrated using the linefitting tool. Using the line fitting tool instead of directly integrating the peaks leads to an approximately 2-fold decrease of the relative error. The three integrals of the NH_4^+ peaks were added together to calculate the total NH_4^+ integral. From the ratio of the integral of NH_4^+ and MA the concentration of NH_4^+ was calculated with absolute quantification according to Equation 2.2. The linewidth of NH_4^+ is calculated by averaging the full width half maximum (FWHM) of the three NH_4^+ peaks. The signal-to-noise ratio (SNR) was calculated using the "SNR Calculation" tool in MestReNova with the noise region defined from 11 to 13 ppm. The SNR values were calculated by averaging 3 measurements of the average SNR of the three peaks of the NH_4^+ triplet. The relative error was calculated according to:

$$relative\ error = \frac{c_{calc} - c_{grav}}{c_{grav}} 100 \tag{2.5}$$

where, c_{calc} and c_{grav} are the concentration of NH_4^+ calculated from absolute quantification and from the weight and purity of the NH_4Cl that was added to prepare the standards, respectively.

The T_1 of NH_4^+ and MA was measured using the ES pulse sequence with default setting. Spectra were acquired at 6 different recycle delays and the function $y(x) = a * (1 - exp(-bx))$ was fitted to the integrated peak intensities of NH_4^+ and MA as a function of d1 using the software OriginPro 2015. Subsequently, the parameter b from the fitting function was inversed to calculate T_1. An example of the T_1 determination using this method can be found in Section 2.5.

2.5. Supporting Information

Calculation: Ammonia accumulation time

In experiments to test materials as electrocatalysts for N_2 reduction, ammonia is accumulated in the electrolyte until the concentration reaches the detection limit. Spectrophotometric methods for ammonia detection are very sensitive but require considerable bench time. ^{1}H NMR detection reduces the bench time but on a standard laboratory NMR (400 MHz) the SNR of a 40 µM NH_4^+ sample is only 13.6 after 13.6 min analysis time. For accurate quantication an SNR of 20 is necessary which increases the required concentration to 58 µM NH_4^+. Taking into account a dilution from the electrolyte to the NMR tube of 1:1.28 this results in a required concentration in the electrolyte of ≈ 75 µM. The amount of ammonia in the electrolyte after electrolysis can be calculated according to:

$$c_{NH_3} = \frac{\dot{n}_{NH_3} t}{V} \tag{2.6}$$

where, $\dot{n}_{NH_4^+}$ is the amount of moles NH_3 produced per second, t is the duration of the experiment and V is the volume of the electrolyte. Reported catalytic activities for N_2 reduction vary from 1 pmol/s to 1 nmol/s NH_3 assuming an electrode area of 1 cm^2.[28] From Equation 2.8, it follows that with an intermediate catalyst (0.05 nmol/s NH_3) and a typical electrolyte volume (10 mL) the required experiment duration to reach 75 µM NH_3 in the electrolyte is ≈ 4 hours. Such long experiments create a bottleneck in the catalyst screening workflow and create a risk of false positives due to contamination as well as a risk of false negatives due to catalyst deactivation. Since many groups only have access to standard NMR spectrometers higher sensitivity is needed.

Calculation: Standardized Sensitivity

It is difficult to compare the sensitivity of ^{1}H NMR spectra which were acquired on different spectrometers. Many parameters affect the sensitivity such as field strength, percentage relaxation, type of probe, water suppression and post processing method. We will attempt to compare our measured sensitivity with the sensitivity measured by Hodgetts *et al.* by calculating a standardized sensitivity that takes into account the influence of the field strength B of the NMR and the type of probe on the sensitivity:[17]

$$Standardized\ Sensitivity = \frac{1}{c_{NH_4^+}} \frac{SNR}{\sqrt{t}} \left(\frac{400}{B}\right)^{\frac{3}{2}} \frac{1}{k_P} \tag{2.7}$$

, where SNR is the signal-to-noise measured at the NH_4^+ concentration $c_{NH_4^+}$ in the NMR tube, t is the total analysis time and B is the field strength of the spectrometer in MHz. The second last term takes into account the influence of the field strength on the sensitivity which is:[15]

$$Sensitivity \propto B^{\frac{3}{2}} \tag{2.8}$$

The last term takes into account the influence of the type of probe. An up to 4-fold higher sensitivity can be measured on an NMR equipped with a cryoprobe compared with a standard room temperature probe.[15] To account for this difference, a probe factor k_P was introduced. The probe factor is 3.5 and 1 for sensitivities that were measured on an NMR equipped with a cryoprobe and a room temperature probe, respectively.

T_1 determination with ES

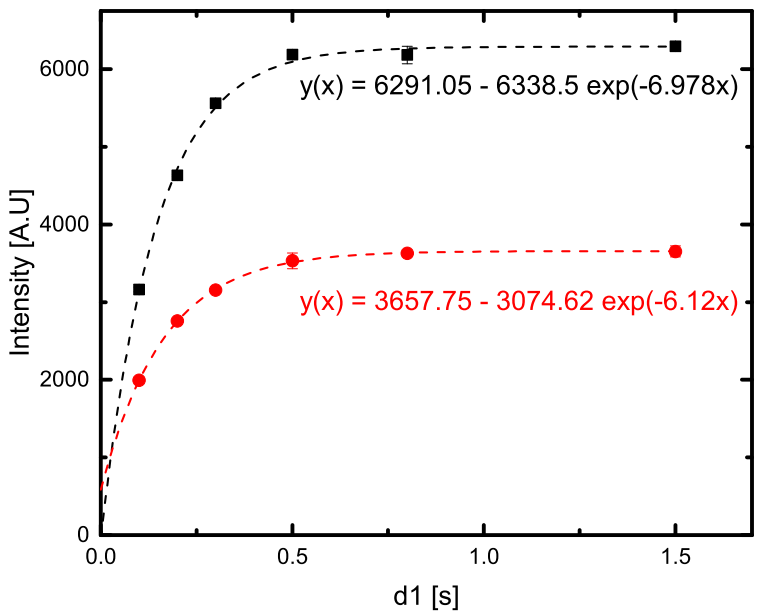

Figure 2.5: T_1 measurement of NH_4^+ **(black)** and MA **(red)** at 1 mM Gd^{3+}. Error bars around each point represent the standard deviation for each duplicate measurement. Parameters: , $c_{NH_4^+}$ = 388 µM, at=0.75 s, nt=512, pulse sequence: ES.

Quantification of $^{15}NH_4^+$ with 1 mM Gd^{3+}

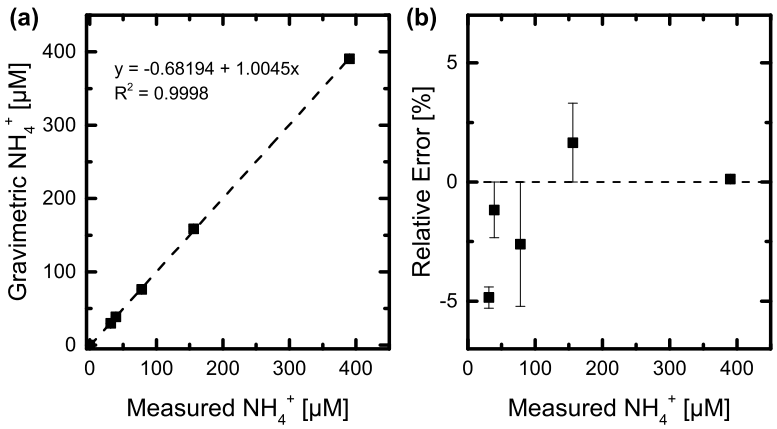

Figure 2.6: **(a)** Linearity and **(b)** accuracy of $^{15}NH_4^+$ quantification with 1 mM Gd^{3+}. Error bars around each point represent the standard deviation for each triplicate measurement. Pulse sequence: ES, recycle delay: 0.5 s, acquisition time: 0.75 s total analysis time: 10.7 min.

Sensitivity comparison with literature

Table 2.1: ^1H NMR sensitivity for $^{14}NH_4^+$ in literature.

Final NH_4^+ [µM]	solvent	pulse sequence	t [min]	gain	probe	B [MHz]	Lb [Hz]	SNR	Ref.
39.36	H_2O	waterES	14.7	46	RT	400	4	47.4	This work
11.9	H_2O	lc1pncwps	22	n.a.	Cryo	600	3	46	[17]
10	EtOH	PGSE	25	40	RT	600	1	19	[12]

References

[1] M. Kolen, W. A. Smith, and F. M. Mulder, *Accelerating ^{1} H NMR Detection of Aqueous Ammonia,* ACS Omega **6**, 5698 (2021).

[2] R. Lan, J. T. Irvine, and S. Tao, *Ammonia and related chemicals as potential indirect hydrogen storage materials,* International Journal of Hydrogen Energy **37**, 1482 (2012).

[3] A. Klerke, C. H. Christensen, J. K. Nørskov, and T. Vegge, *Ammonia for hydrogen storage: challenges and opportunities,* Journal of Materials Chemistry **18**, 2304 (2008).

[4] F. M. Mulder, *Implications of diurnal and seasonal variations in renewable energy generation for large scale energy storage,* Journal of Renewable and Sustainable Energy **6**, 033105 (2014).

[5] D. R. MacFarlane, P. V. Cherepanov, J. Choi, B. H. Suryanto, R. Y. Hodgetts, J. M. Bakker, F. M. Ferrero Vallana, and A. N. Simonov, *A Roadmap to the Ammonia Economy,* Joule **4**, 1186 (2020).

[6] S. Z. Andersen, V. Čolić, S. Yang, J. A. Schwalbe, A. C. Nielander, J. M. McEnaney, K. Enemark-Rasmussen, J. G. Baker, A. R. Singh, B. A. Rohr, M. J. Statt, S. J. Blair, S. Mezzavilla, J. Kibsgaard, P. C. K. Vesborg, M. Cargnello, S. F. Bent, T. F. Jaramillo, I. E. L. Stephens, J. K. Nørskov, and I. Chorkendorff, *A rigorous electrochemical ammonia synthesis protocol with quantitative isotope measurements,* Nature **570**, 504 (2019).

[7] W. Yu, P. Buabthong, C. G. Read, N. F. Dalleska, N. S. Lewis, H.-J. Lewerenz, H. B. Gray, and K. Brinkert, *Cathodic NH nh_4^+ leaching of nitrogen impurities in CoMo thin-film electrodes in aqueous acidic solutions,* Sustainable Energy & Fuels **4**, 5080 (2020).

[8] J. Choi, H.-L. Du, C. K. Nguyen, B. H. R. Suryanto, A. N. Simonov, and D. R. MacFarlane, *Electroreduction of Nitrates, Nitrites, and Gaseous Nitrogen Oxides: A Potential Source of Ammonia in Dinitrogen Reduction Studies,* ACS Energy Letters **5**, 2095 (2020).

[9] D. L. Boucher, J. A. Davies, J. G. Edwards, and A. Mennad, *An investigation of the putative photosynthesis of ammonia on iron-doped titania and other metal oxides,* Journal of Photochemistry and Photobiology A: Chemistry **88**, 53 (1995).

[10] M. D. Krom, *Spectrophotometric determination of ammonia: a study of a modified Berthelot reaction using salicylate and dichloroisocyanurate,* The Analyst **105**, 305 (1980).

[11] EPA, *Method 350.1: Nitrogen, ammonia (colorimetric, automated phenate), revision 2.0,* (1993).

[12] A. C. Nielander, J. M. McEnaney, J. A. Schwalbe, J. G. Baker, S. J. Blair, L. Wang, J. G. Pelton, S. Z. Andersen, K. Enemark-Rasmussen, V. Čolić, S. Yang, S. F. Bent, M. Cargnello, J. Kibsgaard, P. C. K. Vesborg, I. Chorkendorff, and T. F. Jaramillo, *A Versatile Method for Ammonia Detection in a Range of Relevant Electrolytes via Direct Nuclear Magnetic Resonance Techniques,* ACS Catalysis **9**, 5797 (2019).

[13] Y.-X. Lin, S.-N. Zhang, Z.-H. Xue, J.-J. Zhang, H. Su, T.-J. Zhao, G.-Y. Zhai, X.-H. Li, M. Antonietti, and J.-S. Chen, *Boosting selective nitrogen reduction to ammonia on electron-deficient copper nanoparticles,* Nature Communications **10** (2019), 10.1038/s41467-019-12312-4.

[14] W. Yu, N. S. Lewis, H. B. Gray, and N. F. Dalleska, *Isotopically Selective Quantification by UPLC-MS of Aqueous Ammonia at Submicromolar Concentrations Using Dansyl Chloride Derivatization,* ACS Energy Letters **5**, 1532 (2020).

[15] S. K. Bharti and R. Roy, *Quantitative 1H NMR spectroscopy,* TrAC Trends in Analytical Chemistry **35**, 5 (2012).

[16] G. Wider and L. Dreier, *Measuring Protein Concentrations by NMR Spectroscopy,* Journal of the American Chemical Society **128**, 2571 (2006).

[17] R. Y. Hodgetts, A. S. Kiryutin, P. Nichols, H.-L. Du, J. M. Bakker, D. R. Macfarlane, and A. N. Simonov, *Refining Universal Procedures for Ammonium Quantification via Rapid* ^{1} *h NMR Analysis for Dinitrogen Reduction Studies,* ACS Energy Letters **5**, 736 (2020).

[18] T. Vosegaard and N. C. Nielsen, *Defining the sampling space in multidimensional NMR experiments: What should the maximum sampling time be?* Journal of Magnetic Resonance **199**, 146 (2009).

[19] J.-H. Ardenkjaer-Larsen, G. S. Boebinger, A. Comment, S. Duckett, A. S. Edison, F. Engelke, C. Griesinger, R. G. Griffin, C. Hilty, H. Maeda, G. Parigi, T. Prisner, E. Ravera, J. van Bentum, S. Vega, A. Webb, C. Luchinat, H. Schwalbe, and L. Frydman, *Facing and Overcoming Sensitivity Challenges in Biomolecular NMR Spectroscopy,* Angewandte Chemie International Edition **54**, 9162 (2015).

[20] T. D. Claridge, *Introduction,* in *High-Resolution NMR Techniques in Organic Chemistry* (Elsevier, Oxford, United Kingdom, 2016) 3rd ed., pp. 469–475.

[21] P. Schanda, . Kupče, and B. Brutscher, *SOFAST-HMQC Experiments for Recording Two-dimensional Deteronuclear Correlation Spectra of Proteins within a Few Seconds,* Journal of Biomolecular NMR **33**, 199 (2005).

[22] H. Gunther, *NMR Spectroscopy*, 3rd ed. (WILEY-VCH, Weinheim, Germany, 2013) pp. 239–247.

[23] F.-X. Theillet, A. Binolfi, S. Liokatis, S. Verzini, and P. Selenko, *Paramagnetic relaxation enhancement to improve sensitivity of fast NMR methods: application to intrinsically disordered proteins,* Journal of Biomolecular NMR **51**, 487 (2011).

[24] S. Cai, C. Seu, Z. Kovacs, A. D. Sherry, and Y. Chen, *Sensitivity Enhancement of Multidimensional NMR Experiments by Paramagnetic Relaxation Effects,* Journal of the American Chemical Society **128**, 13474 (2006).

[25] P. Caravan, J. J. Ellison, T. J. McMurry, and R. B. Lauffer, *Gadolinium(III) Chelates as MRI Contrast Agents: Structure, Dynamics, and Applications,* Chemical Reviews **99**, 2293 (1999).

[26] J. Newman and K. E. Thomas-Alyea, *Electrochemical Systems*, 3rd ed. (WILEY-INTERSCIENCE, Hoboken, N.J, 2004) pp. 10–13.

[27] T. Burdyny and W. A. Smith, *CO_2 reduction on gas-diffusion electrodes and why catalytic performance must be assessed at commercially-relevant conditions,* Energy & Environmental Science **12**, 1442 (2019).

[28] X. Zhu, S. Mou, Q. Peng, Q. Liu, Y. Luo, G. Chen, S. Gao, and X. Sun, *Aqueous electrocatalytic N_2 reduction for ambient NH_3 synthesis: recent advances in catalyst development and performance improvement,* Journal of Materials Chemistry A **8**, 1545 (2020).

3

Overcoming nitrogen reduction to ammonia detection challenges: The case for leapfrogging to gas diffusion electrode platforms

The nitrogen reduction reaction (NRR) is a promising pathway towards the decarbonization of ammonia (NH_3) production. However, unless practical challenges related to the detection of NH_3 are removed, confidence in published data and experimental throughput will remain low for experiments in aqueous electrolyte. In this perspective, we analyze these challenges from a system and instrumentation perspective. Through our analysis we show that detection challenges can be strongly reduced by switching from H-cell to gas diffusion electrode (GDE) cell design as a catalyst testing platform. Specifically, a GDE cell design is anticipated to allow for a reduction in the cost of crucial $^{15}N_2$ control experiments from €100–2000 to less than €10. A major driver is the possibility to reduce the $^{15}N_2$ flow rate to less than 1 mL/min which is prohibited by an inevitable drop in mass-transport at low flow rates in H-cells. Higher active surface areas and improved mass transport can further circumvent losses of NRR selectivity to competing reactions. Additionally, obstacles often encountered when trying to transfer activity and selectivity data recorded at low current density in H-cells to commercial device level can be avoided by testing catalysts under conditions close those in commercial devices from the start.

Parts of this chapter have been published in ACS Catalysis **12,10**, 5726–5735 (2022) [1].

3.1. Introduction

Novel electrochemical reactions provide hope for a scalable means of storing intermittent electricity within chemical bonds, simultaneously aiding in the buffering of renewable energy while providing a route for offsetting carbon-based fuels. Nitrogen reduction electrochemistry in particularly has the potential to directly offset 1–1.4% of global CO_2 emissions currently emitted during ammonia (NH_3) production, with additional potential for using ammonia as an energy carrier in further applications (e.g. shipping, aviation).[2–4] Such promise has led to a large number of researchers entering the nitrogen electrochemistry field in recent years, with substantial effort placed on developing selective catalysts capable of driving nitrogen reduction to ammonia over the more favourable hydrogen evolution reaction (HER).[5] If parallel electrochemical reactions with low solubility gaseous reagents are taken as precedent (e.g. electrochemical reduction of CO_2 and O_2), once high selectivity catalysts have been identified there are established approaches for increasing reaction rates, reducing overpotential, increasing stability and eventually incorporating promising catalysts supported on a high surface area support such as a gas-diffusion electrode (GDE) in commercial devices.[6, 7] However, currently the academic field appears to be at a standstill because, due to the inefficiency of the reaction in aqueous electrolyte, no selective N_2 reduction catalyst has been conclusively presented, yet.[8, 9]

The difficulty of achieving dominant faradaic efficiencies (FE) for the nitrogen reduction reaction (NRR) is commonly attributed to the slow kinetics of breaking the nitrogen triple bond in a 6-electron transfer process compared to only 2-electron transfers for HER. Any catalyst then needs to balance the simultaneous challenge of improving the kinetics for N_2 reduction while suppressing HER.[5] A large body of knowledge is available on altering the selectivity of electrocatalytic reactions including strategies like alloying, doping or introducing defects.[10] For example, the selectivity of the CO_2 reduction reaction (CO2RR) can be tuned towards ethanol (from 30 to 41% FE) or ethylene (from 66 to 80% FE) by alloying Cu with Ag or Al, respectively.[11, 12] Extensive exploration of such strategies might yield a selective catalyst for NRR, too.

Despite the wealth of electrochemical expertise entering this novel research field, substantial detection challenges have persisted. Typical experiments in aqueous electrolyte produce µM levels of NH_3 and NH_4^+ which are on par with common NH_3 contamination levels.[8, 9, 13] Adventitious NH_3/NOx often found in membranes, catalyst precursors, electrolytes and N_2 feedstocks commonly occurs at concentrations between 2–20 µM in the electrolyte (see Table 3.2).[14–18] To highlight this issue, we calculate the accumulated ammonia in the electrolyte for an NRR partial current of 100 µA which is among the highest reported rates in literature. Even at this high rate the accumulated ammonia in the electrolyte after 30 min of electrolysis without catalyst deactivation (electrolyte volume: 30 mL) is only 20.7 µM which is too close to common contamination levels for unambiguous quantification.

These measurement challenges have led to false positive measurements of NRR activity and in some cases to retractions and refutations of publications that were initially believed to be groundbreaking.[8, 9, 14–20] To overcome the measurement challenges associated with NRR, extensive experimental protocols were introduced which—if executed correctly—are able to avoid false positives. According to those protocols, it is particularly important to show that NH_3 yield from experiments with $^{14}N_2$ quantitatively agrees with $^{15}N_2$ experiments and that the $^{15}N_2$ used in those experiments is free of $^{14/15}NH_3$ and $^{14/15}NOx$ contamination.[8, 13, 21] Critical reviews agree that very few published reports meet these criteria.[8, 9, 13] As such only a small reliable data set is available for potentially-invaluable computational studies.[12] In short, if the challenges of detecting electrochemically produced NH_3 were removed, there would be an undeniably propulsion forward of the research field due to increased reproducibility and a larger reliable data set.

When analyzing the typical electrochemical NH_3 synthesis system, however, it becomes clear that researchers face the dilemma of choosing either reliable data or affordable, fast experiments. As we will discuss in more detail below, carrying out reliable protocols is time-consuming and expensive due to the long electrolysis steps involved and the use of expensive $^{15}N_2$. We found, that this dilemma is linked to the H-cell-type cell design used in most studies. On the other hand, if the same experiments were performed in a gas diffusion electrode cell, then testing restrictions due to detection challenges have the potential to be overcome. We will show that the compact design of gas diffusion electrode cells and their high N_2 mass transport, which is decoupled from the gaseous flow rate, makes them advantageous to use for NRR studies.

In this perspective we provide a technological motivation for leapfrogging catalyst development within H-cells, and promoting gas-diffusion electrodes as a substrate for the development of NRR catalysts. We first analyze what limits the progress of the field with H-cells. Then the benefits for NH_3/NH_4^+ detection of supplying N_2 from a near N_2 gas-phase are discussed from a system and instrumentation perspective and contrasted to the current approach of supplying N_2 from the bulk electrolyte. We then argue what other implications the use of higher surface area electrodes and a reduced liquid diffusion pathway have for NRR catalyst screenings. Lastly, we examine the potential and limitations of gas diffusion electrodes as a platform to benchmark NRR catalysts.

3.2. Limits of product detection by configuration and operating conditions

The most commonly used electrochemical cells for NRR are H-cells which are comprised of a working, reference and counter electrode submerged in two electrolyte-filled compartments separated by a membrane (see Figure 3.1a). The N_2 is supplied by bubbling into the electrolyte while stirring. NH_3 production is typically quantified from liquid samples of the electrolyte.

Using H-cells for NRR studies leads to several limitations which are illustrated in Figure 3.1b–d. Electrodes in H-cells have low electrochemical surface area (ECSA) for NRR (Figure 3.1b) which makes them prone to deactivation for example due to deposition of impurities from the electrolyte on the electrode surface.[22, 23] In addition, the only marginally water-soluble nitrogen gas has to be supplied from the bulk electrolyte which leads to a relatively large boundary layer thickness and therefore low mass transport.[24] These two limitations will be discussed in greater detail later in this perspective.

In Figure 3.1c we compare the NH_3 production from NRR with commonly observed NH_3/NOx contamination levels. To quantify NH_3/NOx contamination levels we summarized the available literature on the magnitude of different contamination sources in Table 3.2. Most contamination sources are in the range of 2–20 µM but up to 150 µM of NH_3 is possible. Reports of NH_3 contamination with very sensitive and selective detection methods have shown that an NH_3 background of 0.5–2 µM cannot be removed, even with extensive cleaning.[8, 17, 25] Therefore, we propose that the risk of NH_3 contamination is highest if the NH_3 production from NRR does not exceed 2 µM and gradually decreases with increasing NH_3 production. This is illustrated using a colour gradient in Figure 3.1c. NH_3 production from NRR should at least exceed 20 µM to avoid the region with the most contamination sources (2–20 µM). The reported NH_3 production rates in literature vary from 3–300 µA cm^{-2} NRR partial current density.[26] In the comparison in Figure 3.1c, we chose a production rate of 30 µA NRR partial current density which we refer to as an intermediate NH_3 production rate throughout this perspective (unless otherwise noted we will assume an electrode area of 1 cm^2 in all calculations). With this intermediate production rate and the median electrolyte volume of 30 mL used in H-cell studies (see Table 3.3), the electrolysis time required to reach 20 µM NH_3 is 1.6h (see Figure 3.1c). Therefore, to reach an NH_3 concentration that is large enough to at least exceed the most common NH_3 contaminations, NH_3 from electrolysis must be accumulated for almost 2h. Our calculation agrees well with the electrolysis time that is used in practice in NRR studies (median from Table 3.3: 2h). While such long experiments are necessary for durability tests once an active catalyst has been identified, initial experiments to measure the NRR activity of promising materials should be much shorter to enable fast advancement in NRR research. In addition, shorter experiments reduce the risk of contamination entering the cell, for instance from a not properly purified N_2 feed gas.

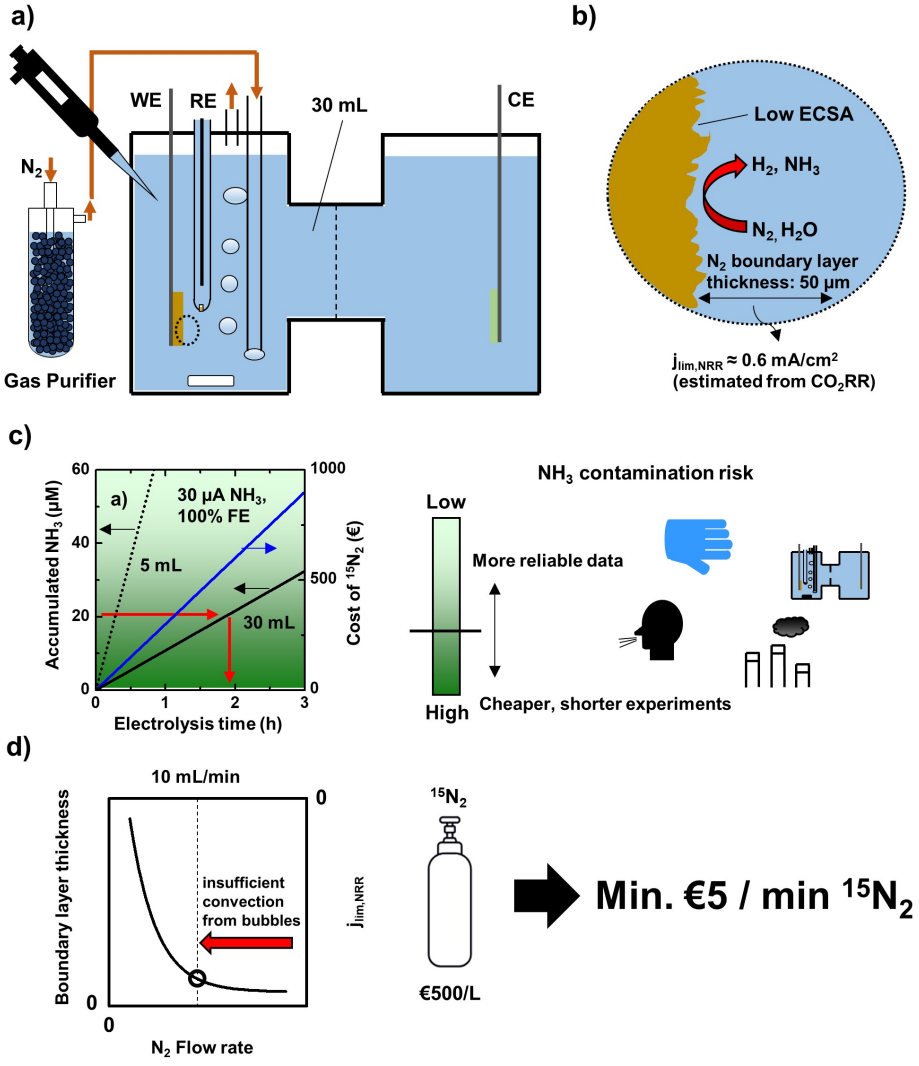

Figure 3.1: Limitations of H-cell cell design for NRR studies. a) Schematic of an H-cell and gas purification. b) Schematic of the electrode surface with 50 µm boundary layer and resulting mass-transport limiting current for NRR jlim,NRR. c) Dependence of the accumulated NH_3 and the cost of an isotope labelling experiment on the electrolysis time and the electrolyte volume. Ammonia production from NRR: 30 µA, flow rate during $^{15}N_2$ experiments: 10 mL/min. The green colour gradient represents the risk of NH_3 contamination (summarized from Table 3.2). d) Dependence of N_2 mass transport to the cathode on the N_2 flow rate and resulting minimal cost of isotope labelling. Adapted with permission from Clark et al.[27] Copyright 2018 American Chemical Society.

While most NH_3 contaminations in Table 3.2 are below 20 µM, this threshold is somewhat arbitrary and accurate quantification is also possible below 20 µM, which comes at the cost of a higher risk of false positives that must be reduced with more frequent control experiments and more extensive cleaning steps the lower the NH_3 concentration gets. Due to the unavoidable NH_3 background of 0.5–2 µM in the electrolyte, reports of catalysts that do not exceed this threshold are highly questionable.[8, 16, 17] Besides NH_3 contamination, another factor that can limit the experimental throughput is the detection limit of some NH_3 analytical methods.

The detection limit of the most commonly used NH_3 detection method in literature—the indophenol method—is sufficiently low but the method requires time consuming sample preparation with unstable reagents, which leads to long bench time. Therefore, the indophenol method is undesirable for NRR research from a practical perspective.[25, 28, 29] It is widely accepted that control experiments with $^{15}N_2$ which quantitatively agree with $^{14}N_2$ experiments are essential to prove that NH_3 production originated from NRR, and not from contamination of either 14N and/or ^{15}N species.[8, 17, 25] The detection of the isotopologue $^{15}NH_3$ requires an isotopically selective detection method which in most cases is liquid state ^{1}H-NMR that can detect the triplet and doublet ^{1}H spectra of $^{14}NH_3$ and $^{15}NH_3$, respectively. ^{1}H-NMR allows for quick sample preparation but unless expensive spectrometers are available, the sensitivity is limited which leads to either a long electrolysis time to accumulate enough ammonia to reach the detection limit or a long analysis time per sample to acquire and average enough scans to increase the detection limit sufficiently. Adding Gd^{3+} to the NMR solution as a paramagnetic relaxation agent increases the sensitivity but even then, 17 µM NH_3 must be reached for quantitative analysis (400 MHz NMR, no cryoprobe, 15 min analysis time per sample).[30] According to Figure 3.1c reaching 17 µM NH_3 with a catholyte volume of 30 mL takes 1.4h. The long electrolysis time in NRR studies is therefore not only caused by NH_3 contamination but also by the limited sensitivity of ^{1}H-NMR. We note that the extent to which both of these factors limit the electrolysis time depends strongly on a cell parameter—the electrolyte volume.

Several reasons make NH_3 contaminations so difficult to avoid that some authors believe that no catalyst has been unambiguously proven to be active for NRR in aqueous electrolyte.[8, 9] NH_3 contamination can originate from many, often unexpected sources (see Table 3.2). These can easily look like genuine NRR because the NH_3 increase can be time dependent (e.g. NH_3 that slowly leaches from a Nafion membrane) and potential dependent (e.g. NOx that gets reduced electrochemically to NH_3).[9, 31] Some contamination sources can contaminate a whole batch of experiments (e.g. contaminated catalyst precursor) or only a single experiment (e.g. touched electrolyte with a nitrile glove).[8, 17] The identification and elimination of NH_3 contamination sources should precede any NRR measurement. As early as 2018, Greenlee et al. reported that there is a high risk of false positives in NRR experiments and that there is a gap between what experimental protocols should be like for unambiguous measurements and what is done in practice. They

proposed a protocol for unambiguous measurement of NRR activity which is still valid today.[13] In the following years several authors reassessed the reliability of NRR research and found that the gap still exists, although it is slightly smaller since more papers include background measurements and at least qualitative $^{15}N_2$ experiments.[8, 9, 15] Because the paper by Greenlee et al. was published over three years ago, we think that a lack of knowledge about reliable protocols can no longer explain why the gap still exists. Instead, we think there must be practical barriers that prevent the implementation of reliable protocols.

To examine if there are any practical barriers to implementing reliable detection protocols, we examine the most important step of such protocols—the isotope labelling step. All proposed NRR protocols agree that properly executed isotope labelling experiments that quantitatively agree with $^{14}N_2$ data are essential for an unambiguous proof of NRR activity.[8, 13, 15] We calculate that one experiment with $^{15}N_2$ in an H-cell with typical operating conditions (experiment time: 2h, flow rate: 40 mL/min, see Table 3.3) would cost about €2400 due to the high cost of $^{15}N_2$ (≈ €500 per liter). At this cost, isotope labelling experiments are obviously prohibitively expensive. Some authors try to circumvent this problem by using drastically reduced flow rates[32], operating in fed batch mode[33], using a static gas atmosphere[34] or recirculating the gas[35] during $^{15}N_2$ experiments. While reducing or interrupting gas flow reduces cost, Clark et al. showed that a minimum flow rate of 10 mL/min into an 1.6 mL H-cell is necessary to prevent a sharp decrease of the mass transport of the dissolved gas to the electrode surface (quantified by measuring the boundary layer thickness with ferrocyanide reduction).[27] The reason for the reduced mass transport is that the gas that is bubbled into the cell is a source of convection which helps transporting the dissolved gas to the electrode. As the flow rate is reduced, less convection from the gas bubbles leads to lower mass transport of dissolved gas to the electrode surface and an increase in boundary layer thickness as shown in Figure 3.1d.[27] To understand if reduced mass transport can be tolerated for NRR, we estimate the mass transport limiting current of NRR in an H-cell from the limiting current of CO2RR to CO in an H-cell (10 $mA\,cm^{-2}$) by taking into account the different solubility and diffusion coefficient of CO_2 and N_2 and the different number of electrons involved in each reaction (see Equation 3.1).[27, 36–39] The resulting mass transport limiting current for NRR is ≈ 0.6 $mA\,cm^{-2}$ which means that at the upper end of the range of reported NH_3 production rates (3–300 $\mu A\,cm^{-2}$) NRR is most likely already influenced by mass transport limitations.[26] This is undesirable because mass transport limitations will reduce the ammonia production and make results difficult to reproduce, because the transition from activation controlled to mass transfer controlled kinetics is not well-defined in an H-cell.[23] A further reduction of the mass transport limiting current due to a reduction of the gas flow rate below 10 mL/min can therefore not be tolerated. The sharply decreasing mass transport below 10 mL/min explains why reports with reduced flow rate are unable to achieve quantitative agreement between $^{14}N_2$ and $^{15}N_2$ data because mass transport limitations will lower the NH_3 production rate with $^{15}N_2$ if too low flow rates are

used.[32, 33] Another issue that increases the cost of isotope labelling in H-cells is that the electrolyte must be pre-saturated with $^{15}N_2$ prior to electrolysis (typically for 30 min) which adds to the cost.[40] Nielander et al. showed that the cost per experiment can be reduced by recirculating $^{15}N_2$, but the remaining cost is still high (€100 per experiment) because the whole volume of the home-build gas recirculation setup must be flushed with $^{15}N_2$.[8, 35] Thus, the necessity for flow rates >10 mL/min in H-cells is a fundamental barrier to reliable data collection in an H-cell. None of the available solutions reduces the cost sufficiently to make quantitative $^{15}N_2$ control experiments as accessible as they have to be.

The above analysis has shown that while it is possible to reduce the electrolyte volume in H-cells to decrease the electrolysis time, the N_2 flow rate cannot be reduced below 10 mL/min, which creates an unavoidable cost barrier towards implementation of reliable protocols for NRR research. Unless this limitation is removed, the uncertainties about the reliability of results in the NRR field are unlikely to go away, or the field set to become exclusive to those who can afford regular isotope labelling. To avoid this, $^{15}N_2$ experiments have to become affordable (e.g. around €10 per experiment), and short (15–20 min). In the following section, we explore if these requirements can be implemented with a gas diffusion electrode (GDE) cell design.

A typical gas diffusion electrode cell (see Figure 3.2a) consists of three compartments. For the NRR, the main difference to H-cells is that in a GDE cell N_2 is not bubbled directly into the catholyte but flows past a hydrophobic gas diffusion electrode which separates the catholyte and gas compartment. The catalyst is positioned on the GDE at the interface of the catholyte and gas phase (Figure 3.2b). The hydrophobicity of the GDE prevents the electrolyte from entering the gas phase. Due to the small distance that the reactant gas has to travel from the gas phase to reach the catalyst (≈50 nm compared to 50 µm in an H-cell) mass transport is much higher than in H-cells.[24] Therefore, higher mass transport limited current densities for NRR can be reached in GDE cells.[41, 42] Both the anolyte and catholyte are recycled between the cell and a reservoir. During electrolysis insoluble reaction products will enter the gas compartment and leave the cell with the feed gas. Soluble products such as NH_3 will mostly remain in the electrolyte.[24]

To reach the ^{1}H-NMR detection threshold of 17 µM NH_3 in the catholyte within 15 minutes electrolysis time with an intermediate NH_3 production rate, the volume of the catholyte should be less than 5 mL (see Figure 3.1c).[30] The volume of the catholyte is comprised of 4 parts, the internal volumes of: half-cell, reservoir, tubing connections and peristaltic tubing for the pump. For a standard GDE cell these volumes can be as low as 0.8 mL, 0.4 mL, 2 mL, 1.6 mL, respectively assuming a 8 mm thick catholyte compartment, 20 cm 1/8" inner diameter (ID) peristaltic pump tubing and 1 m 1/16" ID tubing connections.[24] To reduce this further, the tubing size can be reduced to smaller, commercially available sizes (1/16" ID peristaltic tubing and 1/32" ID tubing for the remaining connections). This leads to volumes of 0.8 mL, 0.4 mL, 0.5 mL, 0.4 mL, respectively and a total volume of 2.1 mL which

is sufficient to reduce the electrolysis time to less than 15 min.

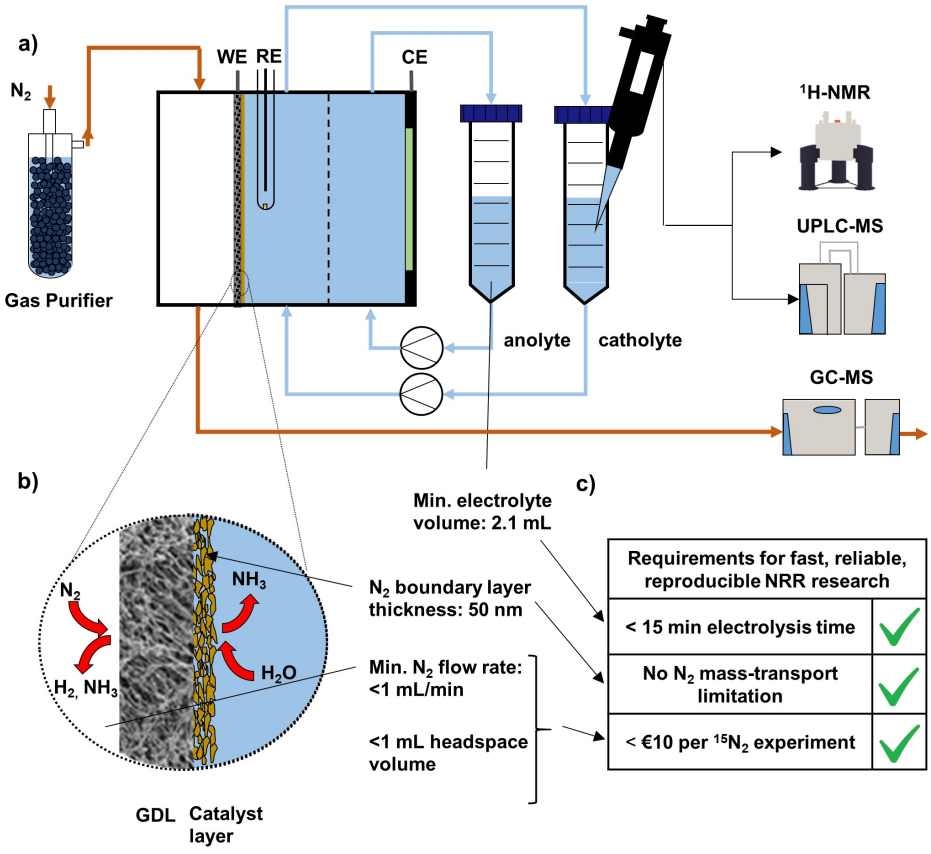

Figure 3.2: Schematic illustrating how cell parameters of the gas diffusion electrode cell design are influencing reliability and speed of NRR research. a) Schematic of a gas diffusion electrode cell and NH_3 detection. b) Schematic of the surface of a gas diffusion electrode. c) Checklist for fast, reliable, reproducible NRR research.

To reduce the cost of isotope labelling to €10 per experiment, the $^{15}N_2$ consumption must be less than 20 mL per experiment. For a 15 min experiment, this means that the flow rate should be less than 1 mL/min (plus 5 mL to flush the system). As discussed above, the flow rate in H-cells must be higher than 10 mL/min for sufficient mass transport of dissolved N_2 from the bulk electrolyte to the catalyst surface.[27] On the other hand, in GDE cells N_2 has to travel first through a gas-filled gas diffusion layer and then through an electrolyte-filled catalyst layer to reach the surface where the reaction takes place (see Figure 3.2b). In this configuration, the flow rate of N_2 can only influence the N_2 mass transport through the gas phase. However,

N_2 diffuses much faster through gas than through liquid. Therefore, the N_2 mass transport through the gas phase is not limiting the N_2 mass transport to the catalyst surface unless very high N_2 consumption rates are reached. To estimate if the N_2 flow rate influences N_2 mass transport at typical N_2 consumption rates in NRR experiments (< 300 $\mu A\,cm^{-2}$ NRR partial current density), we draw on experience from the CO2RR again.[26] Tan et al. showed that a GDE cell for CO_2 reduction (electrode area: 2 cm^2) can be operated at 200 $mA\,cm^{-2}$ at flow rates as low as 5 mL/min without observing differences in potential or H_2 FE compared to higher flow rates.[43] Since NRR current densities are at least three orders of magnitude lower than that, the N_2 mass transport in GDE cells is independent of the N_2 flow rate in the relevant current density range for NRR experiments. Therefore, flow rates <1 mL/min are possible in GDE cells. To stay below 20 mL total $^{15}N_2$ consumption, the total headspace of the system should be minimal (< 1mL) so that 5 mL $^{15}N_2$ are sufficient to flush the system before starting a $^{15}N_2$ experiment. The total headspace is comprised of the volumes of the gas compartment of the cell, the purifier to remove contamination from the feed gas and tubing connections. State of the art flow fields have a flow channel thickness of around 1 mm and 20 cm 1/32" ID tubing should be sufficient for the connections which adds only 100 µL to the headspace, respectively.[44] For proper isotope labelling experiments it is crucial that NOx is effectively removed from the incoming gas stream because especially $^{15}N_2$ is likely to be contaminated with NH_3/NOx (see Table 3.2). NH_3/NOx impurities can be removed with little additional headspace using impurity traps filled with Cu-Zn-Al oxide catalysts as described by Andersen et al. or with a miniaturized version of the oxidising trap proposed by Choi et al. using an alkaline $KMnO_4$ solution (see Figure 3.4).[8, 9] Both purifier types only add a few 100 µL to the headspace so that the total headspace is sufficiently small for €10 isotope labelling experiments. In summary, all requirements for fast, reliable, reproducible NRR research shown in Figure 3.2c can be fulfilled with GDE cells.

We want to briefly highlight the opportunity of combining the low isotope labelling cost in a GDE cell with very sensitive ^{1}H-NMR spectrometers or the recently developed, highly sensitive detection methods for aqueous and gaseous ammonia detection using ultrahigh performance liquid chromatography-mass spectrometry (UPLC-MS) and gas chromatography-mass spectrometry (GC-MS), respectively (see Figure 3.2a).[25, 45, 46] Unlike $^{14}NH_3$, $^{15}NH_3$ is not affected by contaminations, other than the ones coming from the $^{15}N_2$ itself which can be removed with a proper gas purification step. Therefore, $^{15}NH_3$ from NRR can be quantified accurately as soon as the detection limit of the detection method is reached which is 1 ppm for GC-MS and less than 1 µM for very sensitive ^{1}H-NMR spectrometers and UPLC-MS, respectively.[25, 45, 46] By using these very sensitive detection methods, $^{15}N_2$ experiments can become even shorter and cheaper so that catalysts could potentially be tested only with $^{15}N_2$ instead of $^{14}N_2$ requiring only a few mL of $^{15}N_2$ per catalyst and consequentially enabling rapid, unambiguous NH_3 quantification. With GC-MS gaseous $^{14}NH_3$/$^{15}NH_3$ can be detected in operando with no external sample

manipulations and at very low NH_3 production rates (on the order of 10–13 mol/s at 1 mL/min) which makes the detection more reliable and more sensitive than the commonly used NH_3 accumulation in an acid trap.[45]

3.3. Electrochemical benefits of a high surface area NRR catalyst

The choice of cell design has several other implications for NRR research besides the ones discussed in the previous section. An important implication to consider when switching from H-cell to GDE cell is that the electrode changes from a low electrochemical active surface area (ECSA) 2D electrode to a high ECSA 3D electrode. In the following, we want to discuss the implications of this transition for NRR research.

Three dimensional (3D) nanostructured electrodes such as GDE's have a 10 to 1000-fold higher roughness factor (defined as ECSA available for nitrogen reduction normalized by geometric surface area) than two dimensional (2D) electrodes which are commonly used in H-cells.[6, 23] It is noteworthy that even if an electrode with a 3D morphology is used in an H-cell the active surface area for NRR will be approximately 2D because the active sites in the bulk of the electrode are insufficiently supplied with nitrogen at very low current densities. Not only is most of the catalyst layer then not active for NRR, but there are much larger ECSA's available for HER than NRR.[24] To understand how the roughness factor of an electrode can influence selectivity and product detection, we compared the NH_3 production of two electrode configurations, one 2D electrode in an H-cell and one 3D electrode in a GDE cell. We assumed a 10-fold higher roughness factor for the 3D electrode in the GDE cell. We assumed that both electrode configurations have the same specific activity (i.e. ECSA normalized current density). As shown in Figure 3.3a, due to its higher surface area, the current density normalized by the geometric surface area is higher for the 3D GDE than for the 2D H-cell electrode. We include ammonia production into the model by assuming that the kinetically possible NRR faradaic efficiency (i.e. no mass transport limitation) can be described with a parabolic function. We distinguish two cases in the model of the faradaic efficiency. In the first case, we assume that a potential window where NRR is selective exists at low specific activity (Figure 3.3b). In the second case, we assume that the selective potential window exists at a high specific activity (Figure 3.3d).

For the first case, we show in Figure 3.3c what happens to the ammonia production when using a low/high ECSA electrode, respectively. As we showed in the previous section, there is a minimum amount of NH_3 which has to be produced by the catalyst for the NRR activity to be detectable and distinguishable from contamination. In Figure 3.3c, we assume that the ammonia production of the 2D electrode in an H-cell is too low to reach this detection limit and hence the NRR activity will not be discoverable. On the other hand, with a 3D GDE, larger current densities (and therefore larger ammonia production rates) can be reached at lower overpotentials due to its higher ECSA. In consequence, the NRR activity which was previously

undiscoverable in an H-cell becomes discoverable in a GDE cell. Therefore, using 3D GDE's instead of 2D electrodes in an H-cell makes it possible to measure the selectivity of materials at lower overpotentials. Testing materials in this low overpotential region might yield catalysts with improved selectivity. For example, in the CO2RR scientific field a shift towards more desirable product distributions was discovered by testing materials in a GDE cell which is believed to be caused by the fact that higher current densities can reached at lower overpotentials.[6]

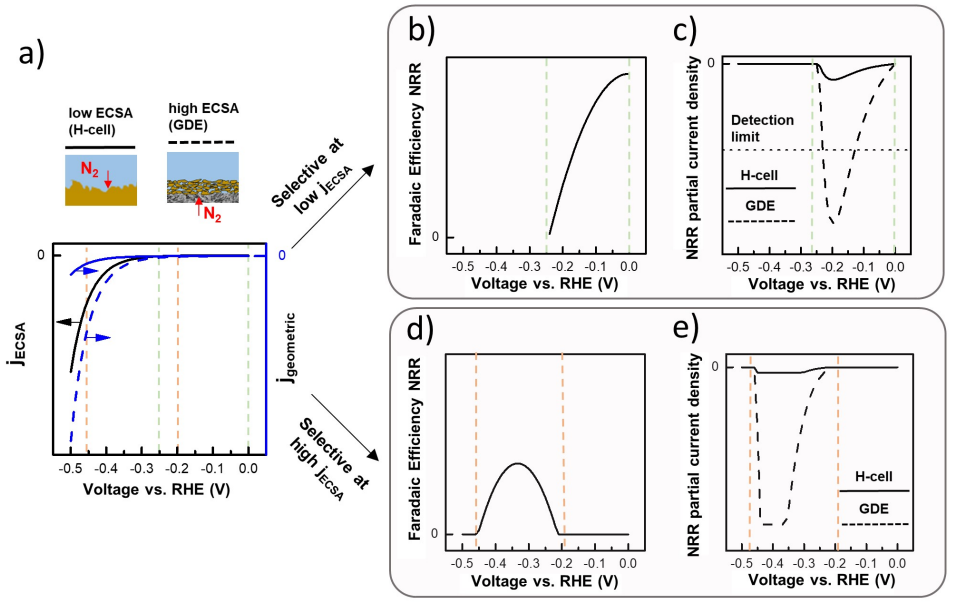

Figure 3.3: Comparative activity of different surface area systems assuming the same specific activity and faradaic efficiency. a) Specific activity (ECSA-normalized, black) and resulting current density normalized by geometric surface area (blue) for low-ECSA and high-ECSA electrode. b) / d) Assumed faradaic efficiency if NRR is favourable over HER at low/high specific activity, respectively. c) / e) NRR partial current density assuming the specific activity in a) and the faradaic efficiency in b) and d), respectively. We assumed that the high-ECSA electrode has a 30-fold higher mass-transport limiting current than the low-ECSA electrode. Specific activity and faradaic efficiency were modelled by using the Butler-Volmer equation and quadratic functions, respectively.

Figure 33.3 shows the ammonia production in the case that a selective potential window exists at high specific activity. In this case, the corresponding NH_3 production is high enough for mass transport limitations to play a role. We assume a mass transport limiting current that is 30-fold higher for the 3D electrode than for the 2D electrode corresponding to the approximate difference in mass transport between H-cell and GDE cell.[27, 47] Both electrodes do not reach their kinetically possible maximum faradaic efficiency due to mass transport limitations. However, the faradaic efficiency is higher for the 3D GDE because the mass transport limitation occurs at higher currents. Therefore, using 3D GDE's can increase the selectivity

compared to 2D electrodes in an H-cell in cases where the latter is operated in the mass transport limited current region. The potential of GDE's to achieve high NH_3 production rates by circumventing N_2 mass transport limitations has been demonstrated by Lazouski et al. who showed that NH_3 partial current densities up to 8.8 $mA\,cm^{-2}$ can be obtained using a lithium-mediated approach with stainless steel gas diffusion electrodes.[48]

Stable catalysts are essential when using detection methods that rely on the accumulation of NH_3, because if a catalyst deactivates before the threshold NH_3 concentration is reached it will not be detectable. The stability of a catalyst can be compromised by impurity deposition onto its surface, surface reconstruction and morphology changes.[23] In NRR experiments the risk of impurity deposition on the electrode surface is particularly high because over long electrolysis times, high negative overpotentials and alkaline electrolytes are used which increase the risk of impurity deposition.[40] This risk can be reduced by using high ECSA GDE's because their higher ECSA reduces the fraction of the surface that can be affected by impurity deposition for a fixed amount of impurities. Furthermore, impurities will deposit preferably on the side of the electrode that is facing the electrolyte, not on the N_2 side of the GDE where NRR can be expected to take place preferably.[22, 23, 40] Surface reconstruction and morphology changes might also affect high ECSA electrodes less, because the overpotential to reach a certain current density will be lower which might reduce the magnitude of such effects.[47]

3.4. Parallel examples of GDE's as a benchmarking cell design

A benchmark consists of a clearly defined electrochemical setup and set of protocols describing how to carry out a measurement with a well-defined catalyst to reproduce a known catalyst performance. Benchmarks are useful when developing electrocatalysts because they ensure the reliability and reproducibility that is necessary to evaluate and compare new catalysts unambiguously.[49] Currently, the NRR academic community has no benchmarking materials or protocols because there is no generally accepted catalyst for this reaction, yet. However, eventually a benchmark will have to be developed for NRR because it can expedite catalyst development. To understand how a suitable benchmark for NRR might look like we will briefly look at how benchmarks are performed in comparable electrochemical fields with low solubility gaseous reagents.

In the case of the oxygen reduction reaction (ORR), specific values for mass-transport limiting current and mass activity must be reached with a Pt/C catalyst in a rotating disk electrode (RDE) setup to confirm that the setup is comparable to literature.[40, 49] However, as recent results have shown, it is not always possible to transfer the activity of promising catalysts measured at low current density in RDE setups to high current density commercial devices.[50] For example, nanostructured Pt-based ORR catalysts such as Pt-Ni nanoframes have much lower mass activity under real

fuel cell conditions than predicted by low current density RDE measurements.[50] Similarly, for a long time, CO2RR catalysts were compared at low current density in H-cells but when those catalysts were tested at higher current density in GDE cells they had completely different product distributions.[47, 51] The lack of transferability of results can arise from a variety of changes that occur when catalysts are tested in commercial devices instead of low current density catalyst testing devices, for example changes in local mass transport, pH or catalyst layer quality.[24, 52] A possible solution to this problem would be to benchmark catalysts in membrane electrode assemblies (MEA) where they can be tested at high current density. However, the production of MEA's is time consuming and it is challenging to control temperature, pressure, water distribution and prevent gas crossover.[53, 54] Therefore, in both fields, CO2RR and ORR, GDE cells have emerged as an alternative platform to test catalysts at current densities closer to commercial conditions but without the problems associated with using a MEA cell design. For example, Inaba et al. has shown that similar ORR mass activities can be observed in GDE and MEA cell design for a given Pt/C catalyst.[47, 55] Leapfrogging low current density catalyst development and directly adopting a GDE cell design for NRR catalyst search might prevent years and resources spent recording data at low current density which might not be transferrable to commercial devices.

However, the use of GDE cells to benchmark catalysts instead of H-cells or RDE cells has several disadvantages. Using a GDE cell instead of an H-cell can cause practical problems, for example with the electrical contact or the sealing of the GDE. A description of how to deal with such problems goes beyond the scope of this perspective but interested readers are referred to the relevant literature.[56] Additionally, a GDE is an ill-defined 3D nanostructure which can have an inhomogeneous distribution of pH and N_2 concentration due to highly overlapping diffusion gradients. Inside the 3D structure of a GDE many different morphological factors such as grain, porosity, oxidation state etc. might be superimposed which makes it difficult to extract structure-functionality relationships between morphological factors and intrinsic activity. Due to these implications, GDE's might not be suitable for fundamental studies where the goal is to measure intrinsic values for activity and selectivity. For such studies H-cells with a well-defined catalyst surface might be a better platform.[6, 23]

3.5. Conclusions

The poor reliability and experimental throughput of NRR research is linked to the H-cell-type cell design, with its commonly high electrolyte volume and N_2 flow rates. These limitations can be overcome by using GDE cells, because mass transport and gaseous flow rate are decoupled resulting in short (<15 min) and cheap (less than €10 per experiment) isotope labelling experiments. The higher ECSA of 3D nanostructured GDE's enables higher NH_3 production at lower overpotentials and reduces the risk of catalyst deactivation. However, it is less suitable for fundamental or mechanistic studies aiming to measure intrinsic activity/selectivity values, because the surface of the catalyst is ill-defined. Leapfrogging to GDE cell design for NRR

catalyst development will reduce the uncertainty associated with transferring low current density H-cell data to high current density commercial devices. Because the primary objective of NRR research at the moment is to reliably identify a selective catalyst, the advantages of catalyst development in a GDE cell design clearly outweigh its limitations.

3.6. Supporting Information

Miniaturized alkaline impurity trap

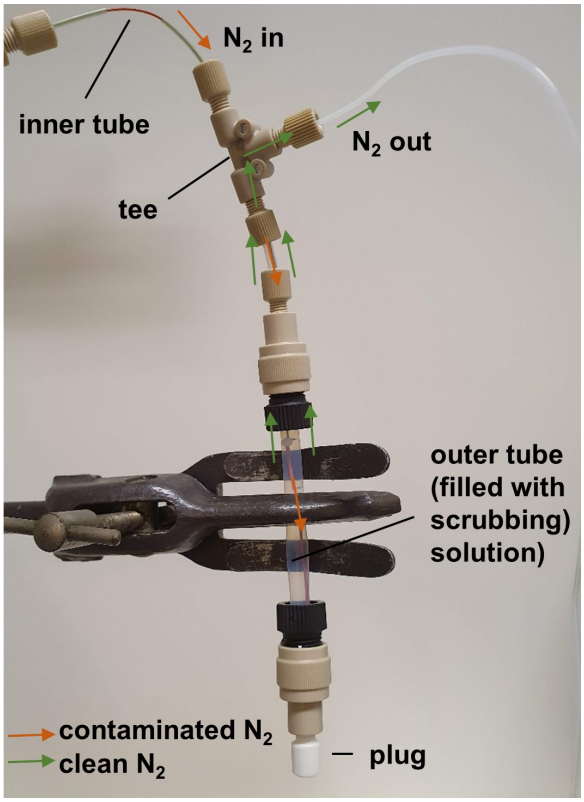

Figure 3.4: Photograph of a miniaturized purifier to clean NH_3/NOx contaminated gas streams with minimal additional headspace.

The removal of NH_3 and NOx contamination from the gas feed of the cell is crucial to avoid false positives while testing catalysts for NRR. Purifiers to achieve this typically consist of an inner and an outer tube. The inner tube is immersed into the outer tube which is filled with an oxidizing solution that traps the NH_3/NOx. During operation, gas is bubbled into the oxidizing solution through the inner tube. The gas exits the outer tube through its headspace. Typically, both outer tube

and inner tube are made of glass, because glass is very inert and easy to reshape. However, the smallest commercially available impurity traps of this design have several mL of headspace volume which would make them very expensive to flush during a $^{15}N_2$ experiment. Therefore, we propose to use an impurity trap made from inert polymers instead, as shown in Figure 3.4. The working principle of the design is identical to that of glass impurity traps but the inner and outer tube are made of inert polymer tubing. The headspace of the 1/32″ outer diameter (OD) inner tubing and the tee is negligible so that the total headspace of the purifier can be estimated from the headspace of the ¼″ outer diameter (OD) outer tube. In our experience approximately 1 cm of headspace in the outer tube is sufficient to prevent liquid from entering the gas channel. With an inner diameter (ID) of 5.6 mm the headspace of the outer tube is approximately 250 µL. This low headspace makes it ideal for cheap $^{15}N_2$ experiments in GDE cell. Additionally, it is comprised of standard connectors for easy, leak-tight, contamination-free connections. Unlike with glass impurity traps, it is possible to easily adjust the length of the outer tube depending on the required removal efficiency. The trap only consists of readily available, off-the-shelf parts which should improve standardization of this critical component.

Table 3.1: Order list for an impurity trap with low headspace volume.

Part #	Name	Quantity	Supplier	Price ($)
1648	Tefzel (ETFE) Tubing Natural 1/8″ OD x .093″ ID x 5ft	1	IDEX Health	33.75
U-665	Adapter Assembly 1/2-20 Female x1/4-28 Female	2	IDEX Health	37.5
P-713	PEEK Low Pressure Tee Assembly 1/8″ PEEK .050 thru hole	1	IDEX Health	38.63
F-247	NanoTight Sleeve Green 1/16″ OD x .033″ ID x 1.6″	4	IDEX Health	*2.84
1569	PEEK Tubing Orange 1/32″ OD x .020″ ID x 5ft	1	IDEX Health	56.93
P-703	Union Assembly PEEK .050 thru hole, for 1/8″ OD	2	IDEX Health	*24.98
P-249	Super Flangeless One-Piece Fitting, 1/4-28 Flat-Bottom, for 1/16″ OD	6	IDEX Health	11.02

P-311	Plug Tefzel (ETFE) - 1/4-28	1	IDEX Health	2.49
20533	PTFE tubing tubing L × OD × ID 25 ft × 1/4 in. (6.35 mm) × 0.228 in. (5.8 mm)	1	Merck Sigma	88.8

Calculation: nitrogen reduction reaction mass-transport limiting current in H-cell

We estimate the mass transport limiting current of the nitrogen reduction reaction $j_{lim,NRR}$ from the mass-transport limiting current of the CO_2 reduction reaction to CO $j_{lim,CO2RR}$ according to:

$$j_{lim,NRR} \approx j_{lim,CO2RR} \frac{S_{N_2} D_{N_2} z_{NRR}}{S_{CO_2} D_{CO_2} z_{CO2RR}} \tag{3.1}$$

$$= 10 \frac{mA}{cm^2} \frac{1.27x10^{-5}\ x\ 1.77x10^{-5} \frac{cm^2}{s}\ x\ 6}{7x10^{-4}\ x\ 1.67x10^{-5} \frac{cm^2}{s}\ x\ 2}$$

$$= 0.6 \frac{mA}{cm^2}$$

, where S_i, D_i, are the solubility and diffusion coefficient of nitrogen and carbon dioxide in water, respectively and z_{NRR}, z_{CO2RR} are the number of electrons transferred in the electrochemical reduction of nitrogen to ammonia and of carbon dioxide to carbon monoxide per molecule of N_2/CO_2, respectively.[27, 36–39]

Calculation: accumulated NH_3 in the electrolyte

The concentration of NH_3 in the electrolyte was calculated according to:

$$c_{NH_3} = \frac{i_{NH_3} t}{zFV} \tag{3.2}$$

, where c_{NH_3} is the concentration of NH_3 after electrolysis, i_{NH_3} is the partial current density of NRR, t is the duration of the experiment, z is the number of electrons transferred per molecule of NH_3 produced, F is the Faraday Constant and V is the half-cell volume of the electrolyte, respectively.

Mathematical modelling of influence of ECSA on ammonia production and faradaic efficiency

The specific activity (defined as the ECSA normalized current density) j_{ECSA} was calculated by assuming Butler-Volmer kinetics according to:

$$j_{ECSA} = j_0(e^{-\alpha f\eta} - e^{(1-\alpha)f\eta}) \quad (3.3)$$

, where j_0 is the exchange current density, α is the symmetry factor, f is the Faraday Constant F divided by the ideal gas constant R and the temperature T and η is the overpotential.[57] The current density normalized by geometric surface area $j_{geometric}$ was calculated by multiplying j_{ECSA} with the roughness factor of the electrode. The faradaic efficiency (FE) was modelled by assuming that a potential window exists where NRR is favourable over HER and that the FE of NRR within this potential window can be described by a quadratic function:

$$FE = a\eta^2 + b\eta + c \quad (3.4)$$

, where a,b,c are constant parameters. The partial current density of NRR j_{NRR} was calculated by multiplying the FE with $j_{geometric}$. The partial current density of NRR including mass transport effects $j_{mt,NRR}$ was calculated by replacing j_{NRR} with the mass transport limiting current $j_{lim,NRR}$ wherever j_{NRR} would otherwise have been lower than $j_{lim,NRR}$:

$$j_{mt,NRR} = max(j_{NRR}, j_{lim,NRR}) \quad (3.5)$$

Literature summary of reported levels of NH_3/NOx contamination

Table 3.2: Literature summary of ammonia and nitrate contaminations observed in nitrogen reduction studies. *To make reports more comparable, contaminations reported as absolute amounts in nmol or as concentrations in a gas stream were converted into concentrations in the electrolyte by assuming the following parameters: electrolyte volume 10 mL, catalyst area: 1 cm^2, catalyst amount: 1 mg, gas flow rate: 30 mL/min duration of gas flow: 2h.

Contamination source	NH_3/NOx concentration	Reference
Human Breath Human Breath	0.3–3 ppm NH_3 in gas 0.28–1.4 ppm NH_3 in gas	[8] [58]
0.05 M H_2SO_4 open to air for 1h	1.7 µM NH_3	[15]
0.05 M H_2SO_4 sealed for 1h	0.6 µM NH_3	[15]
DI water open to air for 400 min	8.8 µM NH_3	[59]
Nitrile gloves sonicated for 1h in DI water	155.1 µM NH_3	[8]
Polypropylene sample storage container (initially)	0.3–49.8 µM NOx	[16]
Polypropylene sample storage container (after 10 days)	3.4–65.3 µM NOx	[16]
Cell, electrolyte, epoxy, electrodes	18.9–21.5 µM NOx	[16]

N impurities in CoMo film	10 μM NH_3	[16]
Rubber septa	630 μM NH_3, 270 μM NOx	[60]
Ar	1.3 ppb NOx in gas (0.02 μM NOx)*	[16]
N2	3.1 ppb NOx in gas (0.046 μM NOx)*	[16]
Ar, $^{14}N_2$, $^{15}N_2$	200 ppb N_2O in gas (3 μM NOx)*	[17]
$^{15}N_2$	0.024–420 ppm ^{15}NOx in gas (0.36–6290 μM ^{15}NOx)* 0.014–1900 ppm $^{15}NH_3$ in gas (0.21–28454 μM $^{15}NH_3$)*	[21]
Bi2O3, Al2O3, Fe2O3	10–120 μmol/g catalyst NOx (1–12 μM NOx)*	[18]
Commercial metallic iron	16343–406469 μM total N	[18]
$^{15}N_2$ scrubbing solution	18.5 μM $^{14}NH_3$, 33 μM $^{15}NH_3$	[16]
Potential induced generation of NH_3 from Fe loaded onto stainless steel	10 μM NH_3	[17]
Release of NH_3 from Nafion 117 membrane soaked in electrolyte containing 0.1 μg/mL of NH_3	17.6 μM NH_3	[61]
Background	1.5 μM NH_3	[25]
Background	2 μM NOx	[17]
Background	0.5 μM NH_3	[8]

Literature summary of experimental parameters used during aqueous nitrogen electroreduction experiments

Table 3.3: Literature summary of experimental parameters used during aqueous NRR studies.

Ref	Gas flow rate (mL/min)	Electrolyte volume (mL)	Electrode area (cm^2)	Electrolysis time (h)	^{15}N? [a]	QT? [b]	Flow rate ^{15}N (mL/min)
[62]	n.a.	n.a.	1	2	yes	no	n.a.

[63]	0.48	100	n.a.	2	yes	no	0.48
[32]	250	n.a.	6.25	1	yes	no	5
[64]	n.a.	30	1	n.a.	yes	no	n.a.
[65]	n.a.	30	1	2	no	no	n.a.
[66]	n.a.	90	2	6	yes	no	20 mL every 10 min
[67]	no flow?	30	2	2	yes	no	n.a.
[68]	20	n.a.	n.a.	2	yes	no	n.a.
[62]	n.a.	50	1	2	yes	no	n.a.
[69]	n.a.	n.a.	1	n.a.	no	no	n.a.
[70]	n.a.	n.a.	1.5	n.a.	no	no	n.a.
[71]	n.a.	30	1	2	yes	yes	n.a.
[72]	n.a.	n.a.	1	2	no	no	n.a.
[73]	n.a.	35	1	2	no	no	n.a.
[33]	n.a.	25	1	n.a.	yes	no	20 mL every 10 min
[74]	10	30	0.07	3	yes	no	n.a.
[34]	60	10	n.a.	n.a.	yes	yes	static
$\tilde{x}$	40	30	1	2			

[a] ^{15}N?: Were control experiments with ^{15}N performed?

[b] QT?: Was a quantitative agreement between $^{14}NH_3$ and $^{15}NH_3$ data demonstrated?

References

[1] M. Kolen, D. Ripepi, W. A. Smith, T. Burdyny, and F. M. Mulder, *Overcoming nitrogen reduction to ammonia detection challenges: The case for leapfrogging to gas diffusion electrode platforms,* ACS Catalysis **12**, 5726 (2022).

[2] D. R. MacFarlane, P. V. Cherepanov, J. Choi, B. H. Suryanto, R. Y. Hodgetts, J. M. Bakker, F. M. Ferrero Vallana, and A. N. Simonov, *A Roadmap to the Ammonia Economy,* Joule **4**, 1186 (2020).

[3] A. Valera-Medina, H. Xiao, M. Owen-Jones, W. David, and P. Bowen, *Ammonia for power,* Progress in Energy and Combustion Science **69**, 63 (2018).

[4] F. M. Mulder, *Implications of diurnal and seasonal variations in renewable energy generation for large scale energy storage,* Journal of Renewable and Sustainable Energy **6**, 033105 (2014).

[5] A. R. Singh, B. A. Rohr, J. A. Schwalbe, M. Cargnello, K. Chan, T. F. Jaramillo, I. Chorkendorff, and J. K. Nørskov, *Electrochemical Ammonia Synthesis—The Selectivity Challenge,* ACS Catalysis **7**, 706 (2017).

[6] S. Nitopi, E. Bertheussen, S. B. Scott, X. Liu, A. K. Engstfeld, S. Horch, B. Seger, I. E. L. Stephens, K. Chan, C. Hahn, J. K. Nørskov, T. F. Jaramillo, and I. Chorkendorff, *Progress and Perspectives of Electrochemical CO_2 Reduction on Copper in Aqueous Electrolyte,* Chemical Reviews **119**, 7610 (2019).

[7] S. Sui, X. Wang, X. Zhou, Y. Su, S. Riffat, and C.-j. Liu, *A comprehensive review of Pt electrocatalysts for the oxygen reduction reaction: Nanostructure, activity, mechanism and carbon support in PEM fuel cells,* Journal of Materials Chemistry A **5**, 1808 (2017).

[8] S. Z. Andersen, V. Čolić, S. Yang, J. A. Schwalbe, A. C. Nielander, J. M. McEnaney, K. Enemark-Rasmussen, J. G. Baker, A. R. Singh, B. A. Rohr, M. J. Statt, S. J. Blair, S. Mezzavilla, J. Kibsgaard, P. C. K. Vesborg, M. Cargnello, S. F. Bent, T. F. Jaramillo, I. E. L. Stephens, J. K. Nørskov, and I. Chorkendorff, *A rigorous electrochemical ammonia synthesis protocol with quantitative isotope measurements,* Nature **570**, 504 (2019).

[9] J. Choi, B. H. R. Suryanto, D. Wang, H.-L. Du, R. Y. Hodgetts, F. M. Ferrero Vallana, D. R. MacFarlane, and A. N. Simonov, *Identification and elimination of false positives in electrochemical nitrogen reduction studies,* Nature Communications **11**, 5546 (2020).

[10] Z. W. Seh, J. Kibsgaard, C. F. Dickens, I. Chorkendorff, J. K. Nørskov, and T. F. Jaramillo, *Combining theory and experiment in electrocatalysis: Insights into materials design,* Science **355**, eaad4998 (2017).

[11] Y. C. Li, Z. Wang, T. Yuan, D.-H. Nam, M. Luo, J. Wicks, B. Chen, J. Li, F. Li, F. P. G. de Arquer, Y. Wang, C.-T. Dinh, O. Voznyy, D. Sinton, and E. H. Sargent,

Binding Site Diversity Promotes CO_2 Electroreduction to Ethanol, Journal of the American Chemical Society **141**, 8584 (2019).

[12] M. Zhong, K. Tran, Y. Min, C. Wang, Z. Wang, C.-T. Dinh, P. De Luna, Z. Yu, A. S. Rasouli, P. Brodersen, S. Sun, O. Voznyy, C.-S. Tan, M. Askerka, F. Che, M. Liu, A. Seifitokaldani, Y. Pang, S.-C. Lo, A. Ip, Z. Ulissi, and E. H. Sargent, *Accelerated discovery of CO2 electrocatalysts using active machine learning,* Nature **581**, 178 (2020).

[13] L. F. Greenlee, J. N. Renner, and S. L. Foster, *The Use of Controls for Consistent and Accurate Measurements of Electrocatalytic Ammonia Synthesis from Dinitrogen,* ACS Catalysis **8**, 7820 (2018).

[14] H. Liu, Y. Zhang, and J. Luo, *The removal of inevitable NO species in catalysts and the selection of appropriate membrane for measuring electrocatalytic ammonia synthesis accurately,* Journal of Energy Chemistry **49**, 51 (2020).

[15] G. Y. Duan, Y. Ren, Y. Tang, Y. Z. Sun, Y. M. Chen, P. Y. Wan, and X. J. Yang, *Improving the Reliability and Accuracy of Ammonia Quantification in Electro- and Photochemical Synthesis,* ChemSusChem **13**, 88 (2020).

[16] W. Yu, P. Buabthong, C. G. Read, N. F. Dalleska, N. S. Lewis, H.-J. Lewerenz, H. B. Gray, and K. Brinkert, *Cathodic NH_4^+ leaching of nitrogen impurities in CoMo thin-film electrodes in aqueous acidic solutions,* Sustainable Energy & Fuels **4**, 5080 (2020).

[17] R. Y. Hodgetts, H.-L. Du, D. R. MacFarlane, and A. N. Simonov, *Electrochemically Induced Generation of Extraneous Nitrite and Ammonia in Organic Electrolyte Solutions During Nitrogen Reduction Experiments,* ChemElectroChem **8**, 1596 (2021).

[18] Y. Chen, H. Liu, N. Ha, S. Licht, S. Gu, and W. Li, *Revealing nitrogen-containing species in commercial catalysts used for ammonia electrosynthesis,* Nature Catalysis (2020), 10.1038/s41929-020-00527-4.

[19] J. Choi, H.-L. Du, C. K. Nguyen, B. H. R. Suryanto, A. N. Simonov, and D. R. MacFarlane, *Electroreduction of Nitrates, Nitrites, and Gaseous Nitrogen Oxides: A Potential Source of Ammonia in Dinitrogen Reduction Studies,* ACS Energy Letters **5**, 2095 (2020).

[20] S. Licht, B. Cui, B. Wang, F.-F. Li, J. Lau, and S. Liu, *Retraction,* **369**, 780 (2020).

[21] R. Dabundo, M. F. Lehmann, L. Treibergs, C. R. Tobias, M. A. Altabet, P. H. Moisander, and J. Granger, *The Contamination of Commercial 15N2 Gas Stocks with 15N–Labeled Nitrate and Ammonium and Consequences for Nitrogen Fixation Measurements,* PLoS ONE **9**, e110335 (2014).

[22] R. Subbaraman, N. Danilovic, P. P. Lopes, D. Tripkovic, D. Strmcnik, V. R. Stamenkovic, and N. M. Markovic, *Origin of Anomalous Activities for Electrocatalysts in Alkaline Electrolytes,* The Journal of Physical Chemistry C **116**, 22231 (2012).

[23] R. Kas, K. Yang, D. Bohra, R. Kortlever, T. Burdyny, and W. A. Smith, *Electrochemical CO_2 reduction on nanostructured metal electrodes: fact or defect?* Chemical Science **11**, 1738 (2020).

[24] T. Burdyny and W. A. Smith, *CO_2 reduction on gas-diffusion electrodes and why catalytic performance must be assessed at commercially-relevant conditions,* Energy & Environmental Science **12**, 1442 (2019).

[25] W. Yu, N. S. Lewis, H. B. Gray, and N. F. Dalleska, *Isotopically Selective Quantification by UPLC-MS of Aqueous Ammonia at Submicromolar Concentrations Using Dansyl Chloride Derivatization,* ACS Energy Letters **5**, 1532 (2020).

[26] X. Zhu, S. Mou, Q. Peng, Q. Liu, Y. Luo, G. Chen, S. Gao, and X. Sun, *Aqueous electrocatalytic N_2 reduction for ambient NH_3 synthesis: recent advances in catalyst development and performance improvement,* Journal of Materials Chemistry A **8**, 1545 (2020).

[27] E. L. Clark, J. Resasco, A. Landers, J. Lin, L.-T. Chung, A. Walton, C. Hahn, T. F. Jaramillo, and A. T. Bell, *Standards and Protocols for Data Acquisition and Reporting for Studies of the Electrochemical Reduction of Carbon Dioxide,* ACS Catalysis **8**, 6560 (2018).

[28] M. D. Krom, *Spectrophotometric determination of ammonia: a study of a modified Berthelot reaction using salicylate and dichloroisocyanurate,* The Analyst **105**, 305 (1980).

[29] R. Zaffaroni, D. Ripepi, J. Middelkoop, and F. M. Mulder, *Gas Chromatographic Method for* In Situ *Ammonia Quantification at Parts per Billion Levels,* ACS Energy Letters **5**, 3773 (2020).

[30] M. Kolen, W. A. Smith, and F. M. Mulder, *Accelerating ^{1}H NMR Detection of Aqueous Ammonia,* ACS Omega **6**, 5698 (2021).

[31] F. Hanifpour, C. P. Canales, E. G. Fridriksson, A. Sveinbjörnsson, T. K. Tryggvason, E. Lewin, F. Magnus, A. S. Ingason, E. Skúlason, and H. D. Flosadóttir, *Investigation into the mechanism of electrochemical nitrogen reduction reaction to ammonia using niobium oxynitride thin-film catalysts,* Electrochimica Acta **403**, 139551 (2021).

[32] M.-C. Kim, H. Nam, J. Choi, H. S. Kim, H. W. Lee, D. Kim, J. Kong, S. S. Han, S. Y. Lee, and H. S. Park, *Hydrogen Bonding-Mediated Enhancement of Bioinspired Electrochemical Nitrogen Reduction on $Cu_{2-x}S$ Catalysts,* ACS Catalysis **10**, 10577 (2020).

[33] Z.-H. Xue, S.-N. Zhang, Y.-X. Lin, H. Su, G.-Y. Zhai, J.-T. Han, Q.-Y. Yu, X.-H. Li, M. Antonietti, and J.-S. Chen, *Electrochemical Reduction of N_2 into NH_3 by Donor–Acceptor Couples of Ni and Au Nanoparticles with a 67.8% Faradaic Efficiency,* Journal of the American Chemical Society **141**, 14976 (2019).

[34] B. H. R. Suryanto, D. Wang, L. M. Azofra, M. Harb, L. Cavallo, R. Jalili, D. R. G. Mitchell, M. Chatti, and D. R. MacFarlane, *MoS_2 Polymorphic Engineering Enhances Selectivity in the Electrochemical Reduction of Nitrogen to Ammonia,* ACS Energy Letters **4**, 430 (2019).

[35] A. C. Nielander, S. J. Blair, J. M. McEnaney, J. A. Schwalbe, T. Adams, S. Taheri, L. Wang, S. Yang, M. Cargnello, and T. F. Jaramillo, *Readily Constructed Glass Piston Pump for Gas Recirculation,* ACS Omega **5**, 16455 (2020).

[36] R. Battino, T. R. Rettich, and T. Tominaga, *The Solubility of Nitrogen and Air in Liquids,* Journal of Physical and Chemical Reference Data **13**, 563 (1984).

[37] R. T. Ferrell and D. M. Himmelblau, *Diffusion Coeffkients of Nitrogen and Oxygen in Water,* Journal of Chemical & Engineering Data **12**, 111 (1967).

[38] J. J. Carroll, J. D. Slupsky, and A. E. Mather, *The Solubility of Carbon Dioxide in Water at Low Pressure,* Journal of Physical and Chemical Reference Data **20**, 1201 (1991).

[39] B. Jähne, G. Heinz, and W. Dietrich, *Measurement of the diffusion coefficients of sparingly soluble gases in water,* Journal of Geophysical Research **92**, 10767 (1987).

[40] C. Wei, R. R. Rao, J. Peng, B. Huang, I. E. L. Stephens, M. Risch, Z. J. Xu, and Y. Shao-Horn, *Recommended Practices and Benchmark Activity for Hydrogen and Oxygen Electrocatalysis in Water Splitting and Fuel Cells,* Advanced Materials **31**, 1806296 (2019).

[41] L. Hu, Z. Xing, and X. Feng, *Understanding the Electrocatalytic Interface for Ambient Ammonia Synthesis,* ACS Energy Letters **5**, 430 (2020).

[42] U. B. Shahid, Y. Chen, S. Gu, W. Li, and M. Shao, *Electrochemical nitrogen reduction: an intriguing but challenging quest,* Trends in Chemistry **4**, 142 (2022).

[43] Y. C. Tan, K. B. Lee, H. Song, and J. Oh, *Modulating Local CO2 Concentration as a General Strategy for Enhancing C–C Coupling in CO2 Electroreduction,* Joule **4**, 1104 (2020).

[44] L. Peng, X. Lai, D. Liu, P. Hu, and J. Ni, *Flow channel shape optimum design for hydroformed metal bipolar plate in PEM fuel cell,* Journal of Power Sources **178**, 223 (2008).

[45] D. Ripepi, R. Zaffaroni, M. Kolen, J. Middelkoop, and F. M. Mulder, *Operando isotope selective ammonia quantification in nitrogen reduction studies via gas chromatography-mass spectrometry,* Sustainable Energy & Fuels **6**, 1945 (2022).

[46] A. C. Nielander, J. M. McEnaney, J. A. Schwalbe, J. G. Baker, S. J. Blair, L. Wang, J. G. Pelton, S. Z. Andersen, K. Enemark-Rasmussen, V. Čolić, S. Yang, S. F. Bent, M. Cargnello, J. Kibsgaard, P. C. K. Vesborg, I. Chorkendorff, and T. F. Jaramillo, *A Versatile Method for Ammonia Detection in a Range of Relevant Electrolytes via Direct Nuclear Magnetic Resonance Techniques,* ACS Catalysis **9**, 5797 (2019).

[47] C.-T. Dinh, T. Burdyny, G. Kibria, A. Seifitokaldani, C. M. Gabardo, J. P. Edwards, P. D. Luna, O. S. Bushuyev, C. Zou, R. Quintero-Bermudez, Y. Pang, D. Sinton, and E. H. Sargent, *CO2 electroreduction to ethylene via hydroxide-mediated copper catalysis at an abrupt interface,* Science **360**, 783 (2018).

[48] N. Lazouski, M. Chung, K. Williams, M. L. Gala, and K. Manthiram, *Non-aqueous gas diffusion electrodes for rapid ammonia synthesis from nitrogen and water-splitting-derived hydrogen,* Nature Catalysis **3**, 463 (2020).

[49] H. Gasteiger, J. Panels, and S. Yan, *Dependence of PEM fuel cell performance on catalyst loading,* Journal of Power Sources **127**, 162 (2004).

[50] I. E. L. Stephens, J. Rossmeisl, and I. Chorkendorff, *Toward sustainable fuel cells,* Science **354**, 1378 (2016).

[51] Y. Hori, H. Konishi, T. Futamura, A. Murata, O. Koga, H. Sakurai, and K. Oguma, *"Deactivation of copper electrode" in electrochemical reduction of CO2,* Electrochimica Acta **50**, 5354 (2005).

[52] B. A. Pinaud, A. Bonakdarpour, L. Daniel, J. Sharman, and D. P. Wilkinson, *Key Considerations for High Current Fuel Cell Catalyst Testing in an Electrochemical Half-Cell,* Journal of The Electrochemical Society **164**, F321 (2017).

[53] C. M. Zalitis, D. Kramer, and A. R. Kucernak, *Electrocatalytic performance of fuel cell reactions at low catalyst loading and high mass transport,* Physical Chemistry Chemical Physics **15**, 4329 (2013).

[54] M. T. M. Koper, ed., *Fuel cell catalysis: a surface science approach*, Wiley series on electrocatalysis and electrochemistry (Wiley, Hoboken, N.J, 2009) pp. 532–540, oCLC: ocn294884358.

[55] M. Inaba, A. W. Jensen, G. W. Sievers, M. Escudero-Escribano, A. Zana, and M. Arenz, *Benchmarking high surface area electrocatalysts in a gas diffusion electrode: measurement of oxygen reduction activities under realistic conditions,* Energy & Environmental Science **11**, 988 (2018).

[56] K. Liu, W. A. Smith, and T. Burdyny, *Introductory Guide to Assembling and Operating Gas Diffusion Electrodes for Electrochemical CO_2 Reduction,* ACS Energy Letters **4**, 639 (2019).

[57] A. J. Bard and L. R. Faulkner, in *Electrochemical methods: fundamentals and applications* (Wiley, New York, 2001) 2nd ed., p. 96.

[58] T. V. Larson, D. S. Covert, R. Frank, and R. J. Charlson, *Ammonia in the Human Airways: Neutralization of Inspired Acid Sulfate Aerosols,* Science **197**, 161 (1977).

[59] C. Saigne, S. Kirchner, and M. Legrand, *ION-CHROMATOGRAPHIC MEASUREMENTS OF AMMONIUM, FLUORIDE, ACETATE, FORMATE AND METHANESULPHONATE IONS AT VERY LOW LEVELS IN ANTARCTIC ICE,* Analytica Chimica Acta, **203**, 11 (1987).

[60] D. L. Boucher, J. A. Davies, J. G. Edwards, and A. Mennad, *An investigation of the putative photosynthesis of ammonia on iron-doped titania and other metal oxides,* Journal of Photochemistry and Photobiology A: Chemistry **88**, 53 (1995).

[61] Y. Ren, C. Yu, X. Tan, H. Huang, Q. Wei, and J. Qiu, *Strategies to suppress hydrogen evolution for highly selective electrocatalytic nitrogen reduction: Challenges and perspectives,* Energy & Environmental Science **14**, 1176 (2021).

[62] L. Zhao, X. Liu, S. Zhang, J. Zhao, X. Xu, Y. Du, X. Sun, N. Zhang, Y. Zhang, X. Ren, and Q. Wei, *Rational design of bimetallic $Rh_{0.6}Ru_{0.4}$ nanoalloys for enhanced nitrogen reduction electrocatalysis under mild conditions,* Journal of Materials Chemistry A **9**, 259 (2021).

[63] X. Wei, D. Vogel, L. Keller, S. Kriescher, and M. Wessling, *Microtubular Gas Diffusion Electrode Based on Ruthenium□Carbon Nanotubes for Ambient Electrochemical Nitrogen Reduction to Ammonia,* ChemElectroChem **7**, 4679 (2020).

[64] Y. Jin, X. Ding, L. Zhang, M. Cong, F. Xu, Y. Wei, S. Hao, and Y. Gao, *Boosting electrocatalytic reduction of nitrogen to ammonia under ambient conditions by alloy engineering,* Chemical Communications **56**, 11477 (2020).

[65] X. Jiang, M. He, M. Tang, Q. Zheng, C. Xu, and D. Lin, *Nanostructured bimetallic Ni–Fe phosphide nanoplates as an electrocatalyst for efficient N2 fixation under ambient conditions,* Journal of Materials Science **55**, 15252 (2020).

[66] Y.-X. Lin, S.-N. Zhang, Z.-H. Xue, J.-J. Zhang, H. Su, T.-J. Zhao, G.-Y. Zhai, X.-H. Li, M. Antonietti, and J.-S. Chen, *Boosting selective nitrogen reduction to ammonia on electron-deficient copper nanoparticles,* Nature Communications **10** (2019), 10.1038/s41467-019-12312-4.

[67] L. Zhang, M. Cong, X. Ding, Y. Jin, F. Xu, Y. Wang, L. Chen, and L. Zhang, *A Janus Fe-SnO_2 Catalyst that Enables Bifunctional Electrochemical Nitrogen Fixation,* Angewandte Chemie International Edition **59**, 10888 (2020).

[68] Y. Li, J. Chen, P. Cai, and Z. Wen, *An electrochemically neutralized energy-assisted low-cost acid-alkaline electrolyzer for energy-saving electrolysis hydrogen generation,* Journal of Materials Chemistry A **6**, 4948 (2018).

[69] J. Wang, Y. Ren, M. Chen, G. Cao, Z. Chen, and P. Wang, *Bismuth hollow nanospheres for efficient electrosynthesis of ammonia under ambient conditions,* Journal of Alloys and Compounds **830**, 154668 (2020).

[70] Y. Tong, H. Guo, D. Liu, X. Yan, P. Su, J. Liang, S. Zhou, J. Liu, G. Q. M. Lu, and S. X. Dou, *Vacancy Engineering of Iron-Doped $W_{18}O_{49}$ Nanoreactors for Low□Barrier Electrochemical Nitrogen Reduction,* Angewandte Chemie International Edition **59**, 7356 (2020).

[71] J. Wang, B. Huang, Y. Ji, M. Sun, T. Wu, R. Yin, X. Zhu, Y. Li, Q. Shao, and X. Huang, *A General Strategy to Glassy M-Te (M = Ru, Rh, Ir) Porous Nanorods for Efficient Electrochemical N_2 Fixation,* Advanced Materials **32**, 1907112 (2020).

[72] F. Wang, X. Lv, X. Zhu, J. Du, S. Lu, A. A. Alshehri, K. A. Alzahrani, B. Zheng, and X. Sun, *Bi nanodendrites for efficient electrocatalytic N_2 fixation to NH_3 under ambient conditions,* Chemical Communications **56**, 2107 (2020).

[73] M. Ohrelius, H. Guo, H. Xian, G. Yu, A. A. Alshehri, K. A. Alzahrani, T. Li, and M. Andersson, *Electrochemical Synthesis of Ammonia Based on a Perovskite $LaCrO_3$ Catalyst,* ChemCatChem **12**, 731 (2020).

[74] P. Song, H. Wang, L. Kang, B. Ran, H. Song, and R. Wang, *Electrochemical nitrogen reduction to ammonia at ambient conditions on nitrogen and phosphorus co-doped porous carbon,* Chemical Communications **55**, 687 (2019).

4

Combinatorial Screening of Bimetallic Electrocatalysts for Nitrogen Reduction to Ammonia Using a High-Throughput Gas Diffusion Electrode Cell Design

The electrochemical nitrogen reduction reaction (NRR) is a promising alternative to the current greenhouse gas emission intensive process to produce ammonia (NH_3) from nitrogen (N_2). However, finding an electrocatalyst that promotes NRR over the competing hydrogen evolution reaction (HER) has proven to be difficult. This difficulty could potentially be addressed by accelerating the electrocatalyst development for NRR by orders of magnitude using high-throughput (HTP) workflows. Available cell designs for HTP workflows are unsuitable for NRR catalyst development because they have not reached sufficient technological maturity or cannot prevent NRR selectivity losses due to N_2 mass-transport limitations. To overcome these limitations, we developed a HTP gas diffusion electrode (GDE) cell to screen up to 16 electrocatalysts in parallel. The key innovation of the cell is the use of expanded Polytetrafluoroethylene (ePTFE) gas diffusion layers (GDL) which simplifies the handling of catalyst arrays compared to carbon fabrics and increases the N_2 mass transport by around two orders of magnitude compared to conventional HTP cell designs. We demonstrate the robustness of the HTP workflow by screening 528 bimetallic catalysts of composition AB (A,B = Ag, Al, Au, Co, Cu, Fe, Mn , Mo, Ni, Pd, Re, Ru, W) for NRR activity. None of the materials produced ammonia significantly over background level.

Parts of this chapter have been submitted for publication.

4.1. Introduction

The unequal distribution of renewable energy generation potential across the globe has created an awareness that a scalable means of storing and transporting electricity is needed to decarbonize the global economy. Green ammonia (NH_3), i.e., ammonia produced from renewable electricity has the potential to fill this gap, with additional potential to decarbonize ammonia production (1-1.4% of global CO_2 emissions) and to replace fossil fuels in the engines of ships and trucks. One of the potentially cheapest routes to produce green NH_3 is the conversion of nitrogen (N_2) to NH_3 via the electrochemical nitrogen reduction reaction (NRR).[1–3] However, it has proven to be very challenging to find a selective catalyst that sufficiently suppresses the more favorable hydrogen evolution reaction (HER) in aqueous electrolyte such that high NH_3 production rates can be achieved.[4]

The difficulty of finding a selective catalyst for NRR is commonly attributed to the slow kinetics of the activation of the N_2 triple bond and the subsequent reduction in a 6-electron process compared to only 2-electron transfers for HER.[4] It is generally believed that the binding energies of key intermediates of the NRR mechanism are correlated (so called scaling relations) which leads to a minimum overpotential requirement of 0.5V for NRR according to density functional theory (DFT) calculations.[5] To overcome these difficulties, strategies are needed to promote NRR while simultaneously suppressing HER.

Alloying two or more metals can effectively tune the selectivity of electrochemical reactions. For example, Cu has been alloyed with Ag and Al to tune the selectivity of the CO_2 reduction reaction (CO2RR) towards ethanol or ethylene, respectively.[6, 7] The improved electrocatalytic performance of alloys is often ascribed to strain, ligand and ensemble effects that create active sites with more optimal binding energies for key intermediates.[8–10] Possibly, an intermetallic catalyst exists that has a sufficient concentration of optimal active sites for NRR to promote the reaction and reach sufficient rates to prevail over HER.

Many recent studies claim that intermetallic materials such as Pd_3Cu_1, PdRu and AuCu are active catalysts for NRR.[11–14] However, several critical assessments of the NRR literature have concluded that the methodology that has been used thus far to assess the NRR activity of materials is unable to guarantee reliable results, because the performed control experiments were insufficient to exclude the possibility of a false positives from NH_3 and/or nitrogen oxides (NOx) contamination.[15–17] This conclusion has led to a lack of confidence in published NRR results among NRR researchers which further intensified in view of the recent retractions and refutations of papers which were believed to be groundbreaking.[18, 19]

To improve the reliability of NRR research, many control experiments to eliminate contamination sources and reduce the risk of false positives have been proposed.[15–17] In addition, we have recently argued that the choice of cell design has a large influence on the reliability of NRR experiments. By using gas diffusion electrode

(GDE) cells instead of commonly used H-cells, the reliability of NRR experiments can be improved because experiments can be run at lower gas flow rates without limiting the N_2 mass transport to the catalyst surface, which in turn reduces the cost of crucial control experiments with $^{15}N_2$.[20] The widespread adoption of reliable experimental protocols should restore the trust in published NRR results. Nevertheless, even with reliable protocols in place, two issues still slow down the progress of the research field. First, testing materials for NRR activity produces a lot of negative results which are much less likely to be published due to the bias of published literature to report preferably positive results.[21] Therefore new research cannot benefit from the knowledge of previous failed attempts. Second, the experimental workflow to test materials for NRR activity is too slow. With a median electrolysis time of 2h per NRR experiment (cleaning steps and control experiments not included) catalyst testing is not fast enough for the thorough exploration of more complex material classes such as intermetallic catalysts.[20]

A promising strategy to accelerate the NRR experimental workflow is the implementation of parallelization and automation techniques. So-called high throughput (HTP) workflows are a powerful tool in heterogeneous catalysis.[22] For example the triply promoted iron catalyst that is currently used in the industrial production of ammonia was discovered by means of a HTP screening.[23] A HTP workflow for NRR catalyst development would not only drastically increase the likelihood of finding a promising catalyst but also produce large datasets to improve potentially invaluable computational models.[7] Such datasets would also include a large number of negative results which could inform future research. In short, HTP workflows have the potential to enable more rapid advancements in the NRR research field.

To build a HTP workflow for NRR catalyst development, it is necessary to accelerate every step of the workflow. If one step is much slower than the others it will create a bottleneck and the overall acceleration will be small. Since HTP is a widely used method in other research fields, mature HTP methods for the production and physical characterization of catalyst libraries, and data analysis are available.[24] The key challenge seems to be the development of an electrochemical cell that is capable of rapidly screening materials for the target reaction. Common HTP cell designs to screen electrocatalysts are: single compartment cells with a composition spread as working electrode (WE) or WE array[25–27], scanning capillary/probe/droplet cells[28–30], arrays of single compartment cells[31] and membrane electrode assemblies (MEA).[32] Thus far, papers utilizing HTP workflows make up a negligible fraction of the published electrocatalysis literature which indicates that the available electrochemical cells have not yet reached sufficient technological maturity to replace one-by-one catalyst testing. Common problems with HTP cell designs include insufficient data quality compared to one-by-one catalyst testing[33], short lifetime of cell components like current collectors[25] and catalysts adhesion issues.[26] Clearly, choosing an appropriate cell design is key for a meaningful HTP screening of NRR catalysts.

In all of the previously mentioned HTP cell designs (except MEA) the reactant gas is transported to the catalyst surface from the bulk electrolyte. Due to the low water solubility of N_2 (705.8 µM at 1 bar, 20 °C), the maximum rate of N_2 that can be transported to the catalyst surface in such cells corresponds to an NRR current density of only a few hundred $\mu A\,cm^{-2}$.[20, 34] Screening catalysts under such N_2 limited conditions would lead to NRR selectivity losses.[35] Therefore, such cell designs are unsuitable for an NRR catalyst screening. To our best knowledge, the only HTP cell design in literature with sufficient N_2 mass transport is the MEA cell design with 16 individual WE developed by Liu et al. to screen catalysts for direct methanol fuel cell anodes.[32] In this cell design, carbon fabrics were used as catalyst supports. Our attempts to use carbon fabrics as gas diffusion layer (GDL) in a HTP cell failed due to practical issues. The main problem was that each catalyst required a separate carbon fabric to prevent short circuits between the catalysts during electrochemical tests. Each of these fabrics had to be cut out, transported, installed and electrically connected which proved to be a very time-consuming and error-prone process. In addition, carbon fabrics are very fragile with caused them to break frequently during handling. Since none of the available HTP cell designs are suitable for NRR, a new cell design is needed.

Gas diffusion electrode (GDE) cells have recently gained popularity as a platform to screen electrocatalysts in both the oxygen reduction reaction (ORR) and the CO2RR research field, because they allow testing of electrocatalysts under more realistic reaction conditions than conventional cell designs.[36–38] In GDE cells, the catalyst is positioned on a hydrophobic GDL at the junction between gas phase and liquid electrolyte. This close proximity of the catalyst surface to the gas phase enables high mass transport limiting currents for reactions which have gaseous reagents with low water solubility like N_2.[36, 39] The simplicity of GDE cells in combination with their high N_2 transport and advantages for ammonia detection make GDE cells a preferable platform to screen NRR catalysts.[20, 37] However, the most commonly used type of GDL in GDE cells are carbon fabrics.[36, 39] For the development of a HTP GDE cell, an alternative to carbon fabric GDLs is needed to avoid the practical issues described above.

Recently, Dinh et al. showed that similar CO2RR performance to carbon fabrics can be obtained using a different type of GDL—expanded Polytetrafluoroethylene (ePTFE).[38] Interestingly, ePTFE is not electrically conductive which means that current can only flow through the catalyst layer deposited onto the ePTFE but not through the ePTFE itself. Thus, one piece of ePTFE can support a whole array of electrically insulated catalysts whereas one piece of carbon fabric can only support one catalyst. This not only drastically reduces the complexity of handling catalyst arrays but it also simplifies the electrical connection of catalysts in the electrochemical cell, because each catalyst is located at a well-defined position with respect to its neighbors. Additionally, ePTFE is less fragile than carbon fabrics and it becomes leak-tight under compression which reduces the complexity of a HTP cell even further. These advantageous properties of ePTFE may enable the development of a

new generation of HTP cells with much simpler cell design and sufficient N_2 mass transport for NRR. Such cells have the potential to enable a drastic acceleration of the experimental throughput of NRR research compared to one-by-one catalyst testing.

In this work, we propose a HTP workflow to screen electrocatalysts for NRR and apply it to a screening of bimetallic catalysts. We first introduce a HTP method to produce bimetallic catalysts with well-defined compositions. We then describe the GDE cell design which utilizes ePTFE as GDL and characterize important characteristics of the cell such as reproducibility and N_2 mass transport. Next, we demonstrate that catalyst arrays can be physically characterized with methods that are compatible with a HTP workflow. Then, we use the workflow to screen 528 bimetallic catalysts for NRR activity in the temperature range 21–55 °C. The catalyst screening was optimized for maximum throughput at the expense of resolution to maximize the chance of finding a promising catalyst for NRR.[22] Lastly, we evaluate the speed and robustness of the presented workflow by contrasting it with one-by-one catalyst testing.

4.2. Experimental

Preparation of bimetallic catalyst libraries

16 bimetallic catalysts of varying composition were co-sputtered onto ePTFE (200 nm pore size, Pieper Filter GmbH) using a magnetron sputtering system (AJA International Inc.) equipped with 4 sputter guns (Figure 4.1a,b). The sputter targets (purity: 99.9–99.99%) were purchased from MaTecK. The base pressure of the sputtering chamber was 2e-7 mbar. Before a deposition, samples were sputter-cleaned under argon plasma for 2 min. Then, the sputter guns were turned on with closed shutter for 30 s. After that, the shutters were opened until the deposition was completed. Depositions were carried out under argon flow (flow rate: 20 sccm, purity: 99.9999%) at a pressure of 3 µbar. To control the composition of the co-sputtered composition gradients, the position-dependent deposition rate was measured for each metal by sputtering a thickness gradient on a microscope slide at a sputter gun power of 100 W (Figure 4.1c). The thickness gradients were measured using a Dektak profilometer (Veeco). The catalyst arrays for the electrochemical tests were co-sputtered so that the catalyst layer thickness and composition in the center of the catalyst array were 300 nm and 50:50, respectively. The deposition time and the power of both sputtering guns to achieve this composition and thickness in the center of the catalyst array were calculated based on the deposition rates that were measured for each single metal using a Matlab script. For the calculations, it was assumed that the deposition rate of each metal is proportional to the deposition time and power setting of the sputter gun.[40] During the deposition of the catalyst arrays for the electrochemical tests, the sputter guns were positioned either at an angle of 90° or 180° with respect to each other (Figure 4.1b). Henceforth, catalyst arrays that were sputtered at 90°/180° angle will be referred to as "90°-samples" and "180°-samples", respectively. An example of a 90°-sample and a 180°-sample

is shown in Figure 4.1d. The predicted composition on the ePTFE sample ranged from 20% ± 10% metal A on one side to 80% ± 10% metal A on the other side (Figure 4.1e). The part of the ePTFE surface that was not supposed to be coated with metal was covered with a stainless steel mask (0.2 mm thickness). While we focussed on bimetallic catalysts in this work, many more classes of materials with potentially interesting properties for electrocatalysis can be produced by sputtering, for example high-entropy alloys, metal oxides and metal nitrides.[41, 42]

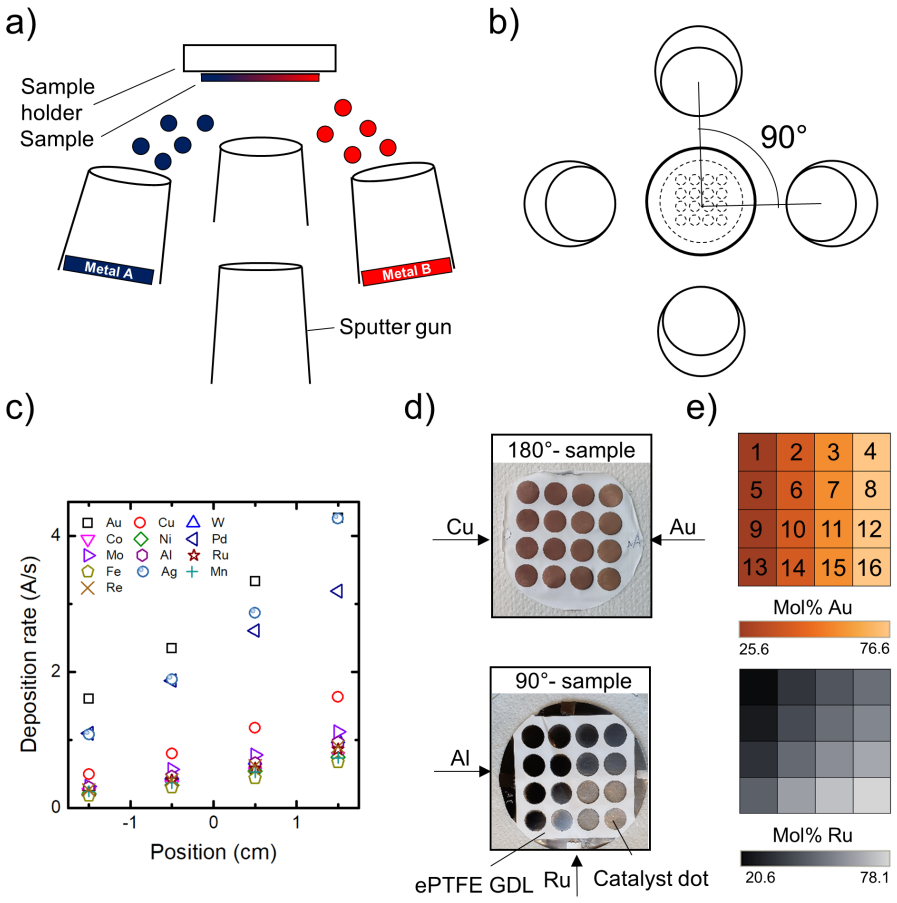

Figure 4.1: Sputtering setup used to deposit the catalyst arrays. a) side view. b) top view. c) Deposition rate of each metal used in this work as a function of position. Position "0" corresponds to the center of the sample. d) Example of a sample sputtered at 90°/180°. e) Predicted composition map of the samples in d).

To minimize the number of times the sputtering chamber had to be opened, all 4 metals in the chamber were co-sputtered with each other resulting in 6 unique bimetallic catalyst arrays (henceforth referred to as a set). The catalyst arrays that were screened for NRR activity in this work are listed in Table 4.1. In total, 33 unique bimetallic catalyst arrays comprising 528 catalysts were screened. The choice of metals to be combined with each other was influenced by a combination of different factors. Practical constraints like the price and availability of sputtering targets, the compatibility of elements with the sputtering process and the need to minimize the number of sputter target changes were considered. The metals in set 1 were chosen based on literature reports claiming that Pd3Cu1, PdRu and AuCu are active catalysts for NRR.[11, 12, 14] For sets 2, 3 and 5, we predominantly choose metals that are active for heterogeneous ammonia synthesis (Fe, Ru, Co, Ni, Mn, Mo) to test if they are active for NRR, too.[23] To choose the metals in set 4, 7629 adsorption energies of nitrogen on bimetallic surfaces were downloaded from the Catalysis-Hub—a public database that contains the results of DFT calculations.[43] According to Skúlason et al., the most promising materials for NRR have a nitrogen adsorption energy in the range -0.5—0 eV.[44] Therefore, the materials with the most entries in this range were chosen for set 4. For set 6, we decided to combine the only element on the left side of the NRR volcano plot—Rhenium—with metals on the right side of the volcano because the resulting bimetallic catalysts might be closer to the peak of the volcano.[45]

Table 4.1: Catalyst arrays that were screened for NRR activity in this work.

Set	Catalysts arrays
1	CuAu, CuPd, CuRu, AuPd, AuRu, PdRu
2	FeCu, FeNi, FeW, CuNi, CuW, NiW
3	PdCo, PdMo, PdNi, CoMo, CoNi, MoNi
4	CoAl, CoRu, CoFe, AlRu, AlFe, RuFe
5	NiCu, NiAg, NiMn, CuAg, CuMn, AgMn
6	ReCu, ReFe, RePd, CuFe, CuPd, FePd

Setup for HTP Catalyst Screening

A schematic of the setup that was used to screen the electrocatalyst arrays for NRR activity is shown in Figure 4.2a. The cell was constructed like a 3-compartment GDE cell but instead of one, an array of 16 WEs was positioned at the interface between the gas compartment and catholyte. The electrolyte reaches the catalyst layer but cannot penetrate the ePTFE due to the hydrophobicity of the material (Figure 4.2b). The abrupt interface between electrolyte and gas ensures high N_2 mass transport to the catalyst surface.[38] All catalysts are in contact with the same catholyte which means that the ammonia production can only be measured for a whole catalyst array at a time, not for individual catalysts. We chose this configuration because inactive catalysts can be filtered out with minimal NH_3 detection

effort. A Celgard 3401 membrane was used as a separator between the catholyte and anolyte. A Mini Hydroflex reversible hydrogen electrode (Gaskatel GmbH) and a nickel foil (thickness: 0.0125 mm, purity: 99.9%, supplier: GoodFellow) were used as reference electrode (RE) and counter electrode (CE), respectively. All electrochemical tests were done using an RT-2000 multichannel potentiostat with 24 independent floating channels (Arbin Instruments) and a Parstat MC potentiostat (Ametek).

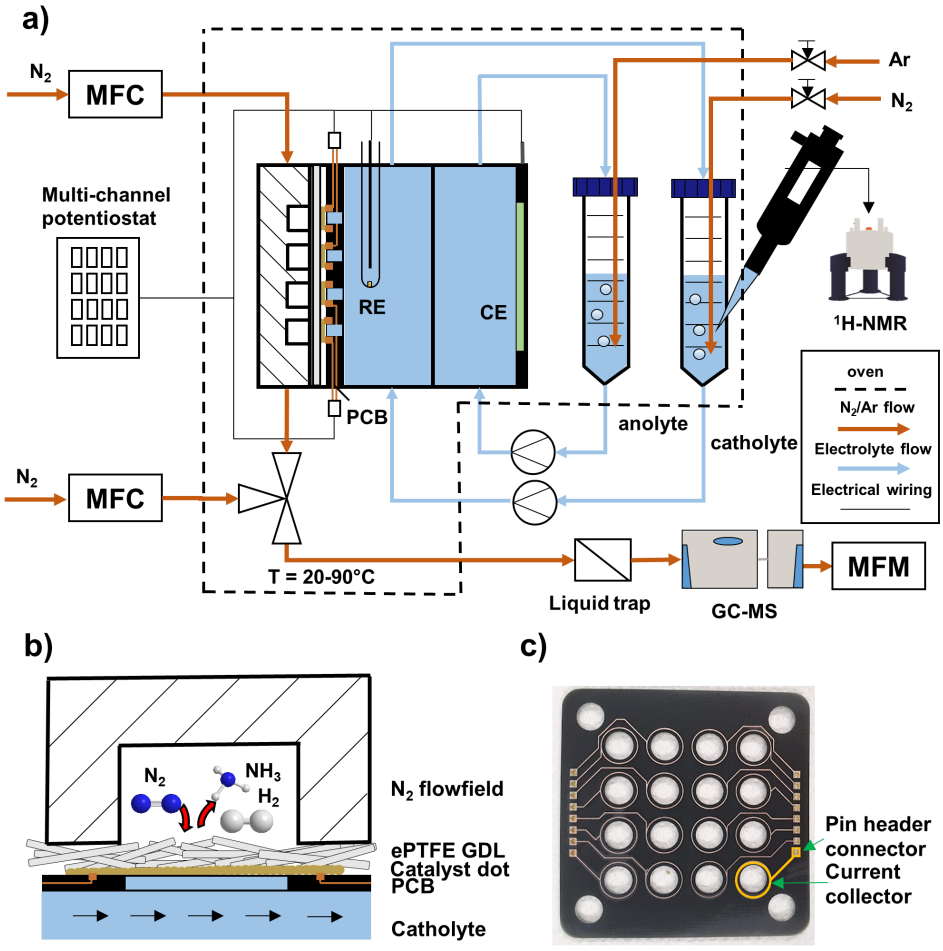

Figure 4.2: a) Schematic of the experimental setup to screen 16 bimetallic electrocatalysts in parallel in a gas diffusion electrode cell. (b) Zoom-in schematic of one catalyst to illustrate how each catalyst was supplied with electrons, N_2 and electrolyte. (c) Photograph of the printed circuit board (PCB) that was used to electrically connect the catalyst array to the potentiostat.

To electrically connect each of the 16 catalysts to the multichannel potentiostat, a printed circuit board (PCB) was custom-designed and manufactured by JLCPCB. The PCB was sandwiched between the gas compartment and the catholyte compartment of the HTP cell to create an electrical contact between the catalysts and the current collectors on the PCB (Figure 4.2b). The current collectors on the PCB are electrically connected to pin header connectors which enables quick connection of the multichannel potentiostat to all 16 catalysts (Figure 4.2c). Each hole in the PCB has a diameter of 6 mm which exposes a catalyst surface area of 0.28 cm^2 to the electrolyte. To prevent contamination of the electrolyte with substances from the PCB, a silicone coating (RS-components) was applied to the PCB. The catholyte and anolyte were recirculated between cell and reservoirs using a Masterflex L/S peristaltic pump. A Bronkhorst mass flow controller (MFC) and mass flow meter (MFM) were installed to control the flow of N_2 into the cell and measure the flow of N_2 leaving the cell, respectively. The temperature of the system was controlled using a home-built oven. Downstream of the gas compartment, a gas chromatography-mass spectrometry (GC-MS) measured the concentration of NH_3, O_2 and H_2 in the gas phase. The details of the GC-MS method have been presented elsewhere.[46] A home-built liquid trap was installed as a precautionary measure to prevent flooding of the GC-MS with electrolyte. However, the liquid trap might be redundant, because electrolyte did not enter the gas compartment a single time during our experiments. N_2 and Ar were supplied by Linde and had a purity of 99.999%. N_2 and Ar were not purified because the concentration of NH_3 in both was below the detection limit of our GC (150 ppb) and the NO concentration in both was less than 10 ppb as measured with an NO analyzer (Teledyne 200E). Since we used low flow rates (1–10 sccm) and short electrolysis durations (<75 min), contaminations at this level are too low to cause false positives.[16] Additionally, we measured both the NH_3 and NOx background in the electrolyte for every experiment with NMR and Ion Chromatography (IC), respectively and found no correlation between the background level and the amount of gas that was in contact with the electrolyte.

Electrochemical Tests

In a typical experiment, a catalyst array was first positioned over the electrical contacts of the PCB. After assembly of the cell, the catalyst array was checked for short-circuits using an ohmmeter. To minimize NH_3 and NOx backgrounds, 0.1 M KOH (prepared fresh daily) was recirculated between cell and reservoirs 2–3 times for 5 min each. The flow rate of the catholyte and anolyte was set to 15 mL/min during all cleaning steps and electrochemical tests. For the electrochemical test, the reservoirs of catholyte and anolyte were filled with 14 mL and 12 mL 0.1 M KOH, respectively. The O_2 in the electrolyte was removed by bubbling N_2 or Ar into the catholyte and anolyte for at least 15 min while recirculating the electrolyte. The flow rate of N_2 and Ar into the reservoirs was set to approximately 10 sccm using a needle valve. The gas compartment of the cell was flushed with N_2 at a flow rate of 10 sccm. To equilibrate any processes that might take place on the catalyst surface once a current is applied (reconstruction, dissolution), a preelectrolysis step was carried out before the electrochemical characterization. During the preelectrolysis step, the same current that would later be applied during the catalyst screening

was applied to each catalyst for 5 min. The electrochemical characterization of the attainable currents and voltages was carried out by applying a chronopotentiometry (CP) staircase in the current density range 1.4–4.3 mA cm^{-2} consisting of 5 steps of 30 s each. Only one catalyst at a time was characterized this way. Since the electrochemical characterization of all 16 catalysts of every catalyst array would have been too time-consuming, only the catalysts at positions 1,6,11,16 and 14,15,16,17 were characterized for a 90°/180°-sample, respectively (catalyst position according to Figure 4.1e). Prior to the electrolysis step to measure the NRR activity of the catalysts, the flow rate of the gas bubbling into the electrolyte reservoirs was reduced to approximately 3 sccm to minimize potential NH_3/NOx contaminations from the feed gas. The N_2 flow rate into the gas compartment was set to 1 sccm unless high oxygen levels made it necessary to increase the flow rate to prevent ORR on the catalyst surfaces. Two CP steps were carried out to measure the NRR activity of the catalyst arrays. During both CP steps a constant current was applied to all catalysts in parallel. The first CP step was carried out at room temperature (henceforth referred to as "RT-experiment") and had a duration of 70 min. The current density that was applied to each catalyst ranged from 1–10 mA cm^{-2} and depended on its position in the cell and the orientation of the sputter guns during co-sputtering of the sample (90° or 180°). A map that shows which current density was applied to each catalyst position for a 90°/180°-sample is shown in Figure 4.11. In general, we tried to minimize redundancy and test as many different current densities and catalyst layer thicknesses for each composition as possible. During the second CP step (henceforth referred to as "55°C-experiment), the same current densities as during the RT-experiment were applied for 60 min while the electrolyte was slowly heated to 55 °C using a custom build oven. The heating profile of the oven (Figure 4.14) allowed a GC-MS injection every 5–10 °C. Water condensation in the gas line had to be prevented to avoid damage to the GC-MS. Therefore, the gas stream exiting the cell was diluted with N_2. The dilution was gradually increased with increasing temperature of the electrolyte from 1:2.5 in the beginning to 1:10 after 30 min. After an experiment, the cell was disassembled and the catalyst array was removed from the PCB. Residues of the previous catalyst were removed from the PCB with grade 1200 abrasive sheets (RS-components). Before reusing, the PCB was washed with soap and rinsed with Milli-Q water. To quantify NH_3/NOx backgrounds a 2 mL sample was taken from the catholyte after the O_2 removal step. The ammonia production during the RT-experiment and the 55°C-experiment was determined by taking a 1 mL sample from the catholyte after each step.

iR-compensation

The uncompensated ohmic resistance between the RE and a catalyst was found to depend on the position of the catalyst in the cell. Figure 4.3a and b show a map of the ohmic resistance between the 16 WEs and the RE as a function of their respective position in the cell for two catalyst arrays consisting of 16 Ag catalysts with identical Ag layer thickness (300 nm), measured by electrochemical impedance spectroscope (EIS). The maximum resistance deviation was 16 Ω which would only cause a 9.6 mV shift in potential at the current of electrochemical characteriza-

tions (600 µA). This potential inaccuracy is negligible for the scope of our screening which is focused on finding selective catalysts. Therefore, we used the resistance map in Figure 4.3a to compensate iR-drops during all electrochemical characterizations (100% post-correction). No iR-compensation was possible for experiments with multiple catalysts running in parallel because during those experiments the electric field of up to 16 WEs overlapped each other which would have made iR-compensation very complex.

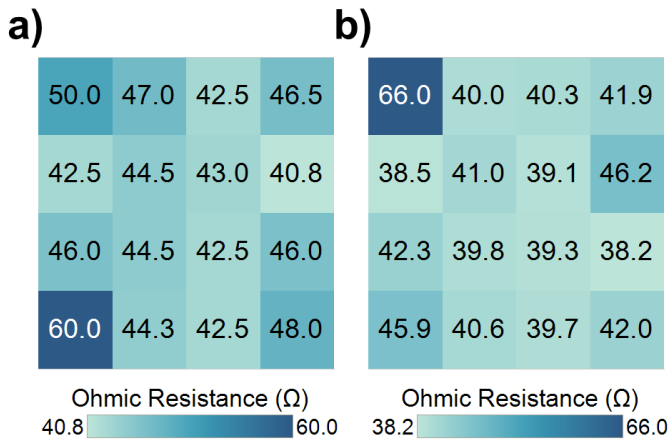

Figure 4.3: Ohmic resistance map for two separate samples containing 16 300 nm Ag catalysts.

4.3. Results and Discussion

Physical Characterisation

To demonstrate that HTP characterization with XRD can be integrated into the workflow, we measured the XRD patterns of a 180°-PdRu-sample. The XRD patterns of the 180°-PdRu-sample and the reference patterns of Pd and Ru are shown in Figure 4.4a. The diffraction peaks at 2θ = 38.3°, 42.2°, 44°, 58.3°, 69.4° and 78.4° could be assigned to the characteristic (100), (002), (101), (102), (110), (103) crystal planes of Ru, respectively and the diffraction peaks at 2θ = 40.1°, 46.7°, 68.1° could be assigned to the characteristic (111), (200), (220) crystal planes of Pd, respectively. Since the catalysts were sputtered at 180°, catalysts in the same column have a similar composition (Figure 4.1e) which leads to similar XRD patterns (Figure 4.4a). A shift from a Pd-rich (catalysts 1 to 4) to a Ru-rich composition (catalysts 13 to 16) can be observed which agrees well with the expected shift in composition for a 180°-PdRu-sample. To examine the morphology of ePTFE with and without catalysts deposited onto it, we recorded SEM images of a PdCu sample (Figure 4.4b–e). Figure 4.4b shows the morphology of the ePTFE before deposition. The material is comprised of macroscopically-small Teflon filaments which form a fibrous network. After deposition of 300 nm PdCu, the surface was almost completely covered with PdCu (Figure 4.4c). After the electrochemical experiments to

measure the NRR activity the morphology seems similar at high magnification but at lower magnification cracks in the surface are visible (Figure 4.4d,e).

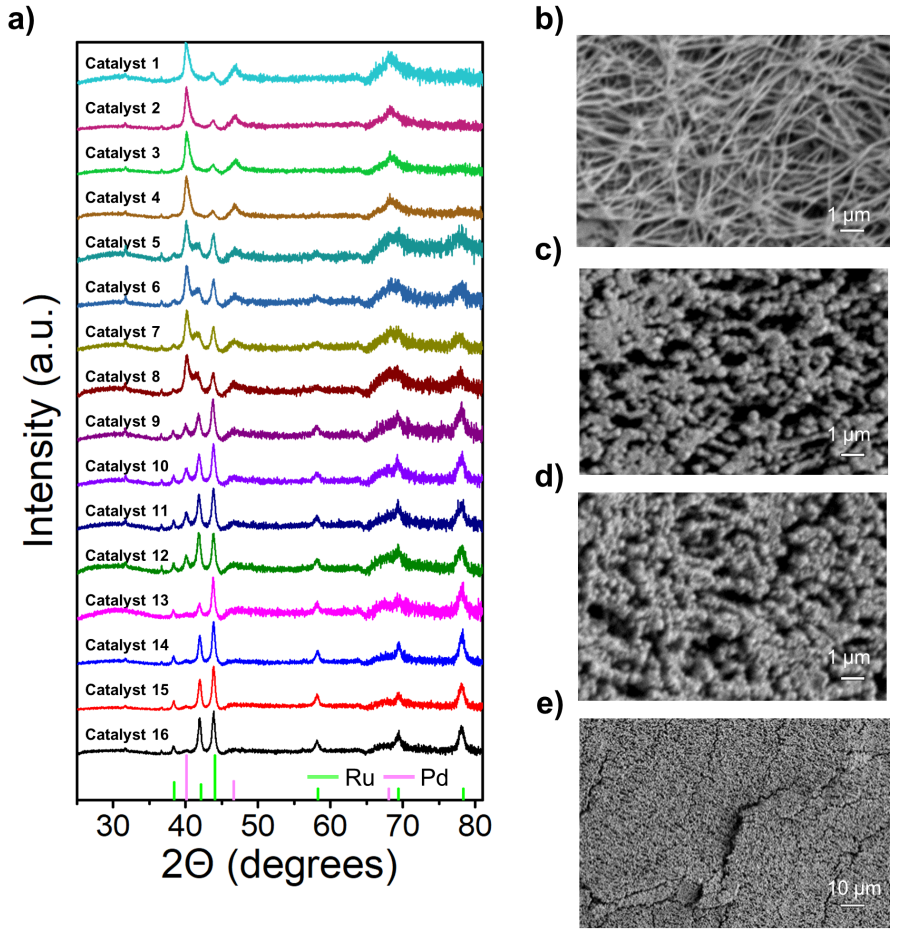

Figure 4.4: a) XRD patterns of a PdRu catalyst array sputtered at 180° and reference patters of Ru and Pd. b) SEM image of ePTFE with 200 nm pore size. c),d) SEM images of 300 nm PdCu sputtered on ePTFE before and after electrolysis, respectively. e) Same position as d) but with lower magnification. Acceleration voltage for SEM images: 5 kV.

Control of thin-film composition

To validate that the composition of material libraries produced for this study can be accurately controlled using co-sputtering, we sputtered a CoMo composition gradient on a microscope slide and measured its bulk composition using EDX (Figure 4.5a). The measured composition gradient agrees well with the predicted compositions from the deposition rates of Co and Mo. This confirms that the bulk compositions of catalyst arrays can be accurately controlled by co-sputtering.

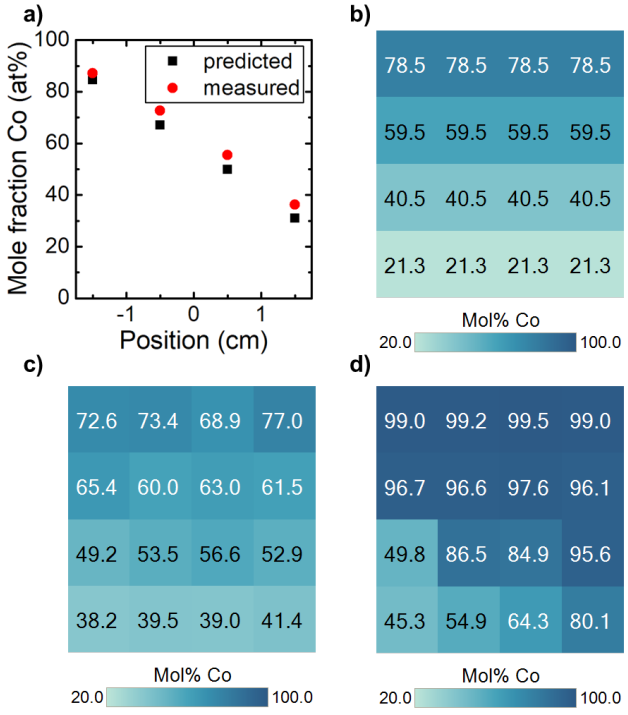

Figure 4.5: a) Comparison of the composition of a CoMo thin film (co-sputtered on a microscope slide) predicted from the sputter rates of Co, Mo and the bulk composition measured by EDX. b) Predicted composition of a 180°-CoMo-sample from the sputter rates of Co, Mo c),d) measured surface composition by XPS before and after electrolysis, respectively.

To measure if the surface composition of CoMo also agrees well with predicted values, the surface compositions of a 180°-sample of CoMo was measured with XPS and compared against the predicted compositions (Figure 4.5b,c). The surface compositions of CoMo agree well with the predicted compositions for the top two catalyst rows whereas a shift towards higher than predicted Co mole fractions can be observed for the bottom two rows. After the electrochemical tests to measure NRR activity, the surface of most catalysts is strongly enriched in Co which indicates that Mo either dissolved into the electrolyte or was replaced by Co on the surface (Figure 4.5d). Interestingly, in the rows with the lowest initial Co concentration (bottom two) the Co composition increases from left to right after electrolysis which indicates that the applied current density during electrolysis might influence how much Mo remains on the surface. The applied current density during the electrochemical tests was 10 mA cm^{-2} on the left side and decreases stepwise to 1 mA cm^{-2} on the right side which indicates that high applied current densities might stabilize Mo on the surface if the initial Co concentration is less than 50 mol%. A detailed investigation of the phenomena underlying these composition changes goes beyond the scope of this work. What is important to know for this study is that initial bulk compositions

of catalysts can be accurately controlled but surface compositions, especially after contact with the electrolyte, might differ strongly from the initial bulk composition. While being able to control initial bulk compositions is sufficient for a preliminary catalyst screening (which is the goal of this study), studies that aim to measure activity-composition relationships must use in situ/operando tools to measure the surface composition during electrolysis.

Characterization of the N_2 mass transport

An important prerequisite for any HTP catalyst screening is that false negatives (i.e. non-discovery of active materials although they were part of the screened library) must be prevented.[22] In the following, we will discuss some of the control experiments that were carried out to confirm that some common causes of false negatives can be excluded in this study. For the sake of brevity, we will only discuss the N_2 mass transport and the reproducibility of electrochemical characterizations in the main manuscript. Further control experiments to confirm that no side reactions occurred and that the ammonia detection worked properly for every sample can be found in Section 4.5.

To confirm that NRR selectivity losses due to N_2 mass transport limitations can be avoided with the HTP GDE cell, we wanted to measure the mass transport limiting current for NRR. However, the mass transport limiting current for NRR cannot be measured directly because there is no selective catalyst for this reaction, yet. Instead, we used ORR to characterize the mass transport which should give comparable results because O_2 and N_2 have similar water solubility.[34, 47] Figure 4.6a shows the polarization curve of a 300 nm Ag catalyst measured in N_2 and in a gas mixture of 5.2% O_2 in N_2. In 5.2% O_2, the onset of ORR begins around 0.8 V vs. reversible hydrogen electrode (RHE) and reaches a plateau around 0.1 V vs. RHE. In N_2, HER starts at around -0.4 V vs. RHE which is sufficiently far away from the start of the ORR plateau in 5.2% O_2 to ensure that HER did not contribute significantly to the ORR limiting current measured in 5.2% O_2. To measure the ORR mass transport limited current density in 5.2% O_2 for each catalyst position in the cell, we applied a potential of 0 V vs. RHE to all 16 Ag catalysts for 150 s, subsequently (Figure 4.6b). As Figure 4.6c shows, the stable current after 150 s is 10–22 $mA\,cm^{-2}$ for three fresh Ag samples. As Figure 4.6d shows, the O_2 mass transport depends linearly on the O_2 concentration which means that the current density measured in 5.2% O_2 can be extrapolated to 100% O_2. The resulting mass transport limited current density in 100% O_2 is 192–423 $mA\,cm^{-2}$. For comparison, other HTP cells such as single compartment cells or scanning droplet cells reach ORR mass transport limitations around 0.6–1.6 $mA\,cm^{-2}$.[25, 30, 33] This demonstrates that the HTP GDE cell reaches mass transport limitations at two orders of magnitude higher current densities than conventional HTP cell designs which is far more than needed to prevent NRR selectivity losses due to mass transport limitations.

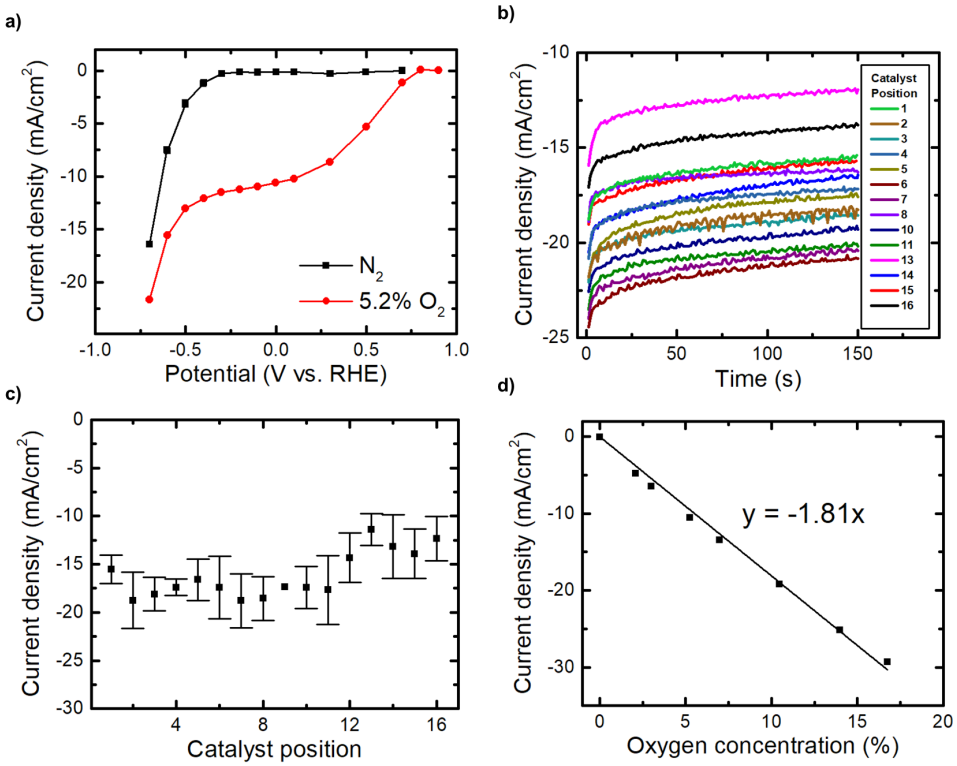

Figure 4.6: a) Polarization curve of a 300 nm Ag catalyst measured in pure N_2 and 5.2% O_2 in N_2. b) Chronoamperometry at 0 V vs. RHE for 150 s in 5.2% O_2 for 16 300 nm Ag catalysts. c) Average current density during the last 5 s of the experiment in b). Error bars represent a triplet measurement with different samples. d) Dependence of current density at 0 V vs. RHE on the oxygen concentration entering the gas compartment of the cell. The data is not iR-compensated.

Reproducibility of the electrochemical characterization

We investigated the reproducibility of electrochemical characterizations with the HTP cell by measuring linear scan voltammetry (LSV) scans for a catalyst array consisting of 300 nm Ag catalysts. As demonstrated in Figure 4.7, the reproducibility across the different catalysts of the array is very good (only around 50 mV maximum potential difference). The potential difference may be caused by morphological inhomogeneities across the ePTFE. GDEs with small geometric surface area are especially prone to these deviations because manufacturing inhomogeneities across the GDE cannot be averaged out as for larger samples.[37] To test the reproducibility of the electrochemical characterization across different samples we repeated the test with a Ag catalyst array produced under identical conditions and found that the LSV's from the second sample closely matches those from the first sample. One LSV from a catalyst of the second sample slightly deviates from the other LSVs at higher current density. The potential difference increases linearly with the current density

which indicates that this catalyst has a higher ohmic resistance than the other catalysts. Presumably, the increase in resistance was caused by a reduced electrical contact between the PCB and the catalyst. The potential difference between the catalyst with higher resistance and the rest was around 50 mV at the current which was used for electrochemical characterizations (600 µA) in the following. Therefore, the electrochemical characterization is very reproducible across different catalysts of an array and different samples but in rare cases increases in resistance can lead to potential shifts up to 50 mV.

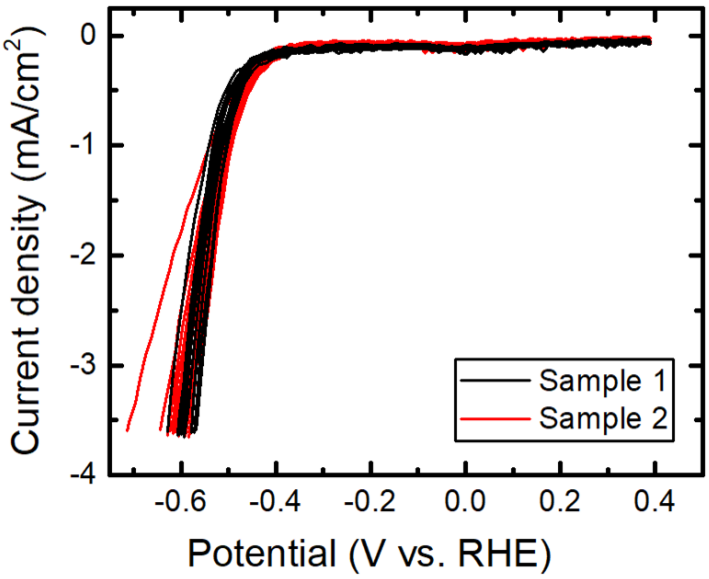

Figure 4.7: Reproducibility of LSVs measured for two catalyst arrays consisting of 300 nm Ag catalysts. Scan rate: 15 mV/s.

Characterization of the electrochemical HER activity

Since HER is the main competing reaction of NRR, a comprehensive dataset of the HER activity of bimetallic catalysts may be useful for the selection of promising catalysts for NRR. However, no such dataset is publicly available, yet. Therefore, we show in Figure 4.8 the electrode potential of 4 compositions from each bimetallic catalyst array at a current density of 2.14 mA cm^{-2} (i.e. 600 µA current). We chose a current density of only 2.14 mA cm^{-2} to minimize errors from uncompensated ohmic resistance between the RE and the catalyst array.

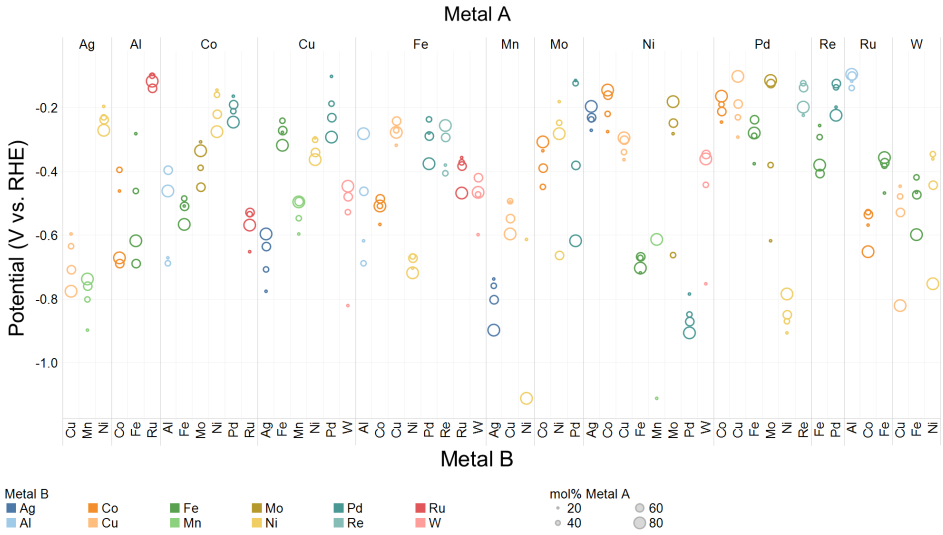

Figure 4.8: Average potential during the last 5 s of the electrochemical characterization at 0.6 mA (2.14 mA cm^{-2}) for each catalyst tested in this work. The size of the symbols represents the predicted mole fraction of metal A in the catalyst (accuracy: ±10%). Some data points of MnNi are outside of the plotted range. Each composition appears twice, both as AB and BA.

Each bimetallic catalyst appears twice in Figure 4.8, both as AB and BA which makes it easier to compare all bimetallic catalysts containing a certain metal. The HER activity was highest (E >-200 mV) for most Ni- and Pd-catalysts and lowest (E < -400 mV) for transition metal oxides (W-, Mn-catalysts). This activity trend agrees well with the expected activity of these metals from literature data.[48–50] Similarly, the activity trend of different Ni-catalysts agrees well with literature.[51, 52] A more detailed comparison of HER activity trends with literature is available in Section 4.5. Due to the difficulty of producing NH_3 concentrations above background level from NRR (see the following section), we were unable to predict promising materials for NRR from the HER activity data. However, the data might benefit future efforts in this direction.

NRR activity of bimetallic electrocatalysts

To quantify the NRR activity of each catalyst array, we measured the difference between the NH_3 concentration in the electrolyte before and after every experiment (henceforth referred to as "NH_3 production") and calculated the corresponding NRR current. Since all 16 catalysts of an array were placed in the same electrolyte, it was only possible to measure the combined NRR current of a catalyst array and not the individual NRR current density of each catalyst. The NRR current of all catalyst arrays is shown in Figure 4.9 and Figure 4.10 for the RT-experiment and the 55°C-experiment, respectively. Besides the color gradient to visualize the NRR current we also reported the NH_3 production underlying the calculation of the NRR current and the NH_3/NOx background for all catalyst arrays. Negative NRR currents (blue)

in Figure 4.9 and Figure 4.10 were most likely caused by larger NH_3 backgrounds in the liquid sample taken before the electrochemical experiment was started. No data from the gaseous NH_3 detection is shown because the detection limit of the GC-MS (1 ppm NH_3 in the gas phase) was not reached by any catalyst array.

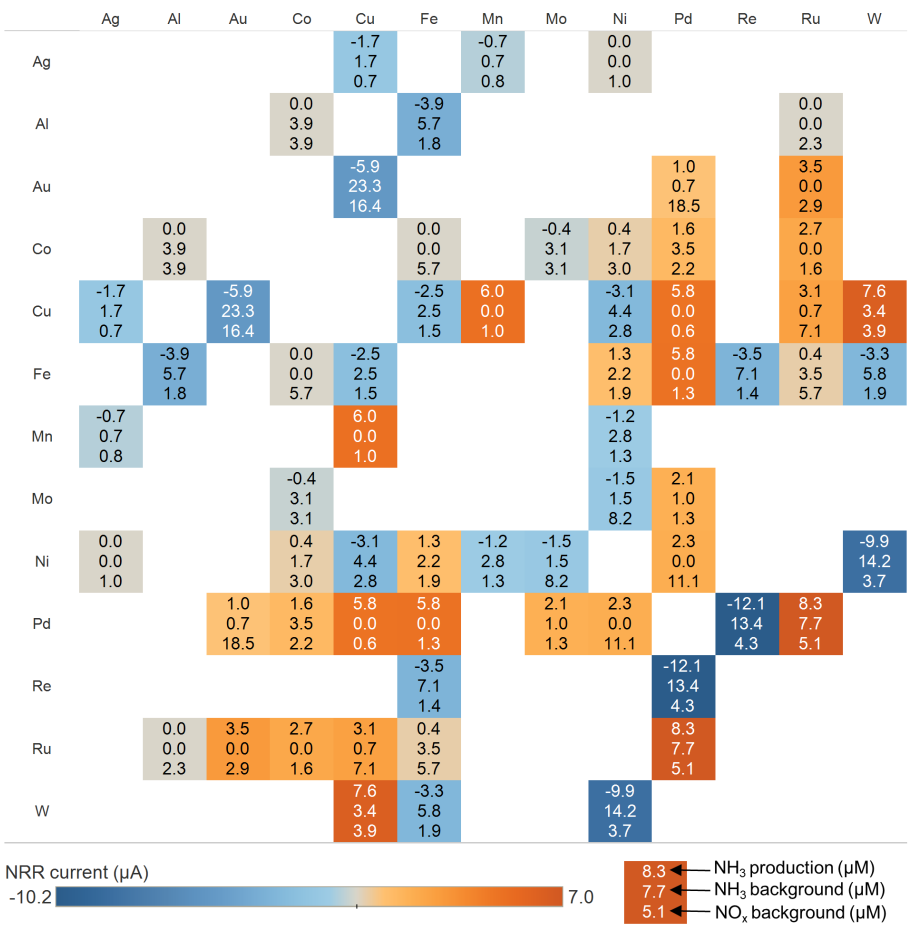

Figure 4.9: NRR activity of the bimetallic catalysts during the RT-experiment. The color represents the NRR current that corresponds to the NH_3 production assuming that all NH_3 was produced from NRR. The NH_3 production, NH_3 background and NOx background are reported for each catalyst array.

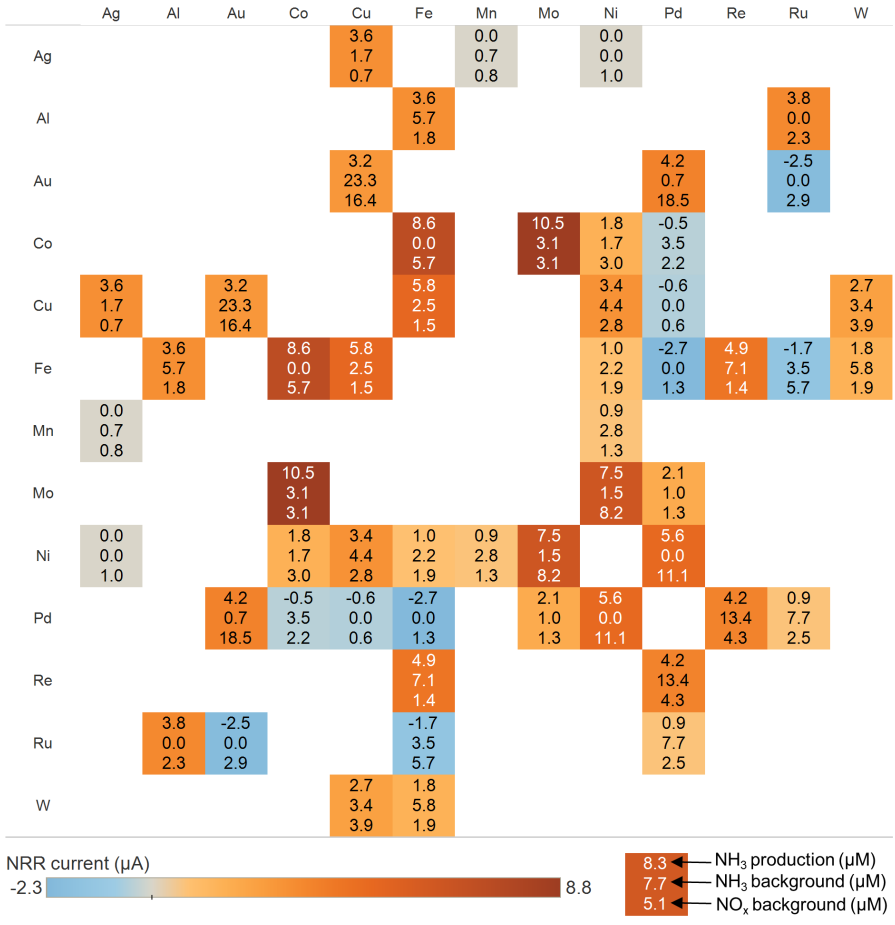

Figure 4.10: NRR activity of the bimetallic catalysts during the 55°C-experiment. The color represents the NRR current that corresponds to the NH_3 production assuming that all NH_3 was produced from NRR. The NH_3 production, NH_3 background and NOx background are reported for each catalyst array.

The largest NRR current that we measured was around 9 µA (CoMo during the 55°C-experiment). Even if all of the 9 µA NRR current were produced by only one of the 16 catalysts of a catalyst array, this corresponds to an NRR current density of ≈30 $\mu A\,cm^{-2}$ (electrode area: 0.28 cm^2) which is only around 10% faradaic efficiency (FE) at the lowest current density used during the screening. Therefore, the most important result of this work is that the 528 bimetallic catalysts that were screened in this work are not promising catalysts for NRR under the tested conditions. If any of the screened catalysts were active for NRR at all their faradaic efficiency was less than 10

It is apparent from Figure 4.9 and Figure 4.10 that NH_3/NOx backgrounds between 0–-4 µM were present for every tested catalyst array. At such low concentrations,

there are many different potential contamination sources. Some of those contamination sources such as the atmosphere, human breath or surfaces that are in contact with the electrolyte are difficult to remove which leads to unavoidable backgrounds.[17, 20, 53, 54] Other research groups have reported unavoidable backgrounds on the order of 0.5–2 µM during their NRR experiments which agrees well with our observations.[17, 53, 54] It is very easy to misinterpret NH_3/NOx backgrounds as NRR activity because some contamination sources can cause a linear increase of the NH_3 concentration over time (e.g. NOx electroreduction to NH_3 or a slow leaching process from a membrane), which looks like NRR activity.[20] To avoid being misled by false positives, we only carried out further experiments with a catalyst array if its NH_3 production was significantly higher than the common NH_3 background. The threshold for further investigation was 3-fold the common NH_3/NOx background of 4 µM (i.e. 12 µM). Unfortunately, the NH_3 production of all catalyst arrays in Figure 4.9 and Figure 4.10 was below this threshold which means that the NH_3 production from NRR (if present if all) of all tested catalyst arrays is indistinguishable from NH_3 contamination.

As a side note, it is noteworthy that both the NH_3 and NOx background had considerable variance over time which suggests that it is insufficient to measure either one of these backgrounds only during one experiment and assume they remain constant for the all following experiments as it is frequently done in the NRR research field to prove that no contaminations were present during experiments.[16] Instead, NH_3/NOx backgrounds must be measured and reported for every NRR experiment, especially if NRR activity is deduced from NH_3 productions on the order of a few µM. In addition, we believe that the NRR research field would benefit from more transparently reported backgrounds because, as we have shown above, the magnitude of backgrounds relative to alleged NH_3 production from NRR is a great indicator of the reliability of a measurement.

We observed spikes in the NH_3 production for NiCu (16.6 µM) at room temperature and for FeCu (17 µM) and PdCu (71 µM) during the 55°C-experiment. However, subsequent attempts to reproduce these results failed which means that the original results were caused by NH_3 contamination. Random spikes of the NH_3 concentration in the electrolyte are common in NRR research. For example gloves, sample storage containers or cell surfaces can randomly introduce large amounts of NH_3 which can lead to false conclusions.[17, 54] In the case of PdCu, the NH_3 contamination might have originated from the reduction of NOx, because an unusually high NOx background (35.9 µM) was measured before the electrolysis was started. This is plausible because Cu is known to be an efficient catalyst for NOx reduction to NH_3.[55] To avoid misleading the reader, we don't report these false positives in Figure 4.9 and Figure 4.10.

The NH_3 production of some catalyst arrays was slightly higher than the common NH_3 background of 4 µM. In some cases (e.g. CuW, RuPd at room temperature) this coincided with the presence of an elevated NH_3/NOx background indicating the

experiment might have been more contaminated than the rest. In other cases, (e.g. CuMn, CuPd, FePd at room temperature) the NH_3 production was slightly elevated while the NH_3/NOx background was low. Yu et al. showed that µM-levels of NH_3 in the electrolyte might originate from nitrogen impurities which were incorporated into sputtered CoMo thin films during the sputtering process.[56] Since CoMo had the highest NH_3 production of all catalysts during the 55°C-experiment we suspect that nitrogen impurities incorporated during the sputtering process might have contributed to the slightly elevated NH_3 productions of some catalyst arrays. However, a systematic investigation of NH_3 contaminations from the sputtering process goes beyond the scope of this work.

Since none of the tested bimetallic catalysts produced NH_3 significantly above background level, it is questionable if bimetallic catalysts are promising for future NRR catalyst development efforts. This view is supported by theoretical considerations based on DFT calculations by Montoya et al. who argued that alloying is not a promising strategy for NRR catalyst development because the scaling relations between the key adsorbates are unlikely to be broken by alloying.[5] However, we have only screened a small fraction of the bimetallic composition space. It is therefore possible that active bimetallic catalysts were missed in this work. In addition, the selectivity of electrocatalytic reactions can be influenced by many factors (e.g. electrolyte, pressure, catalyst morphology etc.) which were not varied in this study. Therefore, bimetallic catalysts which were inactive for NRR in our study might be active under different conditions.[57] Our large dataset of negative results is counteracting the overrepresentation of positive results in literature.[21] Until published positive results of NRR activity meet the requirements of unambiguous NH_3 detection, large datasets of negative results might be more useful to steer future research towards the most promising catalyst development strategies.[15–17]

Screening speed and robustness with the HTP GDE cell

The primary goal of developing a HTP catalyst screening workflow is to increase the speed of a catalyst screening. Therefore, we want to briefly analyze how much quicker catalysts can be screened with the workflow presented in this work and which steps must be accelerated for further improvements. With the HTP workflow presented in this work it took approximately 40 h to screen one set (i.e. 96 catalysts) which is approximately an order of magnitude faster than traditional approaches. Assuming no downtime in a highly automated system, approximately 5000 catalysts could be screened per year at this speed. It took between 6–16 h to sputter the catalyst arrays. The duration of the sputtering step depended strongly on how many sputter rates had to be measured before the sputtering of the catalyst arrays. The characterization steps using XRD and XPS took only around 2 h of bench time per catalyst set because the machines were mostly automated and could run overnight. However, the data processing and analysis of the physical characterization data proved to be a bottleneck which is why we only did this for selected catalyst arrays. The electrochemical experiments to screen one set took around 24 h (including all preparation steps) and the product analysis step took an

additional 2–3 h (including data analysis and visualization). Therefore, future acceleration efforts should focus on accelerating the electrochemical experiments and the catalyst deposition. An electrical contact between catalyst and multichannel potentiostat was successfully established for 97% of the screened catalysts which confirms that the robustness of the cell is comparable to cells used for one-by-one catalyst testing (see Section 4.5 for more information).

4.4. Conclusions

We presented a high-throughput workflow to screen bimetallic electrocatalysts for NRR activity which is approximately an order of magnitude faster than a one-by-one catalyst screening and can be adapted to other reactions of interest and other classes of materials. The GDE cell design used for parallel screening of electrocatalysts enables two orders of magnitude higher mass transport limiting currents for reactions with gaseous reactants such as N_2 or O_2 which circumvents the activity/selectivity losses due to mass transport limitations that can be expected with previous HTP cell designs. A screening of 528 bimetallic catalysts for NRR activity did not yield an active catalyst for the reaction. In the absence of unambiguous positive results, large datasets of negative results for NRR, as the one we presented in this work, might be the best available option to steer future research in the direction of the most promising catalyst development strategies.

4.5. Supporting Information

Chemicals

Maleic acid (≥ 99%), potassium hydroxide (>85%) and sulfuric acid (≥ 99.999%) were obtained from Merck Sigma. Gadolinium(III) nitrate hexahydrate (99.9%) was obtained from Fisher Scientific. DMSO-d6 (99.96% D, 0.03% V/V Tetramethylsilane) was obtained from Euriso-top. Ultrapure water was produced with a Milli-Q Advantage A10 water purification system (resistivity: 18.2 MΩ at 25 °C).

Physical Characterization

X-Ray Diffraction (XRD) patterns of all catalyst arrays were acquired semi-automatically using a Bruker D8 Discover with Cu Kα radiation and equipped with a VANTEC500 2D-detector and a 1 mm collimator. Scanning electron microscopy and energy dispersive X-ray spectroscopy (SEM/EDS, JEOL, JSM-6010LA) was utilized to characterize the surface morphology of the ePTFE GDEs and measure the bulk composition of sputtered composition gradients. A Thermo Scientific Kα X-Ray photoelectron spectrometer (XPS) equipped with an Al Kα X-Ray source was used to measure the surface composition of sputtered composition gradients in a semi-automated way.

Calculation: ammonia production and NRR activity

We define the ammonia production during the RT-experiment as the difference in the NH_3 concentration between the sample that was taken after the room temperature experiment and the background sample. Analogously, we define the ammonia

production during the 55°C-experiment as the NH_3 concentration difference between the sample that was taken after the RT-experiment and the sample that was taken after the 55°C-experiment. The NRR current i_{NRR} for both the RT-experiment and the 55°C-experiment was calculated according to:

$$i_{NRR} = \frac{zFV\Delta c_{NH_3}}{t} \tag{4.1}$$

, where Δc_{NH3} is the ammonia production during the respective CP step, V is the volume of the catholyte before the final sample was taken, t is the duration of the electrolysis, z is the number of electrons transferred per molecule of NH_3 produced (3) and F is the Faraday Constant, respectively.

Experimental protocol for the first two catalyst sets

The experimental conditions were slightly different for the first two catalyst sets that were screened (see Table 4.1). During these experiments we learned a few things that led to slight changes in the experimental protocol for the following sets. These changes were small so that it is still appropriate to report the results of sets 1 and 2 together with the rest but for completeness sake we report them here. For the screening of set 1 the current density range was not 1–10 mA cm^{-2} as for the following sets but 1–20 mA cm^{-2}. The reason for the reduction in current density range was that the large electric fields at higher current density caused a gradual depletion of hydroxyl ions in the anolyte (pH dropped from 13 to 11.8). The depletion of hydroxyl-ions led to a drop in conductivity which in some cases caused the potentiostat to reach its maximum voltage and eventually overload and stop the measurement. To avoid overloads, we reduced the current range for the following measurements. The data from set 1 is still comparable to the rest because if overloads occurred, they occurred after minute 56. Therefore, at least 56 minutes of ammonia production were possible during these experiments which is sufficient for a qualitative measurement of ammonia production. For catalyst set 1, we cleaned the cell by rinsing it with ultrapure water while it was disassembled. This proved to be less effective at removing NH_3/NOx backgrounds which is why we switched to flushing the cell with 0.1 M KOH for the following experiments.

For catalyst set 2, we used ePTFE with 450 nm pore size supported on polypropylene instead of the usual pure ePTFE with 200 nm pore size. This led to larger oxygen leakages so that we had to increase the flow rate to 5 sccm. Therefore, 200 nm pore size ePTFE was used in all following experiments.

Ammonia Detection (Liquid)

The concentration of $^{14}NH_3$ in the solution was quantified using an ^1H NMR method with absolute quantification as previously described.[58] This method enables the quantification of NH_3 without requiring a calibration curve because the interscan delay is sufficiently long (>5T1) to allow full relaxation of the anolyte and the internal standard. To prepare the NMR sample, 550 µL sample solution, 50 µL 3 M sulfuric

acid (freshly prepared) and 50 µL detection solution were mixed inside an Eppendorf tube using a Vortex mixer. Then, 600 µL of this solution were transferred to an NMR tube. The detection solution consisted of 3.21 mM maleic acid (MA) and 12.86 mM gadolinium nitrate hexahydrate diluted in DMSO-d6. Since the chemical shift of MA changes with pH, it could be used to confirm that each sample was sufficiently acidified to shift the equilibrium towards NH_4^+, which is detectable by NMR.[59] The signal-to-noise ratio of MA was calculated to validate that the sensitivity during every measurement was sufficient to detect ammonia if it was present in the sample. In addition, standard samples of 50 µM NH_4^+ were measured regularly to validate the functionality of the liquid NH_3 detection.

^1H NMR spectra were acquired using a 400 MHz Fourier transform NMR spectrometer equipped with an autosampler and an autotunable, temperature regulated Agilent OneNMR room temperature probe. The temperature was set to 25 °C and the receiver gain was optimized automatically. The excitation sculpting pulse sequence "waterES" was used to suppress the resonance of water during acquisition. The acquisition parameter were: acquisition time: 1 s, recycle delay: 0.05 s, number of scans: 1024. The NMR detection method enables quantitative NH_3 detection with a relative error <10% down to 17 µM NH_3 and qualitative detection down to 2.5 µM.[58]

Ammonia Detection (Gaseous)

The NH_3 in the gas stream leaving the gas compartment of the electrochemical cell was detected using GC-MS as described elsewhere.[46] Briefly, the gas stream is first flowing through a multiport switching valve (VICI Valco) before entering the sample loop (internal volume: 500 µL) of the GC-MS (Agilent). At the moment of injection, the sample is transported with He carrier gas through two Select Low Ammonia capillary columns. Using the optimized temperature/pressure profiles described in detail in Ref. [46], the ammonia is then separated from other constituents of the gas stream. Once eluted out of the columns, the sample is partitioned between a pulse discharge detection (PDD) and a single quadrupole mass spectrometer (ISQ) which are used to detect NH_3. O_2 and H_2 are detected using a separate sample loop (internal volume: 250 µL). At the moment of injection, the sample is transported with He carrier gas through a Hayesep N column and a Molsieve 5A column. Once eluted out of the columns, O_2 and H_2 are detected using a PDD detector. The system was assembled by Interscience BV. The mass spectrometer had a detection limit of around 1 ppm for NH_3. Calibration gas standards of 2 pmm NH_3 and 13.8 ppm NH_3 were measured regularly to validate the functionality of the GC-MS.

NOx Detection (Liquid)

The concentration of nitrite and nitrate was determined by ion chromatography (IC; Dionex Integrion HPIC System, Thermo Scientific). The IC was equipped with a conductivity detector and AS18-Fast anion column. Autoneutralization was installed to

enable accurate measurements at high KOH concentrations.

NOx Detection (Gaseous)
A Chemiluminescence Nitric Oxide (NO) Analyzer (200E, Teledyne) was used to measure the NO background of our in-house supply of N_2 and Ar. The detection limit of the NO analyzer was 0.5 ppb.

Data Analysis
Electrochemical data from the Arbin multichannel potentiostat was processed using the open-source software cellpy. Electrochemical data was visualized using the software packages Tableau and Origin Pro. NMR data was processed using the software MestReNova as described earlier.[58] XRD patterns were analyzed using the Diffrac.eva software. GC-MS and IC data were analyzed using the Chromeleon software package.

Prevention of side reactions during NRR catalyst testing
To exclude that side reactions on the current collector occurred we measured the current at a potential of -0.8 V vs. RHE without catalyst (only ePTFE). The resulting current density was less than 0.05 $mA\,cm^{-2}$ on all 16 catalyst positions which is 5% of the lowest current density applied during the catalyst screening and is therefore negligible. Since ORR occurs at lower overpotentials than HER/NRR, high O_2 concentrations in the HTP cell can lead to ORR taking place on the catalyst surface instead of HER/NRR. To investigate if this is the case, we applied a constant potential of 0.1 V vs. RHE to all 16 Ag catalyst dots in parallel while flowing 1 sccm N_2. The resulting ORR current densities were again smaller than 0.05 $mA\,cm^{-2}$ which confirms that the contribution of ORR to the current is negligible. Since the leak-tightness of the cell can change over the course of a screening which can take several months, we validated that the O_2 concentration is sufficiently low during every HTP experiment using GC-MS (Figure 4.17). Since the PDD detector used in this study to measure O_2 is extremely sensitive, the O_2 concentration in the HTP cell was above the linear range of the detector but it was still possible to measure the concentration qualitatively by looking at the peak shape. The O_2 peak that appears at around 1.4 min transitions from a normal peak shape to a wider, cut-off-looking peak shape between 0.03% and 0.2% O_2. We made sure that during every HTP experiment the O_2 peak shape corresponded approximately to the shape labelled "background" in Figure 4.17 which is the concentration at which the ORR current density is smaller than 0.05 $mA\,cm^{-2}$. If the O_2 peak was larger than the peak labelled "background" in Figure 4.17, the flow rate of N_2 was increased until the O_2 concentration was sufficiently reduced. This was only necessary for catalyst sets 1 and 2 because after screening those we realized that PTFE tubing is a source of O_2 leakage and replacing it with stainless steel tubing allowed flow rates of 1 sccm.

HER activity of bimetallic catalysts
The catalysts with the highest electrochemical activity (E >-200 mV) in Figure 4.8 contain almost all either Ni or Pd (exception: AlRu which is in agreement with

expectations because Ni-based catalysts are the most widely studied catalysts for alkaline HER.[48, 49] The high activity of Pd-catalysts is unsurprising because Pd is platinum-group metal and Pt has the highest reported activity for alkaline HER.[60] Among the Ni-based catalysts the activity decreases in the order NiCo > NiMo > NiAg > NiCu > NiW > NiMn > NiFe > NiPd which is quite similar to the trend observed by Raj et al.: NiMo > NiCo > NiW > NiFe.[51] In our screening NiMo is more active than NiCo but the difference between the two is small. The maximum activity for NiMo is obtained in the composition range 60–80 mol% Ni which is in agreement with literature.[61] The activity trend reported by Domínguez-Crespo et al. comparing Ni-catalysts with CoMo agrees with our data: $Co_{30}Ni_{70}$ > $Ni_{30}Mo_{70}$ > $Co_{30}Mo_{70}$.[52] For palladium-based alloys the activity decreases in the order PdCu > PdMo > PdRe > PdCo > PdFe » PdNi. We did not find a dataset to compare this trend with, possibly because Pd is not a promising material for alkaline HER due to its high cost. Interestingly, the bimetallic catalyst that consists of the two most active metals, PdNi, is among the least active catalysts which indicates that it might be promising for reactions that compete with HER. AlRu has the lowest overpotential of all studied catalysts. It is well-known that Raney Ni, i.e. a NiAl alloy, has high activity for alkaline HER because the dissolution of Al in alkaline electrolyte creates a high surface area Ni catalyst.[49, 60] We suspect that a similar reason might explain the high activity of AlRu in our study. Intermediate HER activity (-200 mV > E > -400 mV) was obtained mostly for some Fe-catalysts and NiCu, NiAg. The worst HER catalysts (E < -400mV) were W-,Mn-,Al-catalysts, (exception:AlRu) and Ag-,Co-catalysts (except in combination with Pd or Ni). The poor performance of W- and Mn-catalysts is in agreement with expectations because transition metal oxides are poor HER catalysts unless they are modified to improve HER performance.[50] The typical difference in activity across different compositions is around 100 mV but some bimetallic catalysts (AlFe, CoAl, MoPd, NiW) have much larger differences in activity. All of these catalysts contain at least one metal which should not be stable in 0.1 M KOH according to their Pourbaix diagram (Al, W, Mo) and AlFe, CoAl, NiW showed signs of deactivation after the RT-experiment (described in more detail below) which indicates that the instability of some catalysts might explain the large activity differences.[62]

The previous analysis has shown that HER activity trends that are known from literature can be reproduced using the HTP cell. However, it should be noted that the experimental workflow in this study was optimized for NRR catalyst development, which made it suboptimal for HER activity measurements. For example, the relatively low KOH concentration (0.1 M) used in this study lead to relatively large ohmic drops (Figure 4.3). This was necessary because the electrolyte samples for ammonia quantification had to be acidified with minimal dilution to maximize the NH_3 sensitivity. In addition, the ohmic resistance was not measured for every catalyst to avoid slowing down the experimental throughput for NRR catalyst testing. These limitations precluded the calculation of state of the art HER activity descriptors such as exchange current densities and tafel slopes in our study. Further work with workflows that are optimized for HER might make such measurements possible.

Stability of catalysts and robustness of the HTP cell

Since it might be valuable information for future electrocatalyst development efforts, we here briefly discuss the stability of the catalysts that we screened. We observed no delamination or complete dissolution of catalyst layers except for ReCu and WCu. ReCu completely dissolved upon contact with the electrolyte, and WCu dissolved at high W loadings. This suggests that ePTFE is a suitable substrate for catalyst screenings. For most catalysts, the potential was stable during the RT-experiment and the 55°C-experiment which is another indication of good catalyst stability (Figure 4.19). However, Al,- Mn- ,W-bimetallics were prone to deactivation. From the Al-bimetallics AlCo, AlFe and AlRu, 10/16, 6/16 and 7/16 catalysts lost electrical connection to the potentiostat between the RT-experiment and the 55°C-experiment, respectively. Mn-bimetallics were also unstable as shown by their high overpotentials which in some cases exceeded -1V vs. RHE. As mentioned previously, WCu partially dissolved after electrolysis. The WNi catalyst array completely lost electrical connection to the potentiostat at minute 33 min during the 55°C-experiment due to instability.

To evaluate the robustness of the HTP GDE cell, we calculated how many times a successful electrical connection between potentiostat and catalyst was established. Excluding Mn, Al, W bimetallics and ReCu, a successful electrical connection was established for 560 out of 576 catalysts (97%) that were screened in total in this study (including attempts to reproduce NRR activity). This demonstrates the high robustness of the cell design.

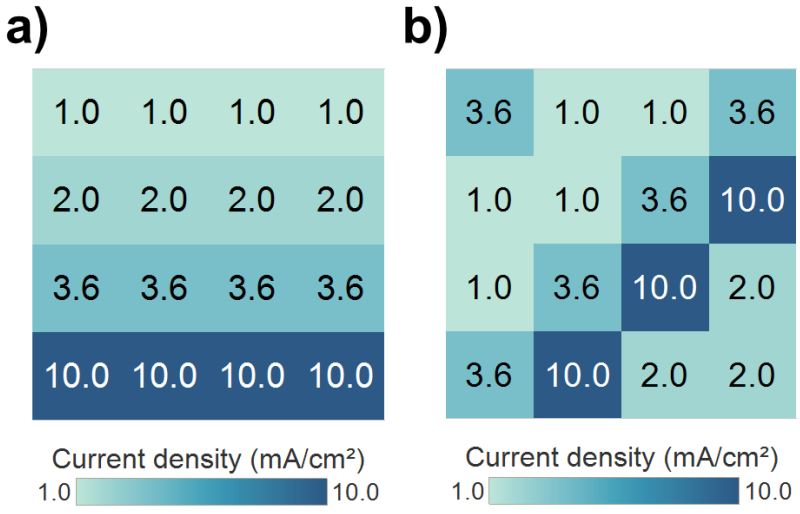

Figure 4.11: Applied current density during parallel screening of electrocatalysts for NRR activity for a 180°/90°-sample, respectively.

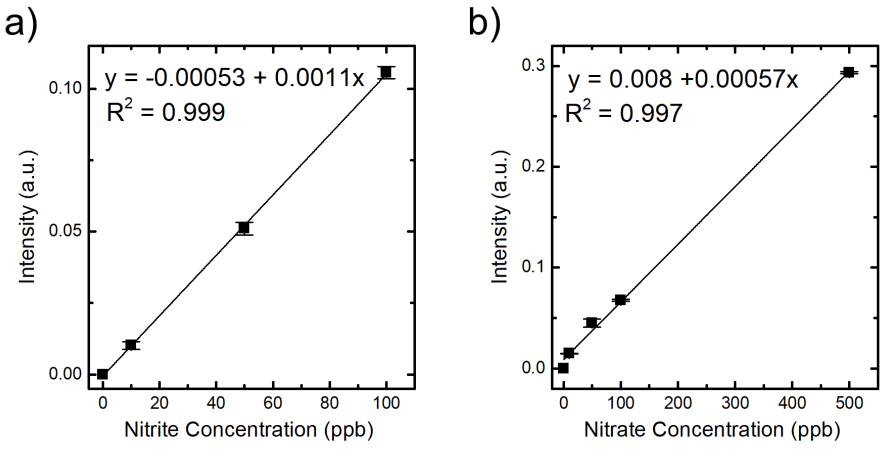

Figure 4.12: Calibration curves used for Nitrite and Nitrate quantification.

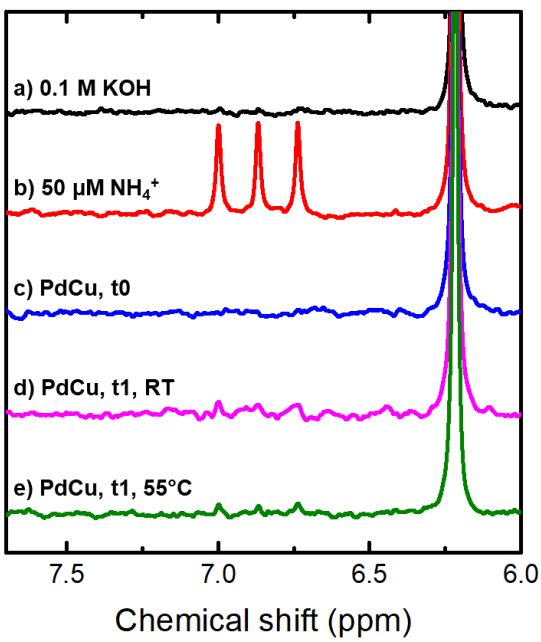

Figure 4.13: ^{1}H NMR spectra of a) a 0.1 M KOH blank , b) a 50 µM NH_4^+ standard, c) the NH_3 background in the catholyte before screening a CuPd catalyst array, d) the catholyte after the RT-experiment and e) after the 55°C-experiment. The 50 µM standard clearly shows the singlet of the internal standard maleic acid at 6.22 ppm and the triplet of NH_4^+ between 6.74–7 ppm.

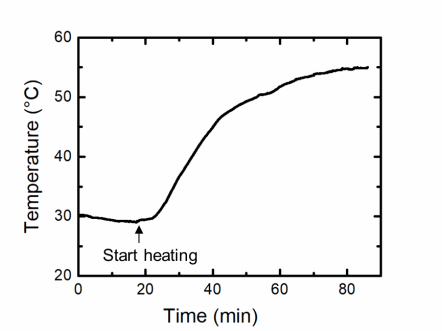

Figure 4.14: Temperature of the catholyte during a 55°C-experiment measured by immersing a K-type thermocouple into the catholyte.

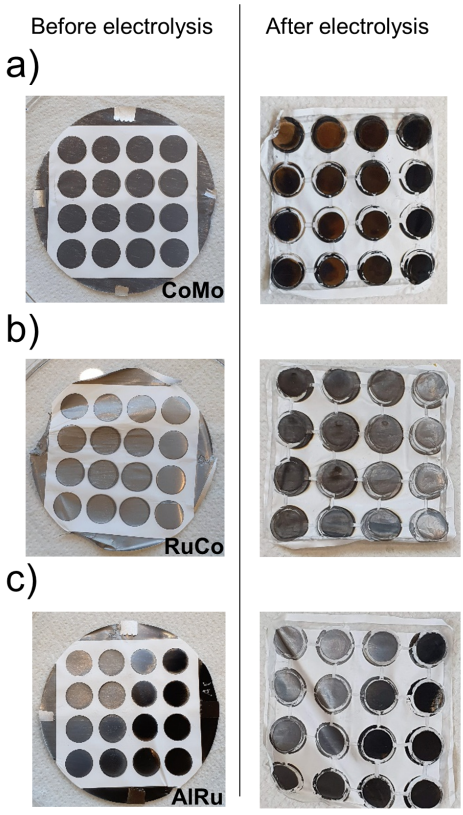

Figure 4.15: Photographs of selected catalyst arrays before (left) and after the electrochemical experiments to measure NRR activity. The area of the catalyst dots that is removed after electrolysis is where the PCB pressed against it during the experiment.

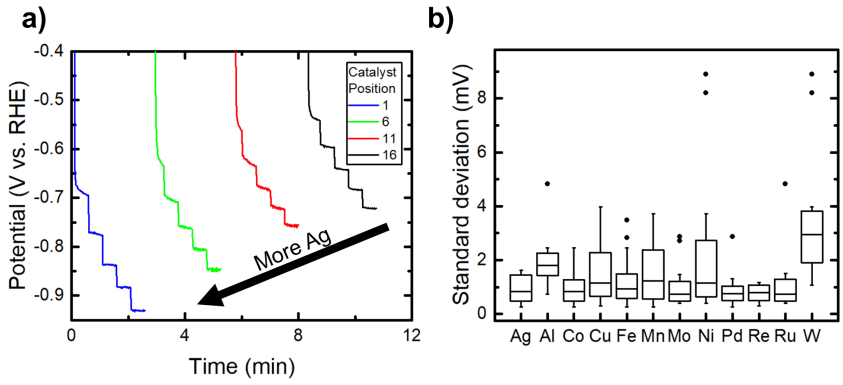

Figure 4.16: Electrochemical characterization of AgCu. b) Box plot of the standard deviation of the potential during the last 5 s of the electrochemical characterization at 0.6 mA (2.14 mA cm^{-2}) for each catalyst tested in this work.

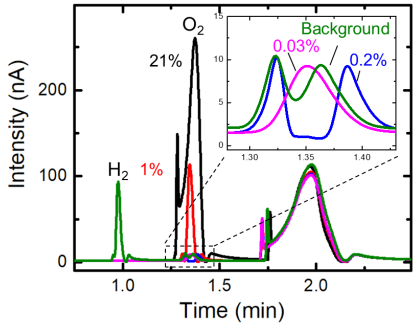

Figure 4.17: GC-MS spectra showing the oxygen background during electrochemical tests.

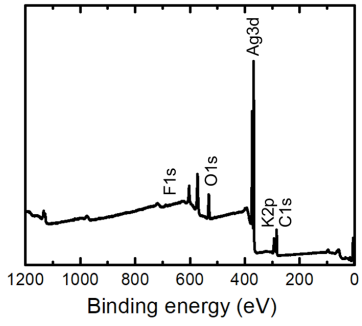

Figure 4.18: XPS survey scan of a 300 nm Ag catalyst dot after the electrolysis protocol used to measure NRR activity (i.e. 75 min CP at room temperature and 60 min CP while heating to 55 °C). No impurities were found which confirms that the cell is clean.

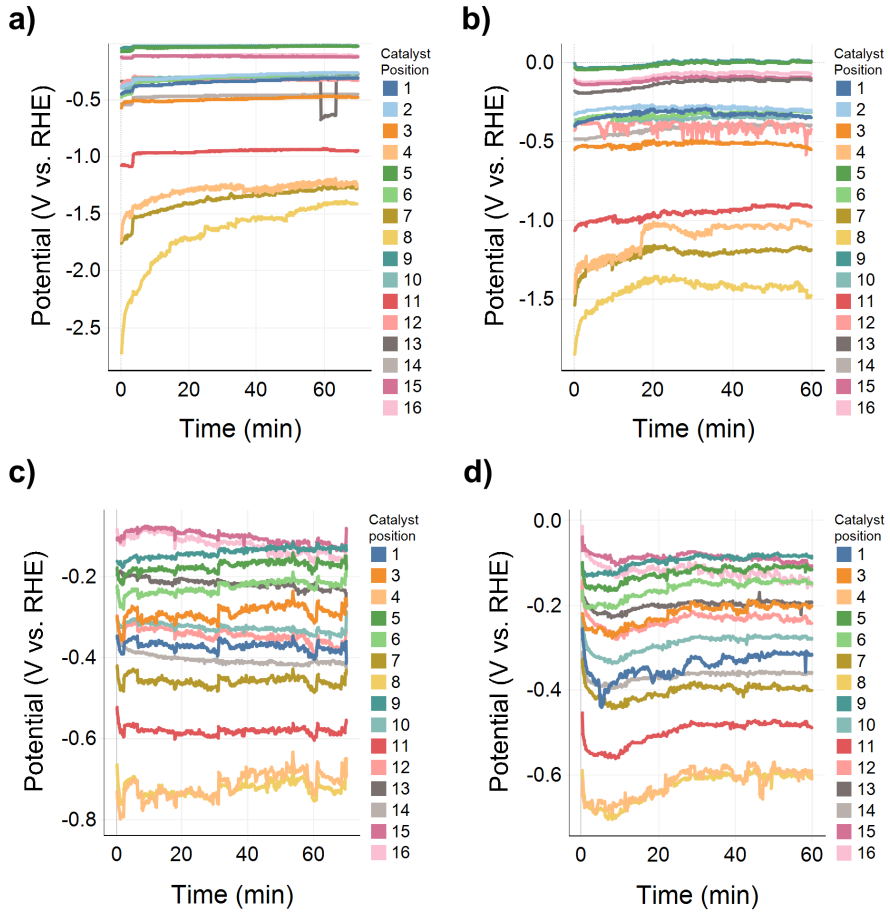

Figure 4.19: Potential over time for a NiMo catalyst array (a,b) and a AgNi catalyst array (c,d) during the RT-experiment (a,c) and during the 55°C-experiment (b,d). The potential was not iR-compensated. No further quantitative analysis of this data was done because the potential is superimposed by considerable iR-drops which depend on the position of the reference electrode with respect to the working electrode and the complex electric field generated by the 16 working electrodes. The fluctuations in potential originated from the GC injections every 5 min and the strokes of the pump used to recirculate the electrolyte.

References

[1] D. R. MacFarlane, P. V. Cherepanov, J. Choi, B. H. Suryanto, R. Y. Hodgetts, J. M. Bakker, F. M. Ferrero Vallana, and A. N. Simonov, *A Roadmap to the Ammonia Economy,* Joule **4**, 1186 (2020).

[2] A. Valera-Medina, H. Xiao, M. Owen-Jones, W. David, and P. Bowen, *Ammonia for power,* Progress in Energy and Combustion Science **69**, 63 (2018).

[3] F. M. Mulder, *Implications of diurnal and seasonal variations in renewable energy generation for large scale energy storage,* Journal of Renewable and Sustainable Energy **6**, 033105 (2014).

[4] A. R. Singh, B. A. Rohr, J. A. Schwalbe, M. Cargnello, K. Chan, T. F. Jaramillo, I. Chorkendorff, and J. K. Nørskov, *Electrochemical Ammonia Synthesis—The Selectivity Challenge,* ACS Catalysis **7**, 706 (2017).

[5] J. H. Montoya, C. Tsai, A. Vojvodic, and J. K. Nørskov, *The Challenge of Electrochemical Ammonia Synthesis: A New Perspective on the Role of Nitrogen Scaling Relations,* ChemSusChem **8**, 2180 (2015).

[6] Y. C. Li, Z. Wang, T. Yuan, D.-H. Nam, M. Luo, J. Wicks, B. Chen, J. Li, F. Li, F. P. G. de Arquer, Y. Wang, C.-T. Dinh, O. Voznyy, D. Sinton, and E. H. Sargent, *Binding Site Diversity Promotes CO_2 Electroreduction to Ethanol,* Journal of the American Chemical Society **141**, 8584 (2019).

[7] M. Zhong, K. Tran, Y. Min, C. Wang, Z. Wang, C.-T. Dinh, P. De Luna, Z. Yu, A. S. Rasouli, P. Brodersen, S. Sun, O. Voznyy, C.-S. Tan, M. Askerka, F. Che, M. Liu, A. Seifitokaldani, Y. Pang, S.-C. Lo, A. Ip, Z. Ulissi, and E. H. Sargent, *Accelerated discovery of CO2 electrocatalysts using active machine learning,* Nature **581**, 178 (2020).

[8] I. E. L. Stephens, A. S. Bondarenko, U. Grønbjerg, J. Rossmeisl, and I. Chorkendorff, *Understanding the electrocatalysis of oxygen reduction on platinum and its alloys,* Energy & Environmental Science **5**, 6744 (2012).

[9] J. Rodriguez, *Physical and chemical properties of bimetallic surfaces,* Surface Science Reports **24**, 223 (1996).

[10] V. Ponec, *Alloy catalysts: the concepts,* Applied Catalysis A: General **222**, 31 (2001).

[11] Z. Wang, C. Li, K. Deng, Y. Xu, H. Xue, X. Li, L. Wang, and H. Wang, *Ambient Nitrogen Reduction to Ammonia Electrocatalyzed by Bimetallic PdRu Porous Nanostructures,* ACS Sustainable Chemistry & Engineering **7**, 2400 (2019).

[12] F. Pang, Z. Wang, K. Zhang, J. He, W. Zhang, C. Guo, and Y. Ding, *Bimodal nanoporous Pd3Cu1 alloy with restrained hydrogen evolution for stable and high yield electrochemical nitrogen reduction,* Nano Energy **58**, 834 (2019).

[13] W. Tong, B. Huang, P. Wang, L. Li, Q. Shao, and X. Huang, *Crystal-Phase-Engineered PdCu Electrocatalyst for Enhanced Ammonia Synthesis,* Angewandte Chemie International Edition **59**, 2649 (2020).

[14] Y. Liu, L. Huang, X. Zhu, Y. Fang, and S. Dong, *Coupling Cu with Au for enhanced electrocatalytic activity of nitrogen reduction reaction,* Nanoscale **12**, 1811 (2020).

[15] L. F. Greenlee, J. N. Renner, and S. L. Foster, *The Use of Controls for Consistent and Accurate Measurements of Electrocatalytic Ammonia Synthesis from Dinitrogen,* ACS Catalysis **8**, 7820 (2018).

[16] J. Choi, B. H. R. Suryanto, D. Wang, H.-L. Du, R. Y. Hodgetts, F. M. Ferrero Vallana, D. R. MacFarlane, and A. N. Simonov, *Identification and elimination of false positives in electrochemical nitrogen reduction studies,* Nature Communications **11**, 5546 (2020).

[17] S. Z. Andersen, V. Čolić, S. Yang, J. A. Schwalbe, A. C. Nielander, J. M. McEnaney, K. Enemark-Rasmussen, J. G. Baker, A. R. Singh, B. A. Rohr, M. J. Statt, S. J. Blair, S. Mezzavilla, J. Kibsgaard, P. C. K. Vesborg, M. Cargnello, S. F. Bent, T. F. Jaramillo, I. E. L. Stephens, J. K. Nørskov, and I. Chorkendorff, *A rigorous electrochemical ammonia synthesis protocol with quantitative isotope measurements,* Nature **570**, 504 (2019).

[18] J. Choi, H.-L. Du, C. K. Nguyen, B. H. R. Suryanto, A. N. Simonov, and D. R. MacFarlane, *Electroreduction of Nitrates, Nitrites, and Gaseous Nitrogen Oxides: A Potential Source of Ammonia in Dinitrogen Reduction Studies,* ACS Energy Letters **5**, 2095 (2020).

[19] S. Licht, B. Cui, B. Wang, F.-F. Li, J. Lau, and S. Liu, *Retraction,* **369**, 780 (2020).

[20] M. Kolen, D. Ripepi, W. A. Smith, T. Burdyny, and F. M. Mulder, *Overcoming nitrogen reduction to ammonia detection challenges: The case for leapfrogging to gas diffusion electrode platforms,* ACS Catalysis **12**, 5726 (2022).

[21] S. L. Scott, T. B. Gunnoe, P. Fornasiero, and C. M. Crudden, *To Err is Human; To Reproduce Takes Time,* ACS Catalysis **12**, 3644 (2022).

[22] A. Hagemeyer, P. Strasser, and A. F. Volpe, in *High-Throughput Screening in Chemical Catalysis* (WILEY-VCH, Weinheim, 2004) pp. 1–60.

[23] H. Liu, in *Ammonia synthesis catalysts: innovation and practice* (Chemical Industry Press ; World Scientific, Beijing : [Hackensack] New Jersey, 2013) p. 32.

[24] T. Muster, A. Trinchi, T. Markley, D. Lau, P. Martin, A. Bradbury, A. Bendavid, and S. Dligatch, *A review of high throughput and combinatorial electrochemistry,* Electrochimica Acta **56**, 9679 (2011).

[25] J. Whitacre, T. Valdez, and S. Narayanan, *A high-throughput study of PtNiZr catalysts for application in PEM fuel cells,* Electrochimica Acta **53**, 3680 (2008).

[26] M. Prochaska, J. Jin, D. Rochefort, L. Zhuang, F. J. DiSalvo, H. D. Abruña, and R. B. van Dover, *High throughput screening of electrocatalysts for fuel cell applications,* Review of Scientific Instruments **77**, 054104 (2006).

[27] J. S. Cooper and P. J. McGinn, *Combinatorial screening of thin film electrocatalysts for a direct methanol fuel cell anode,* Journal of Power Sources **163**, 330 (2006).

[28] J. A. Haber, C. Xiang, D. Guevarra, S. Jung, J. Jin, and J. M. Gregoire, *High-Throughput Mapping of the Electrochemical Properties of (Ni-Fe-Co-Ce)O $_x$ Oxygen-Evolution Catalysts,* ChemElectroChem **1**, 524 (2014).

[29] J. M. Gregoire, C. Xiang, X. Liu, M. Marcin, and J. Jin, *Scanning droplet cell for high throughput electrochemical and photoelectrochemical measurements,* Review of Scientific Instruments **84**, 024102 (2013).

[30] J.-P. Grote, A. R. Zeradjanin, S. Cherevko, A. Savan, B. Breitbach, A. Ludwig, and K. J. Mayrhofer, *Screening of material libraries for electrochemical CO2 reduction catalysts – Improving selectivity of Cu by mixing with Co,* Journal of Catalysis **343**, 248 (2016).

[31] K. C. Neyerlin, G. Bugosh, R. Forgie, Z. Liu, and P. Strasser, *Combinatorial Study of High-Surface-Area Binary and Ternary Electrocatalysts for the Oxygen Evolution Reaction,* Journal of The Electrochemical Society **156**, B363 (2009).

[32] R. Liu and E. S. Smotkin, *Array membrane electrode assemblies for high throughput screening of direct methanol fuel cell anode catalysts,* Journal of Electroanalytical Chemistry **535**, 49 (2002).

[33] A. K. Schuppert, A. A. Topalov, I. Katsounaros, S. O. Klemm, and K. J. J. Mayrhofer, *A Scanning Flow Cell System for Fully Automated Screening of Electrocatalyst Materials,* Journal of The Electrochemical Society **159**, F670 (2012).

[34] R. Battino, T. R. Rettich, and T. Tominaga, *The Solubility of Nitrogen and Air in Liquids,* Journal of Physical and Chemical Reference Data **13**, 563 (1984).

[35] J. Newman and K. E. Thomas-Alyea, in *Electrochemical Systems* (WILEY-INTERSCIENCE, Hoboken, N.J, 2004) third edition ed., pp. 491–499.

[36] J. Schröder, V. A. Mints, A. Bornet, E. Berner, M. Fathi Tovini, J. Quinson, G. K. H. Wiberg, F. Bizzotto, H. A. El-Sayed, and M. Arenz, *The Gas Diffusion Electrode Setup as Straightforward Testing Device for Proton Exchange Membrane Water Electrolyzer Catalysts,* JACS Au **1**, 247 (2021).

[37] K. Ehelebe, N. Schmitt, G. Sievers, A. W. Jensen, A. Hrnjić, P. Collantes Jiménez, P. Kaiser, M. Geuß, Y.-P. Ku, P. Jovanovič, K. J. J. Mayrhofer, B. Etzold, N. Hodnik, M. Escudero-Escribano, M. Arenz, and S. Cherevko, *Benchmarking Fuel Cell Electrocatalysts Using Gas Diffusion Electrodes: Inter-lab Comparison and Best Practices,* ACS Energy Letters **7**, 816 (2022).

[38] C.-T. Dinh, T. Burdyny, G. Kibria, A. Seifitokaldani, C. M. Gabardo, J. P. Edwards, P. D. Luna, O. S. Bushuyev, C. Zou, R. Quintero-Bermudez, Y. Pang, D. Sinton, and E. H. Sargent, *CO2 electroreduction to ethylene via hydroxide-mediated copper catalysis at an abrupt interface,* Science **360**, 783 (2018).

[39] T. Burdyny and W. A. Smith, *CO_2 reduction on gas-diffusion electrodes and why catalytic performance must be assessed at commercially-relevant conditions,* Energy & Environmental Science **12**, 1442 (2019).

[40] A. H. Simon, *Sputter Processing,* in *Handbook of Thin Film Deposition* (Elsevier, 2012) pp. 55–57.

[41] L. Banko, O. A. Krysiak, J. K. Pedersen, B. Xiao, A. Savan, T. Löffler, S. Baha, J. Rossmeisl, W. Schuhmann, and A. Ludwig, *Unravelling Composition–Activity–Stability Trends in High Entropy Alloy Electrocatalysts by Using a Data□Guided Combinatorial Synthesis Strategy and Computational Modeling,* Advanced Energy Materials **12**, 2103312 (2022).

[42] D. Ripepi, R. Zaffaroni, H. Schreuders, B. Boshuizen, and F. M. Mulder, *Ammonia Synthesis at Ambient Conditions via Electrochemical Atomic Hydrogen Permeation,* ACS Energy Letters **6**, 3817 (2021).

[43] K. T. Winther, M. J. Hoffmann, J. R. Boes, O. Mamun, M. Bajdich, and T. Bligaard, *Catalysis-Hub.org, an open electronic structure database for surface reactions,* Scientific Data **6**, 75 (2019).

[44] E. Skúlason, T. Bligaard, S. Gudmundsdóttir, F. Studt, J. Rossmeisl, F. Abild-Pedersen, T. Vegge, H. Jónsson, and J. K. Nørskov, *A theoretical evaluation of possible transition metal electro-catalysts for N_2 reduction,* Phys. Chem. Chem. Phys. **14**, 1235 (2012).

[45] Z. W. Seh, J. Kibsgaard, C. F. Dickens, I. Chorkendorff, J. K. Nørskov, and T. F. Jaramillo, *Combining theory and experiment in electrocatalysis: Insights into materials design,* Science **355**, eaad4998 (2017).

[46] D. Ripepi, R. Zaffaroni, M. Kolen, J. Middelkoop, and F. M. Mulder, *Operando isotope selective ammonia quantification in nitrogen reduction studies via gas chromatography-mass spectrometry,* Sustainable Energy & Fuels **6**, 1945 (2022).

[47] G. Truesdale and A. Downing, *Solubility of Oxygen in Water,* **173**, 1236 (1954).

[48] Z. Chen, X. Duan, W. Wei, S. Wang, and B.-J. Ni, *Recent advances in transition metal-based electrocatalysts for alkaline hydrogen evolution,* Journal of Materials Chemistry A **7**, 14971 (2019).

[49] F. Safizadeh, E. Ghali, and G. Houlachi, *Electrocatalysis developments for hydrogen evolution reaction in alkaline solutions – A Review,* International Journal of Hydrogen Energy **40**, 256 (2015).

[50] Y. Zhu, Q. Lin, Y. Zhong, H. A. Tahini, Z. Shao, and H. Wang, *Metal oxide-based materials as an emerging family of hydrogen evolution electrocatalysts,* Energy & Environmental Science **13**, 3361 (2020).

[51] I. A. Raj and K. I. Vasu, *Transition metal-based hydrogen electrodes in alkaline solution ? electrocatalysis on nickel based binary alloy coatings,* Journal of Applied Electrochemistry **20**, 32 (1990).

[52] M. Domínguez-Crespo, M. Plata-Torres, A. Torres-Huerta, E. Arce-Estrada, and J. Hallen-López, *Kinetic study of hydrogen evolution reaction on Ni30 Mo70, Co30Mo70, Co30Ni70 and Co10Ni20Mo70 alloy electrodes,* Materials Characterization **55**, 83 (2005).

[53] R. Y. Hodgetts, H.-L. Du, D. R. MacFarlane, and A. N. Simonov, *Electrochemically Induced Generation of Extraneous Nitrite and Ammonia in Organic Electrolyte Solutions During Nitrogen Reduction Experiments,* ChemElectroChem **8**, 1596 (2021).

[54] W. Yu, N. S. Lewis, H. B. Gray, and N. F. Dalleska, *Isotopically Selective Quantification by UPLC-MS of Aqueous Ammonia at Submicromolar Concentrations Using Dansyl Chloride Derivatization,* ACS Energy Letters **5**, 1532 (2020).

[55] B. H. Ko, B. Hasa, H. Shin, Y. Zhao, and F. Jiao, *Electrochemical Reduction of Gaseous Nitrogen Oxides on Transition Metals at Ambient Conditions,* Journal of the American Chemical Society **144**, 1258 (2022).

[56] W. Yu, P. Buabthong, C. G. Read, N. F. Dalleska, N. S. Lewis, H.-J. Lewerenz, H. B. Gray, and K. Brinkert, *Cathodic NH_4^+ leaching of nitrogen impurities in CoMo thin-film electrodes in aqueous acidic solutions,* Sustainable Energy & Fuels **4**, 5080 (2020).

[57] S. Nitopi, E. Bertheussen, S. B. Scott, X. Liu, A. K. Engstfeld, S. Horch, B. Seger, I. E. L. Stephens, K. Chan, C. Hahn, J. K. Nørskov, T. F. Jaramillo, and I. Chorkendorff, *Progress and Perspectives of Electrochemical CO_2 Reduction on Copper in Aqueous Electrolyte,* Chemical Reviews **119**, 7610 (2019).

[58] M. Kolen, W. A. Smith, and F. M. Mulder, *Accelerating ^{1}H NMR Detection of Aqueous Ammonia,* ACS Omega **6**, 5698 (2021).

[59] R. Y. Hodgetts, A. S. Kiryutin, P. Nichols, H.-L. Du, J. M. Bakker, D. R. Macfarlane, and A. N. Simonov, *Refining Universal Procedures for Ammonium*

Quantification via Rapid ^{1} *h NMR Analysis for Dinitrogen Reduction Studies,* ACS Energy Letters **5**, 736 (2020).

[60] M. Ďurovič, J. Hnát, and K. Bouzek, *Electrocatalysts for the hydrogen evolution reaction in alkaline and neutral media. A comparative review,* Journal of Power Sources **493**, 229708 (2021).

[61] V. Latyshev, S. Vorobiov, O. Shylenko, and V. Komanicky, *Screening of electrocatalysts for hydrogen evolution reaction using bipolar electrodes fabricated by composition gradient magnetron sputtering,* Journal of Electroanalytical Chemistry **854**, 113562 (2019).

[62] N. Takeno, *Atlas of Eh-pH diagrams*, Tech. Rep. (National Institute of Advanced Industrial Science and Technology, 2005).

5
A Pressure Balancing System for High-Pressure Electrolysis Flow Cells

Pressurization is a promising strategy to increase the selectivity of the nitrogen reduction reaction (NRR) because the electrode potentials of NRR and of the competing hydrogen evolution reaction (HER) can be shifted towards more favourable values for NRR by applying a N_2/H_2 pressure at the cathode. To investigate the influence of a N_2/H_2 pressure on the selectivity of NRR, we developed a high-pressure electrolysis flow cell and a system to pressurize the cell with minimal differential pressure across the cell compartments. A double-GDE flow cell design was designed to minimize the complexity of the system and maximise the sensitivity of the liquid ammonia detection. The system was successfully tested up to a pressure of 10 bar.

5.1. Introduction

Higher selectivities for the nitrogen reduction reaction (NRR) are prevented by the dominating hydrogen evolution reaction (HER) in aqueous electrolyte. More precisely, higher rates of NRR are suppressed because HER occurs at less negative potentials than NRR. The electrocatalyst plays a key role in promoting NRR over HER because it determines the overpotential that has to be applied in addition to the thermodynamically required electrode potential to drive the reaction.[1] For this reason, we have thus far in this work focussed on strategies to develop better electrocatalysts for NRR. However, another promising strategy to promote NRR is to shift the electrode potentials of NRR and HER thermodynamically towards more favourable values for NRR. The electrode potential of an electrochemical reaction depends on the concentration of reactants and products at the catalyst surface (Nernst Equation):

$$E = E_0 + \frac{RT}{zF} ln(\frac{c_{O,surf}}{c_{R,surf}}) \quad (5.1)$$

,where E is the equilibrium potential, E_0 is the standard reduction potential, $c_{O,surf}$ and $c_{R,surf}$ are the concentration of oxidising agent and reducing agent at the surface and z is the number of electrons transferred in the reaction.[2] According to Equation 5.1, the electrode potential of NRR can be shifted to less negative potentials by increasing the concentration of molecular nitrogen at the surface of the electrode. Similarly, the electrode potential of HER can be shifted to more negative values by increasing the hydrogen concentration at the electrode surface. Both effects should shift the selectivity towards NRR. According to Henry's Law an increase in N_2 pressure above the electrolyte leads to a proportional increase of the N_2 solubility in the electrolyte.[3] Therefore, the electrode potentials for NRR and HER can be shifted towards more favourable values for NRR by applying a N_2 and/or H_2 pressure above the electrolyte.

To take advantage of the benefits of a N_2/H_2 pressure for NRR, a pressurizable electrochemical cell is needed. The easiest pressurizable cell design is a single compartment cell which is partially filled with a static electrolyte and two electrodes which are submerged into the electrolyte.[4] However, this cell design is not suitable for NRR catalyst development because without a separator to prevent NH_3 crossover from the cathode to the anode, NH_3 oxidation to NOx will take place at the anode.[5] Therefore, catholyte and anolyte must be separated into two compartments. Electrochemical cells with more than one compartment are much more difficult to pressurize because the separator is often just a thin membrane which can bulge or rupture easily if the pressure on both sides is not equal. To prevent this, a system to balance the pressures in multi-compartment electrochemical cells is needed.

We have outlined in Chapter 3 that using GDE cells for NRR electrocatalyst development has many advantages such as more reliable NH_3 detection and higher experimental throughput. Therefore, it would be beneficial to combine these advantages

with the advantages of high-pressure operation. However, GDE cells typically have flowing electrolyte/gas instead of compartments with static electrolyte, because produced gases (such as H_2 and O_2) must be transported away from the catalyst surface.[6] This complicates pressurization because each flow of electrolyte/gas has to be pressurized independently of the others while maintaining minimal differential pressure between the compartments. The goal of this Chapter is the development of a pressure balancing system for high-pressure electrolysis flow cells which enables the use of pressurized GDE cells. Such a pressure balancing system may even enable the pressurized operation of the high-throughput GDE cell design described in Chapter 4 which would strongly accelerate the screening of catalysts under pressurized conditions. In addition a pressurized system that is designed such that it can work for GDE cells could also work for closed membrane cells like proton exchange membranes (PEM), anion exchange membranes (AEM) or metallic permeation electrodes.

5.2. Process Engineering for High-Pressure Electrolysis Flow Cells with Pressure Balancing

The process flowsheet of the pressure balancing system which was designed and built for this work is shown in Figure 5.1a. As the cell design, we chose a 4-compartment GDE cell with a GDE as both anode and cathode. The cell design will be described in more detail in the following section. To minimize cost and complexity, the system was pressurized through the gas flows. The static anolyte and catholyte were pressurized through the porous GDEs that separated them from the gas flows. With this system design, no high pressure pumps and no pressurized reservoirs for anolyte and catholyte were necessary. At the cathode side, N_2/H_2 mixtures were supplied to the gas compartment to shift the equilibrium towards NRR. The continuous flow ensures proper mixing of N_2 and H_2 despite their large density difference. The outlet of the gas compartment at the cathode side was connected to a GC for gaseous NH_3 detection. At the anode side, N_2 was supplied to remove evolved gas from the anode.

To balance the pressures, Equilibar back-pressure regulators (BPR) were installed downstream of the electrochemical cell. The back-pressure of an Equilibar BPR is set by applying a pressure to the top connector—the so called dome (Figure 5.1b). Through a mechanical system the BPR ensures that nothing can flow through the BPR unless the pressure upstream of the BPR is equal to the dome pressure. The domes of both BPRs were connected by a pipe to ensure that the pressure is equal on both sides. Using Equilibar BPRs for the pressurization prevents sudden pressure spikes because the pressure can be increased gradually while gas is already flowing. The pressure of the domes were set using an electronic dome pressure regulator (Pressure Control Solutions). We chose an electronic dome pressure regulator instead of a manual version because with the electronic version the pressurization can be fully automated at well-defined rates.

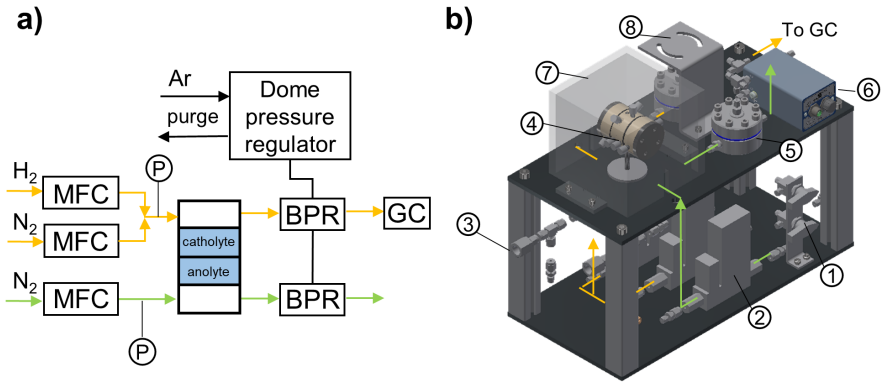

Figure 5.1: Pressure balancing system for high-pressure electrolysis. a) Process flow sheet. b) CAD rendering. Abbreviations: MFC: mass flow controller, BPR: back-pressure regulator, GC: gas chromatograph.

Figure 5.2: An impression of the software that was programmed to control the high-pressure electrolysis system.

An impression of the software to control the system is shown in Figure 5.2. All surfaces that are in contact with the gas stream after it leaves the cathode side of the electrochemical cell were passivated with a SilcoNert (SilkoTek) coating to minimize NH_3 adsorption. The pressure balancing system was built and commissioned successfully up to a pressure of 10 bar. We used it to balance the pressures in an electrochemical cell to produce NH_3 via the H-perm mechanism (Figure 1.2). Preliminary results showed that the NH_3 production can be increased by increasing the N_2 pressure. The details of these experiments will be presented in a future publication.

5.3. A Double-GDE Flow Cell Design for High-Pressure Electrolysis

There are only a few reports of cell designs for high-pressure electrolysis with GDEs.[7–9] Gabardo et al. utilized a 3-compartment GDE cell with flowing electrolyte and gas (Figure 5.1) and Equilibar back-pressure regulators for pressure balancing (similar to our pressure balancing system in Figure 5.1) to study the effect of pressurization on the selectivity of the CO_2 reduction reaction (CO2RR).[9] A flowing catholyte and anolyte increases the complexity of the system because of the additional equipment (pumps, reservoirs) that is needed to recirculate a pressurized electrolyte safely and robustly. In addition, the recirculation increases the overall electrolyte volume which is undesirable for NH_3 detection (see Chapter 3). However, flowing electrolyte is not needed for NRR experiments because the current density for NRR experiments is at least an order of magnitude lower than for CO2RR experiments which means that the complications that will occur at the high current density of CO2RR experiments (concentration polarization) will not occur during NRR experiments. Therefore, we wanted to develop a more simple high-pressure GDE cell design for NRR without flowing electrolyte.

A CAD rendering of the 4-compartment GDE cell designed for this work is shown in Figure 5.3. Expanded PTFE GDEs were used as both anode and cathode (not shown in Figure 5.3). This double-GDE design prevents gas accumulation in the static electrolyte, because O_2 and H_2 produced during the electrochemical reactions can escape through the GDE. Expanded PTFE GDEs were used instead of carbon-fabric GDEs because they have much higher resistance to flooding which makes them more suitable for high-pressure studies.[9] The electrodes were electrically contacted according to the same principle that was used for the HTP cell (Figure 4.2) by pressing a current collector against the catalyst layer on the electrolyte side of the GDE. The gas flowing through the gas compartments on both sides of the cell enables simple pressurization using the pressure balancing system described in the previous section. If electrolyte flow becomes necessary at some point, the plugs in the electrolyte compartments can be replaced with tubing connectors.

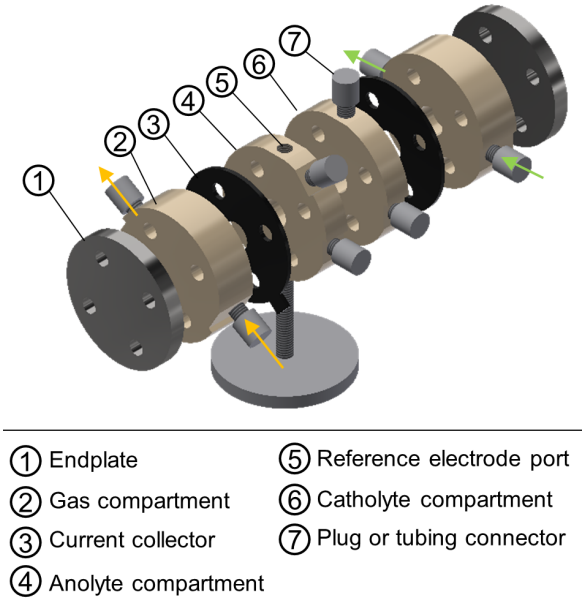

Figure 5.3: CAD rendering of a 4-compartment electrochemical cell for high-pressure experiments.

References

[1] A. R. Singh, B. A. Rohr, M. J. Statt, J. A. Schwalbe, M. Cargnello, and J. K. Nørskov, *Strategies toward Selective Electrochemical Ammonia Synthesis,* ACS Catalysis **9**, 8316 (2019).

[2] J. Newman and K. E. Thomas-Alyea, *Electrochemical Systems*, 3rd ed. (WILEY-INTERSCIENCE, Hoboken, N.J, 2004) pp. 10–13.

[3] J. J. Carroll, J. D. Slupsky, and A. E. Mather, *The Solubility of Carbon Dioxide in Water at Low Pressure,* Journal of Physical and Chemical Reference Data **20**, 1201 (1991).

[4] F. Allebrod, C. Chatzichristodoulou, and M. B. Mogensen, *Alkaline electrolysis cell at high temperature and pressure of 250 °C and 42 bar,* Journal of Power Sources **229**, 22 (2013).

[5] S. Z. Andersen, V. Čolić, S. Yang, J. A. Schwalbe, A. C. Nielander, J. M. McEnaney, K. Enemark-Rasmussen, J. G. Baker, A. R. Singh, B. A. Rohr, M. J. Statt, S. J. Blair, S. Mezzavilla, J. Kibsgaard, P. C. K. Vesborg, M. Cargnello, S. F. Bent, T. F. Jaramillo, I. E. L. Stephens, J. K. Nørskov, and I. Chorkendorff, *A rigorous electrochemical ammonia synthesis protocol with quantitative isotope measurements,* Nature **570**, 504 (2019).

[6] T. Burdyny and W. A. Smith, *CO_2 reduction on gas-diffusion electrodes and why catalytic performance must be assessed at commercially-relevant conditions,* Energy & Environmental Science **12**, 1442 (2019).

[7] L. A. Diaz, N. Gao, B. Adhikari, T. E. Lister, E. J. Dufek, and A. D. Wilson, *Electrochemical production of syngas from CO_2 captured in switchable polarity solvents,* Green Chemistry **20**, 620 (2018).

[8] B. Endrődi, G. Bencsik, F. Darvas, R. Jones, K. Rajeshwar, and C. Janáky, *Continuous-flow electroreduction of carbon dioxide,* Progress in Energy and Combustion Science **62**, 133 (2017).

[9] C. M. Gabardo, A. Seifitokaldani, J. P. Edwards, C.-T. Dinh, T. Burdyny, M. G. Kibria, C. P. O'Brien, E. H. Sargent, and D. Sinton, *Combined high alkalinity and pressurization enable efficient CO_2 electroreduction to CO,* Energy & Environmental Science **11**, 2531 (2018).

Summary

Ammonia synthesis via the direct nitrogen reduction reaction mechanism has the potential to be more flexible in production level and scale of operation and may enable cost reductions compared to alternative technologies for green NH_3 synthesis. For the research field to advance to higher Technology Readiness Levels selective electrocatalysts that promote the reaction over the competing hydrogen evolution reaction are needed. The aim of this work was to build tools that enable the development of selective electrocatalysts for NRR with high NH_3 production rate. We have identified two limitations in the workflow which is typically used to test promising materials for NRR activity, that hindered the development of selective electrocatalysts thus far: 1) NRR activity measurements are found to be unreliable due to NH_3 contaminations and 2) the experimental throughput of the workflow is too slow to enable rapid progress, due to single catalyst studies that require elaborate ammonia detection and calibration methods. In Chapter 2 and 3 we systematically analyzed the steps involved in an NRR activity measurement to develop alternative methods that overcome these limitations. For even more effective NRR catalyst development, we explored in Chapters 4 and 5 how to accelerate the experimental workflow even further by enabling combinatorial catalyst screenings and by carrying out experiments under thermodynamically more favourable conditions for NRR, respectively.

In Chapter 2, we evaluated the NH_3 detection step of the NRR catalyst testing workflow and found that conventionally used spectrophotometric NH_3 detection methods are unsuitable for the quantification of NRR activity because they require too much bench time per sample and they are unable to distinguish between isotopologues of NH_3 which is crucial for reliable detection. Therefore, we evaluated quantitative ^1H NMR as a potential replacement for spectrophotometric methods and found that $^{14}NH_3/^{15}NH_3$ can be quantified accurately and isotopically selective with ^1H NMR but the required analysis time to reach sufficient sensitivity for NRR experiments is too long for routine analysis with a standard 400 MHz NMR without cryoprobe. To overcome this limitation, we developed a new detection method which utilizes a paramagnetic relaxation agent to improve the sensitivity of ^1H NMR. We showed that by adding 1 mM paramagnetic Gd^{3+}-ions to the NMR sample, the required analysis time can be reduced by an order of magnitude to around 15 min per sample which is acceptable for NRR catalyst development. The strong reduction of the analysis time was explained by a much faster relaxation back to equilibrium of the nuclear spins responsible for the NH_3 signal in the presence of Gd^{3+}-ions. This enables a reduction of the time delay between NMR scans so that more scans can be acquired in the same amount of time which increases the signal-to-noise ratio for

a given measurement duration.

In Chapter 3, we analysed the cell design and operating conditions of NRR experiments and found that the choice of cell design is crucial for the speed of catalyst testing and the reliability of results. The choice of cell design determines the volume of the cell compartments and the way in which N_2 is supplied to the catalyst surface which, in turn, influences how long ammonia has to be accumulated in the electrolyte to reach the detection limit and how much N_2 reaches the catalyst surface, respectively. We reported that the most frequently chosen cell design for NRR experiments—the H-cell—is an unfavourable choice for NRR catalyst development because due to the occurrence of mass transport limitations at low N_2 flow rates the cost of crucial control experiments with $^{15}N_2$ cannot be decreased below €100 per experiment without lowering the NRR selectivity at the same time. In addition, with the typical electrolyte volume of H-cells (30 mL), it takes many hours of continuous NH_3 production at typical NRR production rates to accumulate enough ammonia in the electrolyte to exceed the level of common NH_3 contamination sources. We showed that such limitations can be circumvented by switching from H-cells to gas diffusion electrode cells because gas diffusion electrode cells can be operated with lower electrolyte volume and at lower N_2 flow rates without a drop in N_2 mass transport. Further, we showed that the high electrochemical surface area of gas diffusion electrodes lowers the overpotential required to produce sufficient amounts of NH_3 for detection and reduces the risk of catalyst deactivation. Finally, we argued that gas diffusion electrodes might be a more suitable platform to screen catalysts for NRR because in parallel electrochemical research fields they have been adopted to make results obtained in a laboratory devices more transferable to commercial devices which operate at high current density.

In Chapter 4 we integrated parallelization and automatition techniques into the catalyst testing workflow to accelerate it even further. We developed a high-throughput gas diffusion electrode cell design to screen up to 16 bimetallic electrocatalysts in parallel for NRR activity, which accelerated the workflow by an order of magnitude compared to one at a time catalyst testing. The gas diffusion electrode cell design enabled two orders of magnitude higher mass transport limiting currents for reactions with gaseous reactants such as N_2 or O_2 than conventional all-liquid high-throughput cell designs, which circumvents activity losses due to mass transport limitations. We then screened 528 bimetallic catalysts for NRR activity in the temperature range 21–55°C. No catalyst showed NRR activity significantly above background level. Background measurements for both NH_3 and NOx before every experiment were crucial to evaluate the reliability of the results. The reported materials database may act as a future reference for NRR research.

In Chapter 5 we described a pressure balancing system for electrochemical flow cells with multiple compartments. The pressure balancing system enables flow of electrolyte or gas through parallel cell compartments with minimal differential pressure. This enables pressurized operation of gas diffusion electrode cells which

were found to be favourable for NRR in Chapter 3. Due to the thermodynamically more favourable conditions for NRR under N_2 pressure, such a system is expected to increase the selectivity and NH_3 production rate of a selective catalyst. A proof-of-concept experiment confirmed that the fully automated pressure and flow control works according to specification.

Samenvatting

Ammonia synthese via directe elektrochemische stikstof reductie heeft potentie om flexibeler en/of goedkoper te worden dan alternatieve technologieën. Om dit te realiseren en relevante 'Technology Readiness Level' in het onderzoeksveld aan te tonen zijn er echter selectieve elektrokatalysatoren nodig die deze reactie bevorderen ten opzichte van de concurrerende waterstof-evolutie reactie. Het doel van dit werk is om hulpmiddelen te ontwikkelen die het vinden van selectieve elektrokatalysatoren voor de stikstofreductie reactie (NRR) met een hoge NH_3 productiesnelheid mogelijk maken.

Er zijn bij de ontwikkeling van selectieve elektrokatalysatoren voor NRR-activiteit twee belangrijke beperkingen geïdentificeerd in de werkzaamheden die uitgevoerd worden tijdens het testen van interessante kandidaat elektrokatalysator-materialen: 1) NRR-activiteit metingen zijn onbetrouwbaar door NH_3 en NOx contaminaties en 2) de experimentele snelheid en uitvoering van de werkzaamheden is te traag om tot veel testresultaten te komen. In Hoofdstukken 2 en 3 analyseren we systematisch de stappen in een NRR-activiteit meting, om alternatieve methodes te ontwikkelen die deze twee beperkende factoren weg nemen. Voor nog effectievere ontwikkeling van NRR-katalysatoren, hebben we in Hoofdstukken 4 en 5 onderzocht hoe de experimentele werkzaamheden nog verder versneld kunnen worden en hoe experimenten uitgevoerd kunnen worden onder thermodynamisch gunstigere condities voor NRR.

In Hoofdstuk 2 evalueren we dat de NH_3-detectiestap van de meest gebruikte spectrofotometrische NH_3-detectiemethoden in de NRR-katalysatortesten ongeschikt zijn voor een snelle en betrouwbare kwantificering van NRR-activiteit, omdat ze te veel wachttijd vereisen per monster en geen onderscheid kunnen maken tussen stikstof isotopologen van NH_3. Het laatste is cruciaal is voor een betrouwbare detectie. Daarom evalueerde we kwantitatieve ^{1}H NMR als een potentiële vervanging voor spectrofotometrische methoden en constateerden we dat: NH_3 nauwkeurig en isotoop-selectief kan worden gekwantificeerd met ^{1}H NMR, maar dat de benodigde analysetijd om voldoende gevoeligheid voor NRR-experimenten te bereiken te lang is voor routineanalyse met een standaard 400 MHz NMR zonder cryoprobe. Om deze beperking weg te nemen, hebben we een nieuwe methode ontwikkeld die gebruik maakt van een paramagnetisch zout in de oplossing die dankzij de versnelde T1 relaxatie binnen een beperkte meettijd de gevoeligheid van ^{1}H NMR te verbeteren. We toonde aan dat, door 1 mM paramagnetische Gd^{3+}-ionen aan het vloeistof NMR monster toe te voegen, de vereiste analyse tijd kan worden gereduceerd tot ongeveer 15 min per monster, wat een acceptabele tijd is voor NRR-katalysator ontwikkeling. De sterke afname van de analysetijd wordt mogelijk gemaakt door

de snellere T1 relaxatie van de verantwoordelijke kernspins voor het NH_3-signaal in aanwezigheid van Gd^{3+}-ionen.

In Hoofdstuk 3 analyseerde we het celontwerp en de operationele condities van NRR-experimenten en ontdekten dat de keuze voor cel ontwerp cruciaal is voor de snelheid van het testen van katalysatoren en de betrouwbaarheid van de resultaten. De keuze van het celontwerp bepaalt het volume van de celcompartimenten en de manier waarop N_2 aan het oppervlakte van de katalysator wordt toegevoerd. Dit heeft op zijn beurt respectievelijk invloed op hoe lang ammonia moet worden geaccumuleerd in de elektrolyt om het detectielimiet te bereiken en op hoeveel N_2 het katalysator oppervlakte bereikt. We constateerden dat het meest gebruikte celontwerp voor NRR-experimenten (de H-cel) een ongunstige keuze is voor de ontwikkeling van NRR-katalysatoren, want de kosten van cruciale controle experimenten met $^{15}N_2$ kunnen niet worden gereduceerd onder de €100 per experiment zonder ook de NRR-selectiviteit te verlagen, vanwege de aanwezige massa-transport limitaties bij lage N_2 stroomsnelheden. Bovendien, met het typische elektrolytvolume van H-cellen (30 mL), kost het vele uren aan continue NH_3 productie bij normale NRR productiesnelheden om genoeg ammonia in het elektrolyt te accumuleren om meetbaar het niveau van veelvoorkomende NH_3 contaminatiebronnen te overschrijden. We lieten zien dat dit soort beperkingen vermeden kunnen worden door over te stappen van H-cellen naar gas-diffusie-elektroden, aangezien gas-diffusie-elektrode kunnen opereren met lager elektrolyt volume en bij lagere N_2 stroomsnelheden zonder een daling van N_2 massa transport te veroorzaken. Verder, hebben we laten zien dat het grote elektrochemische oppervlakte van gas diffusie elektrode, de overpotentiaal verlaagt hetgeen nodig is om voldoende NH_3 te produceren voor de succesvolle detectie en hetgeen het risico op deactiveren van de katalysator ook vermindert. Ten slotte, hebben we betoogd dat gas diffusie elektroden een geschikter platform zijn om NRR-katalysatoren te screenen, aangezien ze in andere elektrochemische onderzoeksvelden ook zijn toegepast om resultaten in laboratoriumapparatuur beter op te kunnen schalen naar condities die relevant zijn voor commerciële apparatuur, die werkt bij hoge stroomdichtheden.

In Hoofdstuk 4, integreren we de parallellisatie- en automatiseringstechnieken in de katalysatortest werkzaamheden om deze nog verder te versnellen. Hier wordt een 'high-throughput' gas-diffusie-elektrode cel waarin tot 16 bimetallische elektrokatalysatoren in parallel te testen zijn op NRR-activiteit gepresenteerd. Hiermee kunnen de werkzaamheden met een orde van grootte worden versneld vergeleken met het één voor één testen van katalysatoren. Het gas-diffusie-cel ontwerp maakt twee ordes van grootte hoger massa transport mogelijk dan conventionele volledigvloeistof high-throughput cel ontwerpen voor reacties met gasvormige reactanten zoals N_2 of O_2. Dit ontwerp omzeilt hiermee mogelijke activiteit verliezen door massa transport limitaties. Vervolgens zijn 528 bimetallische katalysatoren getest op hun NRR-activiteit binnen een temperatuurbereik van 21-55°C. Opmerkelijk is dat geen enkele katalysator NRR-activiteit vertoonde die significant hoger dan het achtergrondniveau van verontreinigingen. Achtergrond metingen voor zowel NH_3

als NOx voor iedere meting, zijn cruciaal om de betrouwbaarheid van de resultaten te bepalen.

In Hoofdstuk 5 hebben we een drukbalanceringssysteem beschreven voor elektrochemische cellen met meerdere compartimenten voor gas en elektrolyt stromen. Het drukbalanceringssysteem maakt stroming van elektrolyt of gas door parallelle cel compartimenten mogelijk met minimale differentiële druk over membranen. Dit maakt toepassing van gas diffusie elektrode cellen onder hogere drukken mogelijk voor NRR zoals in Hoofdstuk 3 beschreven. Vanwege de thermodynamisch gunstigere condities voor NRR onder N_2-druk, wordt verwacht dat zo een systeem de selectiviteit en NH_3 productie snelheid van een selectieve katalysator verbetert. Een initieel proof-of-concept experiment bevestigde dat de volledig geautomatiseerde druk- en stromingsregeling werkt volgens specificatie.

Acknowledgements

The past four years have been unlike any other period of my life so far. Now, I have a small book with science in it. Science that I discovered. That's pretty cool. The journey to produce this book was fun and exciting but also frustrating and stressful at times. I met awesome people (some are now my friends), went to summer schools, had successes and failures, endured pandemics and explored the Netherlands. This period is now coming to a close. Thankfully, I was not alone on this journey but some of you accompanied me during the good and the bad and helped me with your advice, your company or your comfort to find my way through it.

First of all, I would like to thank my supervisors for their advice, their guidance and their patience with me. Thank you for motivating me and investing in my education. I would also like to express my gratitude to the members of my committee for reading my thesis, providing feedback and for participating in the defence ceremony.

The MECS group and the people from other research groups that I had the chance to meet during my PhD have been a source of fun, inspiration and support over the past years. I am very thankful that I was part of such a inclusive group of wonderful people during my PhD and I regret that I couldn't spend as much time with you as I wanted during the pandemic. Thank you all for the good time!

My research would not have been possible without the excellent technicians who have mastered the art of converting research instruments from malfunctioning nightmares into plug-and-play solutions. Your contribution to my dissertation and my development cannot be overstated. I was fortunate to (co-)supervise the Master's thesis of two bright students. The difficulty of the topic is great but you lived up to the challenge. Thank you for your hard work.

Finally, I'd like to thank my closest friends and family. Your unconditional support means a lot to me. You helped me tremendously to maintain some work-life balance, even during the stressful times. I consider myself incredibly lucky that I could always rely on your support during the last four years.

Curriculum Vitae

Martin Kolen was born on the 13^{th} of January 1994 in Essen, Germany. In 2016, he graduated from RWTH Aachen University with a Bachelor's in Mechanical Engineering. During his Bachelor's he completed engineering internships at RWE Power AG, Access e.V. and Cerobear GmbH and worked as a student assistant at the Helmholtz-Institute for Biomedical Engineering where he developed simulation models for biomedical shockwave transducers. Martin stayed at RWTH Aachen for his Master's in Chemical Process Engineering and graduated in 2017 with the distinction *summa cum laude*. For his Master's thesis, Martin visited the laboratory of Prof. Louis Bouchard at the University of California, Los Angeles to conduct research on reaction monitoring with magnetic resonance imaging. From March 2018 to March 2022 he worked as a PhD candidate at the Delft University of Technology in the Materials for Energy Conversion and Storage (MECS) group under the supervision of Prof. Fokko Mulder. During his time as a PhD candidate, Martin worked on electrocatalyst development for electrochemical ammonia synthesis.

List of Publications

M. Kolen, D. Ripepi, G. Antoniadis, H. Schreuders, B. Boshuizen, D. van Noordenne, D. Ripepi, W.A. Smith, F.M. Mulder, *Combinatorial Screening of Bimetallic Electrocatalysts for Nitrogen Reduction to Ammonia Using a High-Throughput Gas Diffusion Electrode Cell Design*, J. Electrochem. Soc. **169** 124506 (2022).

D. Ripepi, B. Izelaar, D. van Nordenne, P. Jungbacker, **M. Kolen**, P. Karanth, D. Cruz, P. Zeller, V. Perez-Dieste, I. Villa-Garcia, W.A. Smith, F.M. Mulder *In situ study of hydrogen permeable electrodes for electrolytic ammonia synthesis using near ambient pressure XPS*, ACS Catal. **12,21** 13781–13791 (2022).

D. Ripepi, R. Zaffaroni, **M. Kolen**, J. Middelkoop, F.M. Mulder, *Operando isotope selective ammonia quantification in nitrogen reduction studies via gas chromatography-mass spectrometry*, Sustainable Energy Fuels **6** 1945–1949 (2022).

M. Kolen, D. Ripepi, W.A. Smith, T. Burdyny, F.M. Mulder, *Overcoming nitrogen reduction to ammonia detection challenges: The case for leapfrogging to gas diffusion electrode platforms*, ACS Catal. **12,10** 5726–5735 (2022).

M. Sassenburg, R. de Rooij, N.T. Nesbitt, R. Kas, S. Chandrashekar, N.J. Firet, K. Yang, K. Liu, M.A. Blommaert, **M. Kolen**, D. Ripepi, W.A. Smith, T. Burdyny, *Characterizing CO2 Reduction Catalysts on Gas Diffusion Electrodes: Comparing Activity, Selectivity, and Stability of Transition Metal Catalysts*, ACS Appl. Energy Mater. **5,5** 5983–5994 (2022).

M. Kolen, W.A. Smith, F.M. Mulder, *Accelerating ^{1}H NMR Detection of Aqueous Ammonia*, ACS Omega **6** 5698–5704 (2021).